Republic of Iraq
Ministry of Higher Education and Scientific Research
University of Babylon
College of Engineering
Electrical Engineering Dept.

A BUILT-IN SELF-TEST FOR MICRO-ELECTRO-MECHANICAL RESONATOR

A Thesis
Submitted to the Department of Electrical Engineering / College of Engineering / University of Babylon in Partial Fulfillment
of the Requirements for the Degree of Master of Science in Engineering / Electrical Engineering / Electronics.

By

Ali Jasim Mohammed Obaid

Supervised by

Prof. Dr. Qais Karim Omran

2023 A.D. 1444 A.H.

بِسْمِ اللَّـهِ الرَّحْمَـٰنِ الرَّحِيمِ

﴿يَرْفَعِ اللَّهُ الَّذِينَ آمَنـــــــوُا مِنكُمْ
وَالَّذِينَ أُوتُـــــــوا الْعِلْمَ دَرَجَاتٍ﴾

صدق الله العظيم

سورة المجادلة : 11

Supervisors Certification

I certify that this thesis titled "**A BUILT-IN SELF-TEST FOR MICRO-ELECTRO-MECHANICAL RESONATOR**" was prepared by Ali Jasim Mohammed Obaid under my supervision at the Electrical Engineering Department, College of Engineering at University of Babylon, in partial fulfillment of the requirements for the degree of Master of Science in Electrical Engineering/Electronics.

Supervisors

Signature:

Name*:* ***Prof. Dr. Qais Karim Omran***

Date: / / 2023

In view of the available recommendation, we forward this thesis for debate by the examining committee.

Head of the Electrical Engineering Department

Signature:

Name:

Date: / / 2023

Acknowledgements

Thanks be to God for the insight that inspired me, and praise be to Him for the blessings He has bestowed upon me, and to Him is the credit for achieving what I aspire to in this research. Praise be to God, who by His praise opens every book and by His remembrance every speech is issued, and by His praise the people of blessings enjoy the abode of reward.

*It gives me great pleasure to extend my thanks and gratitude to (**Prof. Dr. Qais Karim Omran**), who provided me with the information I needed in my research*

And for the great efforts he made for me since he proposed the subject of the research and his continuous supervision, and for his advice that helped me a lot in overcoming the difficulties I faced, calling from God success and brilliance in the scientific career.

I would like to extend my thanks and gratitude to the Deanship of the College of Engineering and the Presidency of the Electrical Engineering Department for the facilities and administrative procedures they provided me, which effectively contributed to the completion of the requirements of this research.

.

Researcher

Dedication

To my kind father.... *who taught me how to stand firmly above the earth, my role model, and my ideal in life; He is the one who taught me how to live with dignity and honor.*

To my tender mother... *the source of love, altruism and generosity, I cannot find words that can give her her due, for she is the epic of love and the joy of a lifetime, and an example of dedication and giving.*

To my brothers... *my support and I share my joys and sorrows.*

To all my friends and to all those from whom I received advice and support;

I dedicate to you the summary of my scientific effort.

Abstract

Throughout the course of recent years, micro electromechanical systems (MEMS) have illustrated the critical potential for detecting high-recurrence signal handling applications. This is because of their astounding highlights like little extent, enormous recurrence quality element item, low power utilization, minimal expense clump creation. Radio repeat correspondence circuits like reference oscillators, channels, with blenders considering such MEMS resonators may be utilized for meeting the growing count of RF parts inclined to be requested by the front-line multi-band/multi-mode far-off devices. MEMS resonators might give an attainable option in contrast to the present-day grounded quartz crystal that is loaded with significant downsides like big size, and significant cost, besides low similarity with IC chips.

In this thesis, recent technology was designed and simulated for the self-test design, which represents the work of a resonant pass band filter that generates the required frequencies by entering data related to the physical properties of piezoelectric materials. For the proposed system and the extracted design values of resistors, capacitors and equivalent inductors the self checking and correction technique could be used to delete any deviation in the resonator performance. The proposed system was simulated and tested at high pass frequencies fp = 10 GHz, and high-quality factor Q=85% in detecting changes in frequencies and parameter. The motional capacitance was main parameter that effected the output frequency where it has been considered as a function of MEMS material failure mode. The stop frequency has shifted down from 8.5 GHz to 3.47 GHz while the pass frequency has shifted up from 10 GHZ to 10.88 GHz. On the other hand, the other parameter Static Capacitance (Co), Motional

Inductance (Lm) and Motional Resistance (Rm) had a less effect on the output frequency of the resonator.

List of Contents

List of Contents

List of Contents

List of Tables

List of Tables

List of Tables

List of Figures

List of Figures

List of Figures

List of Figures

List of Figures

List of Figures

List of Figures

List of Abbreviations

Abbreviation	Definition
AI	Acoustic Impedance.
AlN	Aluminum Nitride.
AV	Acoustic Velocity.
BAW	Bulk Acoustic Wave.
BIST	Built In Self Test.
BPF	Band Pass Filter.
BPFD	Band Pass Filter Design.
c-c	clamped-clamped.
C_m	Motional Capacitance.
C_o	Static Capacitance.
CPU	Central Processing Unit.
Df_S	Delta stop frequency.
Df_p	Delta pass frequency.
DUT	Device Under Test.
f %	The percentage change in frequency.
f_s	stop frequency.
f_p	pass frequency.
FBAR	Film Bulk Acoustic Resonator.
FBARPP	FBAR Piezoelectric Physical.
IC	Integrated Circuit.
IDT	Inter-Digital Transducer.
L_m	Motional Inductance.
MEMS	Micro-Electro-Mechanical System.
OoB	Out-of-Band.
Op-Amp	Operational Amplifier
PVDF	polyvinylidene fluoride.
PPD	Piezoelectric Physical Density
PZT	lead zirconate titanate.

List of Abbreviations

Abbreviation	Definition
Q	Quality factor.
RF	Radio-Frequency.
RGT	Resonant Gate Transistor.
R_m	Motional Resistance.
SAW	Surface Acoustic Wave.
SMR	Solidly Mounted Resonator.
TD	Thickness Deviation.
TFT	Thin Film Thickness.
TFBAR	Thin-Film Bulk Acoustic Resonator.
UHF	Ultra High Frequency.
VCOs	Voltage controlled oscillators.
VHF	Very High Frequency.
ZnO	Zinc oxide.
Zmax	maximal electrical impedance.
Zmin	Minimum electrical impedance.

List of Symbols

Symbol	Definition
ε	The piezoelectric material permittivity
A	The thin film area (m)
d	The piezoelectric material thickness (m)
Z Acoustic	The FBAR acoustic impedance (ohm)
V	The FBAR acoustic velocity (m/s)
D	The piezoelectric material density (Kg/m2)
h	The FBAR thickness (m)

Chapter One

INTRODUCTION

Chapter one

INTRODUCTION

1.1 Introduction

Using manufacturing processes, The Micro-Electro-Mechanical System (MEMS) technology allows for the creation and construction of intricate mechanical systems and devices as well as their integrated electronics. MEMS emerged gradually from research labs into commonplace goods after a very early vision in the early 1950s. Inkjet printer heads, pressure sensors for medical use, and accelerometers used to control airbag deployment in vehicles are just a few examples of the commercial products and uses that started to use MEMS components in the middle of the 1990s. MEMS devices are now used in data storage systems for precision positioning devices and screens. However, new uses in the areas of communications (optical and wireless), biomedicine, and process control hold the greatest promise for MEMS devices. These systems as a manufacturing technology have numerous clear benefits[1].

As a first step, the microtechnologies and interdisciplinary character of MEMS have allowed for a wide range of devices and synergies to be developed in previously unrelated areas. (such as biology and microelectronics). In addition to the apparent advantages of reduced size, weight, and cost, MEMS also enables the production of components and devices with enhanced performance and reliability [1], [2].

Micro-electro-Mechanical System consists of micromechanical structures, microsensors, microactuators and micro-electronics, all this embedded in the same chip as illustrated in figure 1.1 [1].

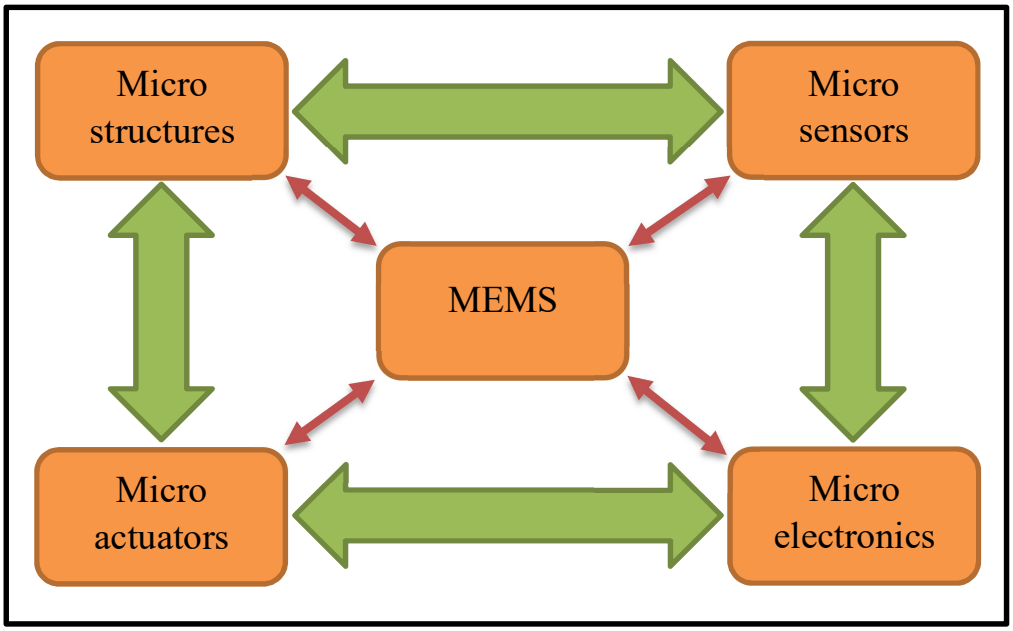

Fig 1.1: Schematic diagram of the components of micro-electromechanical systems [1].

1.2 Micromechanical Resonator

Because of the straightforward micro scale example of a guitar string made of nickel and steel alloy, which has a specific length, and when plucked, resonates at a specific resonance frequency, the idea of a micromechanical resonator is simple to understand. Because of this, it is able to choose a particular frequency automatically, and it also has a Quality factor (Q) that is in the hundreds, which makes it a significant improvement over passive electronic resonators. Now, if the dimensions of such a string are shrunk to the micron level, fabricated with IC-compatible materials such as silicon, polysilicon, etc., and excited electrostatically or piezoelectrically rather than by simply plucking, a microscopic-guitar is created. In MEMS terminology, this instrument is referred to as a clamped-clamped (c-c) beam resonator as depicted in figure 1.2, [2].

The following three elements make up the majority of such a MEMS resonator [2]:

1. An input-transducer that transforms an electrical signal into an electrostatic force and a mechanical indication.

2. The mechanical resonant structure that, as a result of the electric force generated, is capable of vibrating in one or more modes.

3. A device that converts the mechanical signal from the vibrating structure back into an electronic signal by sensing its motion.

Every mechanical structure will vibrate at one or more natural frequencies of resonance, such as a disk or a beam. Similar to how juice glasses vibrate after being forcefully hit at a particular audible frequency. These usually appear in such massive sizes at frequencies of just a few kiloHertz. Higher resonant frequencies can be attained by shrinking to a microscale. (e.g., several MHz or even up to GHz).By exerting pressures on mechanical structures at particular frequencies, referred to as the resonant frequencies, resonance is forced into mechanical structures [2].

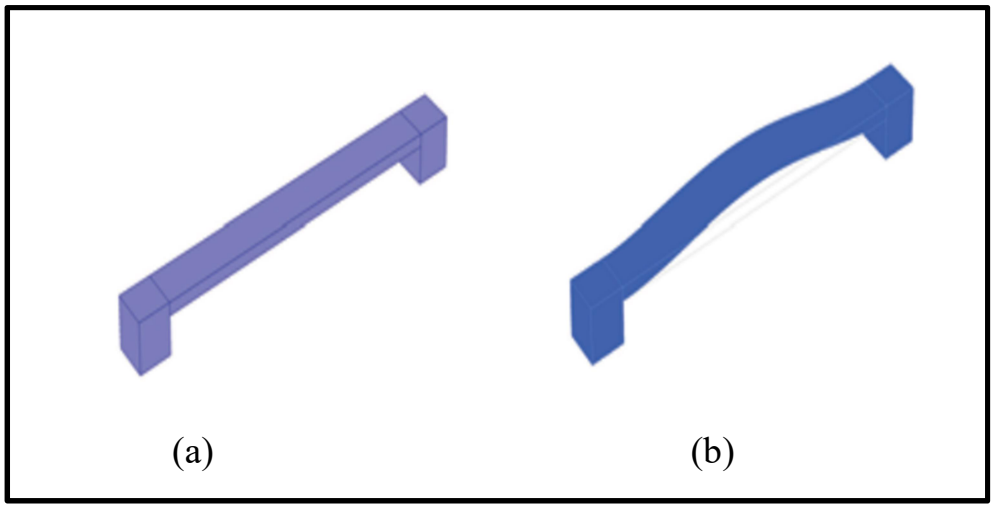

Fig 1.2: (a) Clamped-clamped beam (b) The deformed beam in three dimensions at its native eigenfrequency [2].

A beam with its movement restrained at both extremities is depicted in figure 1.2(a). "clamped-clamped" is another name for this type of beam configuration. (c-c). The "first" flexural-mode, depicted in figure 1.2(b) of the deformed forms, has the lowest resonant frequency and is so-called because its motion is parallel to the beam's breadth[3], [4].

As can see the potential use of MEMS in different applications require the self test in microsystems, that become an essential part of the design steps.

Built In Self Test (BIST) for MEMS is more complex than integrated circuits. Due to the different and diverse reasons and patterns of failure, which makes the online and offline testing complex[5], [6]. Compared to IC testing, MEMS testing is generally more expensive, and in some cases accounts for up to 50% of the final product price[7]–[9]. Built In Self Test methods can help to increase the reliability and offset the cost of these solutions for testing across multiple power domains and interfaces[10]. BIST can be described as a detection methodology or error handling strategy, where the checking system only refers to error detection[11], [12].

1.3 Literature Survey

The important articles and papers which have discussed the electromechanical resonator behaviors have been collected and reviewed in the following paragraphs.

B. John et al. 2015 [13]proved that the test behavior performed with the achievement of BIST is to be sufficient to balance the discouragement of the hardware overhead produced by the additional BIST circuitry. This method can

offer smaller test time compared to an outwardly used test and leads to the use of low-price test equipment through all steps of production.

Zhang et al. (2017) [14]Use acoustic wave-based filters that are among the most widely used filters in wireless communication devices. This is due to a number of factors, including their small size to avoid complicating the front end of devices, particularly smartphones, and their high-quality factor and efficient performance. developed the use of MEMS resonators in place of traditional electrical analogs for Radio-Frequency (RF) uses. These parts are assembled into the gadget by connecting them with high-quality mechanical resonators and integrated circuits. This technology helps restrict Central Processing Unit (CPU) overload while also reducing hardware (transmit and receive). Mechanical vibration is employed due to its small footprint, high quality factor, low power requirements, and compatibility with integrated circuitry. the filter is switched on and off to achieve the center frequency at ~7.81 and ~8.35 GHz separately . The filter performance shows a sharp at the frequency of (f0±0.5 GHz).

Roy et al. (2018) [15]suggested a methodology with oscillating-based test for an attractive sensor of the field for a certain device, this device has various direct test boundaries. It is very difficult to measure these limits all the time, and in this way, a full instrument shoot is an expensive course. Using an oscillator-based test approach, reconfigure it in an oscillating device (using a crit circle) to be visualized by estimating posterior limits such as oscillatory frequency and easily observable abundance.

Dmytro Fedasyuk et al. 2019 [16]presented a solution to the problem of investigating the parameters of the integrated circuits of MEMS accelerometers using self-test and motion detectors, including measurement and detection modes for testing.

Zhao et al. (2019) [17]proposed another technique where the accelerometer is moved twice, one utilizing the right activation finger and one utilizing the left, and the results of disappointment when they are not coordinated. Here overt repetition is used The accelerometer demonstrates a noise floor of 98 ng/$Hz^{1/2}$ and a bias stability of 56 ng under ambient conditions, corresponding to a frequency noise floor of 0.77 ppb/$Hz^{1/2}$and a frequency bias stability of 0.43 ppb.

Y. Liu and Cai et al (2020) [18] In this review, the basic principle and key parameters of the BAW resonator have been described. The literature survey provides details on the different materials, designs, and characteristics of the BAW resonator. High frequency, wide bandwidth, small size, and high-power capacity are the new challenges in 5G communication networks. It is difficult to complete a high-performance filter based on conventional BAW resonator technology. Doped AlN, single AlN, and LN are preferred materials to improve the inherent performance of the resonator. Research on resonator characteristics including spurious mode, temperature compensation, and tuning ability provide technical feasibility for high-performance, stable operation and application expansion of the filter. bulk acoustic wave (BAW) resonators have more potential in fabricating high- quality RF filters because of their lower insertion loss and better selectivity in the middle and high frequency bands above 2.5 GHz.

Yandrapalli, et al. (2021) [19] presented that the most MEMS sense actual signs (speed increase, power, pressure, radiation, and so forth) and change them towards electrical waves handled by the related devices. For self-test, such signs should be produced on-chip along the examination stage which should be small much as small as could really be expected ,Since any BIST method needs a microelectronics control, For the instance of sensor devices, here is conceivable

by electrically instigating on-chip the examination improvements. Simulations and measurements demonstrate that a protocol can be established to reliably design and produce such resonators with desired high frequency for large bandwidth (over 10%).

1.4 Problem Statement

The main problems that occur in the micro-electromechanical resonator systems can be summarized by the following:

MEMS resonator suffers from the problems of difficult-to-control changes in very low frequencies. This is because a high value of the resonator's center frequency (in GHz) will not detect small changes in frequencies (in MHz) and MEMS devices are difficult to be reprogrammed since they are fabricated with special materials and sophisticated techniques. Therefore there is a need for self test crucial to increase the reliability of the system and become more attractive to the investors to be used in different applications.

1.5 Aims of the Thesis

The main aim of this letter is design and simulation a self-test technique for MEMS resonators using suitable methodology with efficient monitoring and controlling sub systems. The BIST give a some benefit such as:

1- Design and simulation a self-test technique for MEMS resonators using suitable methodology with efficient monitoring and controlling sub systems.

2- Examining the performance of the resonator by controlling the design frequencies (fp and fs) and the design values of the piezoelectric materials of the resonator (i.e. the size of the resonator).

3- Design as well as simulate a robust with efficient monitored with controlled micro-electromechanical resonator systems.

1.6 Thesis Organization:

Chapter one: This chapter provided an introduction, problem statements, and objectives of to the thesis.

Chapter two: This chapter introduces basic ideas and situation of micro-electromechanical resonator system along theoretical concepts and mathematical relations.

Chapter three: This chapter presents the details dealing with the proposal micro-electromechanical resonator system with built in self-test.

Chapter four: This chapter provides the simulation results for two designed models using MATLAB program.

Chapter five: This chapter contains the conclusions and the future research direction.

Chapter Two

Theoretical Background

CHAPTER TWO
THEORETICAL BACKGROUND

2.1 Introduction

Mechanical structures with at least one micrometer in size are considered MEMS devices. An electrical effect or output effect is typically used to vibrate a movable part in these devices. These devices' portability, minimal power consumption, and high efficiency are all huge pluses[20].

Microelectromechanical systems (MEMS) allow for the fabrication of miniature integrated devices or systems that syndicate mechanical besides electronic components. Made with batch production techniques, such as Integrated Circuit (IC) fabrication, they range in size as of a few micrometers towards a few millimeters. In addition to their ability to generate macro scale effects, these objects (or systems) can also sense, control, and operate on a microscale level [1].

The interdisciplinary nature of MEMS makes use of design, engineering, and manufacturing expertise from a wide and diverse range of technical fields, including optics engineering, instrumentation, and packaging, mechanical engineering, electrical engineering, and engineering of materials. Systems in the automotive, medical, electronic, telecommunication, and military sectors all make use of MEMS. Examples of modern MEMS devices that are mass-produced and disseminated in the commercial market

1- inkjet printer heads.
2- heads disk drive read/write.
3- blood pressure sensors.
4- optical switches.

5- micro valves.

MEMS, which integrates microelectronics based on silicon with micromachining, has been consider as a cutting-edge technology that could revolutionize both commercial and consumer goods in the 21st century. All of our lives and the way experience them could be drastically altered by its techniques and microsystem-based devices. These systems represent the second revolution in micro manufacturing, if semiconductor micro fabrication was the first[21]

2.2 Physical Principle of MEMS Resonators

The MEMS resonators can produce an endless range of frequencies due to their physical design. Under specific statuses, practically any of these frequencies can be excited to actuate the moving part of the structure into resonance.

2.2.1 The Basics of a MEMS Resonator

For a machine to be in resonance, it must be sensitive to only certain frequencies. Resonance occurs in many different physical realms when a system is able to store energy and transmit energy between modes. If we imagine this system to exist in a mechanical universe, there may be certain frequencies at which it vibrates more powerfully than at others. The R-L-C circuit is a reverberating component in electrical circuits and operates in series and parallel. There are two types of energy storing devices: capacitors, which use an electric field when charged, and inductors, which use a magnetic field when current is passed through them. When the energy is continuously transmitted between the two, the system oscillates. Capacitor and inductor impedances are equivalent when resonance occurs[22].

2.3 MEMS Resonator

To convert energy between the electrical and mechanical fields, a MEMS resonator like the one shown in figure 2.1 uses a transducer. The observed resonant mechanical structures can be treated as spring-mass-damper systems, whether they are beams, disks, rings, or plates [23].

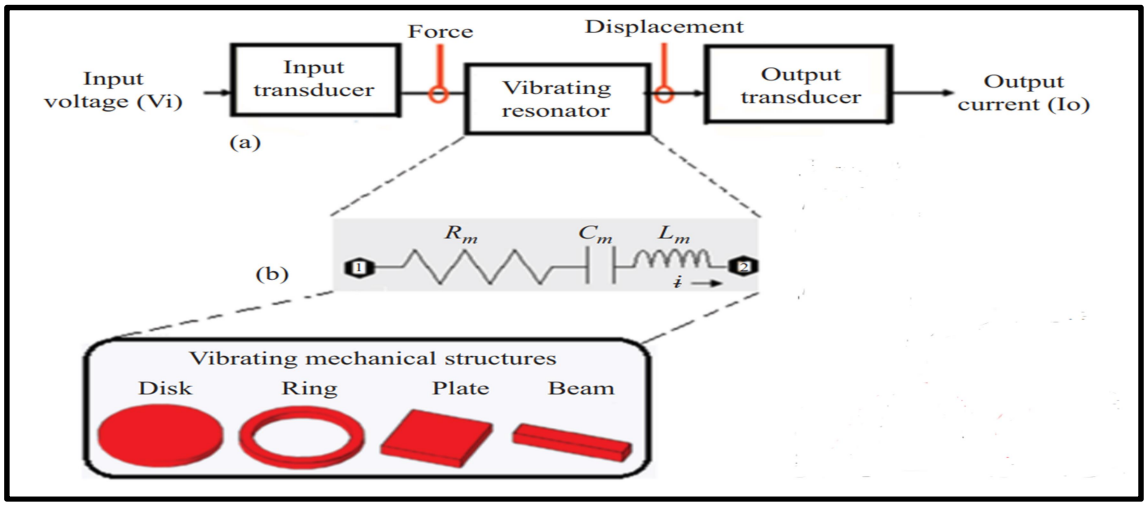

Fig 2.1: (a) Illustration of a MEMS resonator's building blocks in addition (b) a high-level electromagnetic model aimed at MEMS resonators [23].

The MEMS resonator's block schematics are shown in figure 2.1(a), and its general electrical model is shown in figure 2.1(b). The actuation voltage (the incoming electrical energy) is converted into mechanical energy by the electromechanical transducer named the input port. (i.e., strain before stress). At transducer's output terminal, mechanical energy (displacement/deformation) is converted back towards electrical energy.(i.e., output currents). Electromechanical coupling coefficient quantifies the effectiveness of such energy transfer [23].

Because of their stability, reliability, and enormous quality factor (Q), quartz crystal resonators are in great demand. Their manufacturing method is expensive, they are sensitive to shock and vibration, and they aren't compatible with CMOS technology, among other drawbacks. Even if the Q of an on-chip

tank circuit with homogenous inductors and capacitors is above 10, it is still very low.[24].

The MEMS resonator can operate at Very High Frequency (VHF), Ultra High Frequency (UHF), and Radio-Frequency (RF) frequencies while maintaining a very high Q value that is closer to quartz both in vacuum and in air. Less power is used by MEMS resonators, which also have great CMOS compatibility and higher temperature stability. These resonators are also resistant to vibration and shock. Mechanical resonators have replaced quartz crystals in current communication applications because they have a substantially higher Q than their electrical counterparts[24]–[27]. Table 2.1 provides a comparison between MEMS resonator and a quartz resonator.

Table 2.1: Quartz resonators and microelectromechanical system (MEMS) resonators have a lot in common.[28].

Features	Quartz resonator	MEMS resonator
Size	2–5 mm	400 μm smaller
Frequency	1–80 MHz	1–50 MHz
Quality factor (^{x} 103)	100–200	75–150
CMOS compatibility	No	Yes
Shock/vibration immunity	Poor	Good
Cost	High	Better

2.3.1 Methods of Vibration

One simple type of micro machined resonant circuit is the Resonant Gate Transistor (RGT), which consists of a cantilever beam with a fixed end, a mechanical resonant assembly capable of vibrating in one or else more modes, in addition an output transducer for detecting[29]. Beams, rings, disks, square plates, combs, etc. are just some of the micromechanical resonator forms

available. Devices can also be sorted according to the method of operation they use, which can be either flexural, torsional, or bulky[30]. conforming to figure 2.2.

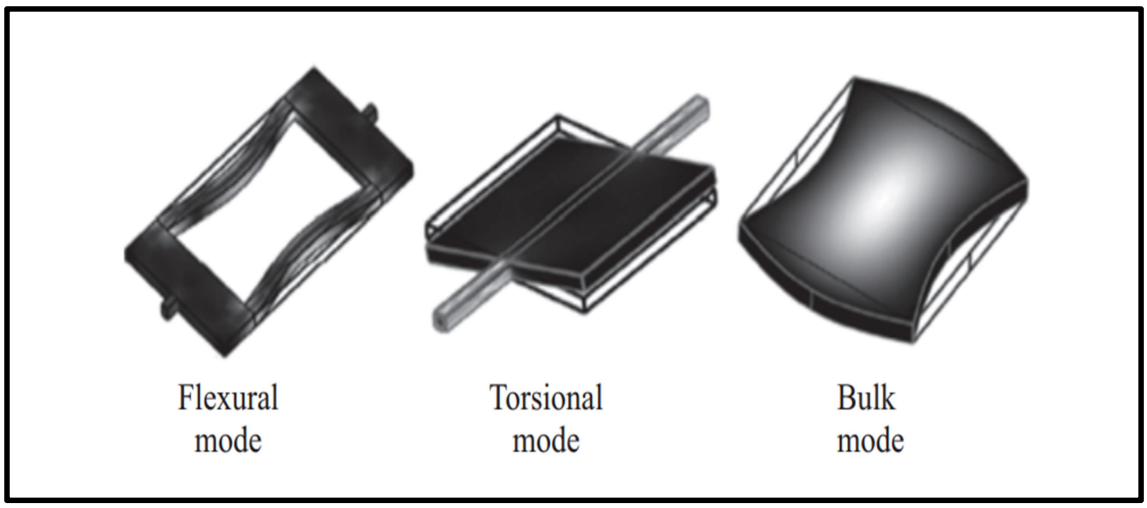

Fig 2.2: Mechanical resonator vibration patterns [30].

A) Flexural Mode

This mode represents the formation of transverse standing waves. The dominant stress is bending stress. Flexural mode resonators are suitable for low-frequency operations, hence are more prone to losses from surface effects.[31].

B) Torsional Mode

This mode is the representation of sheer stress. The displacement produced is rotational in nature. These resonators exhibit lower anchor losses and lower squeeze film damping and hence have very high Q [31].

C) Bulk Mode

This mode represents the formation of longitudinal standing waves. Because of their larger structural stiffness, the bulk mode is preferred for high frequency and high Q operations [31].

2.3.2 Acoustic Micro Resonator Technologies

Acoustic micro resonators have been the subject of research in the telecommunications and sensor sectors for the past few years as a means to shrink the footprint of and lower the power needs of portable radio hardware and detection systems. Acoustic resonators of this type are microelectromechanical devices. When operated under the right conditions, they generate acoustic waves that eventually cause them to vibrate at a reverberation frequency tied to their mechanical setup and characteristics. Resonators can be broken down into two distinct types: those that produce a Surface Acoustic Wave (SAW) and those that produce a Bulk Acoustic Wave (BAW).[32].

2.3.3 FBAR Design Structure

The Film Bulk Acoustic Resonator (FBAR) is analogous to the Solidly Mounted Resonator (SMR). Conventional IC developments allow for the fabrication of devices like SAW, SMR, and FBAR ferroelectric back-to-back acoustic coupler (FBAR) is expedient that uses a piezoelectric material positioned amid II electrodes to create an acoustic seal. It's not uncommon for FBARs to be constructed with piezoelectric elements like Aluminum Nitride (AlN) or Zinc oxide (ZnO). So as to obtain high-quality factors, the FBAR must be released through micromachining, which also serves to provide acoustical isolation among the device also the substrate. In the end, the resonator will have a membrane or air gap beneath its construction. Device release technologies include front- or back-surface micromachining, as well as mass micromachining. [32].

The FBAR design structure with the planar electrode and Hilbert 3 electrode geometry, is shown in figure 2.3.

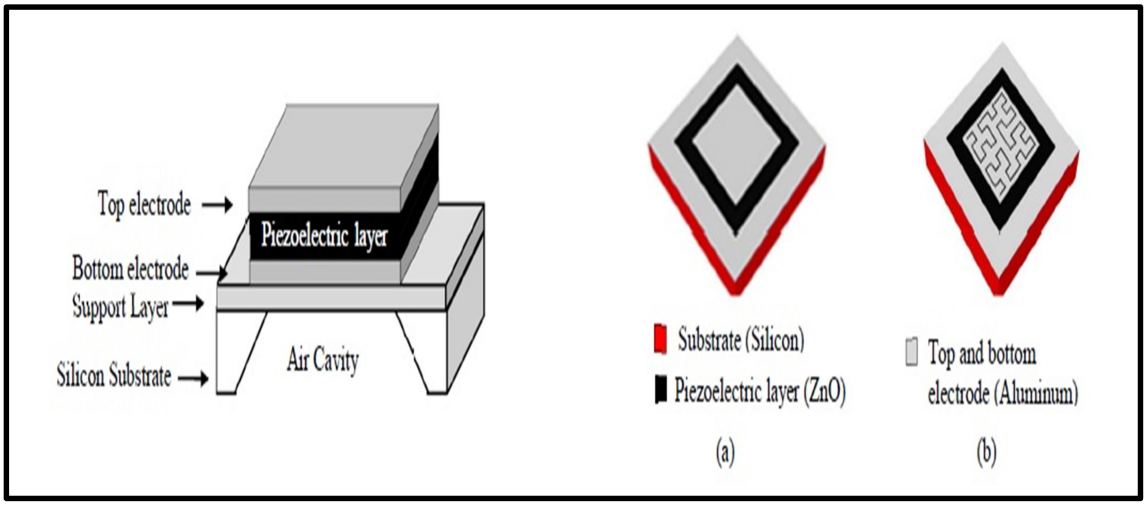

Fig 2.3: Typical FBAR structure, (a) the planar electrode, (b) Hilbert 3 electrode geometry[33].

The schematic diagram of FBAR structure is demonstrated in figure 2.4.

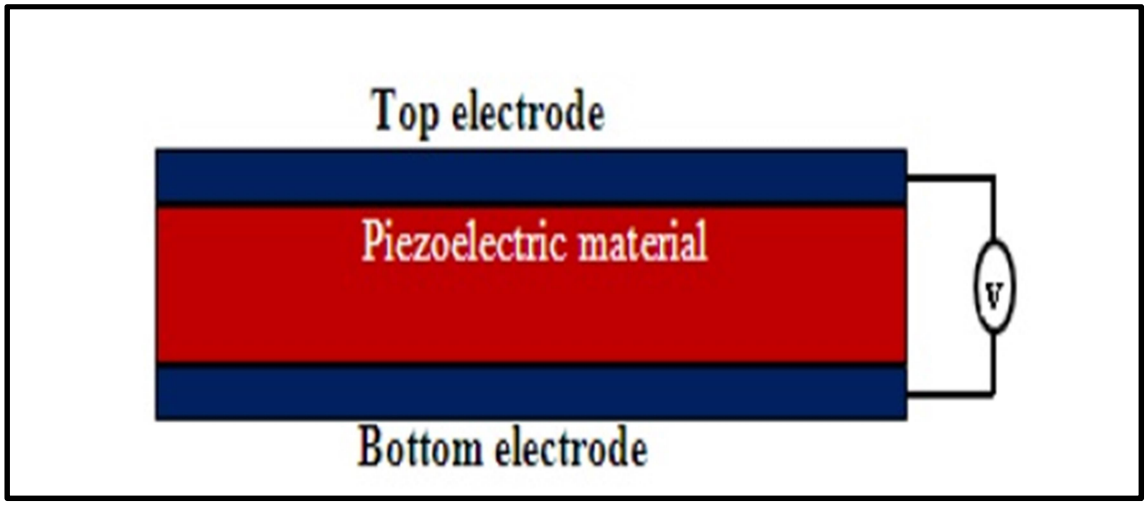

Fig 2.4: Schematic diagram of FBAR structure[34].

The equivalent circuit of single resonator with its typical Band Pass Filter (BPF) are presented in figure 2.5.

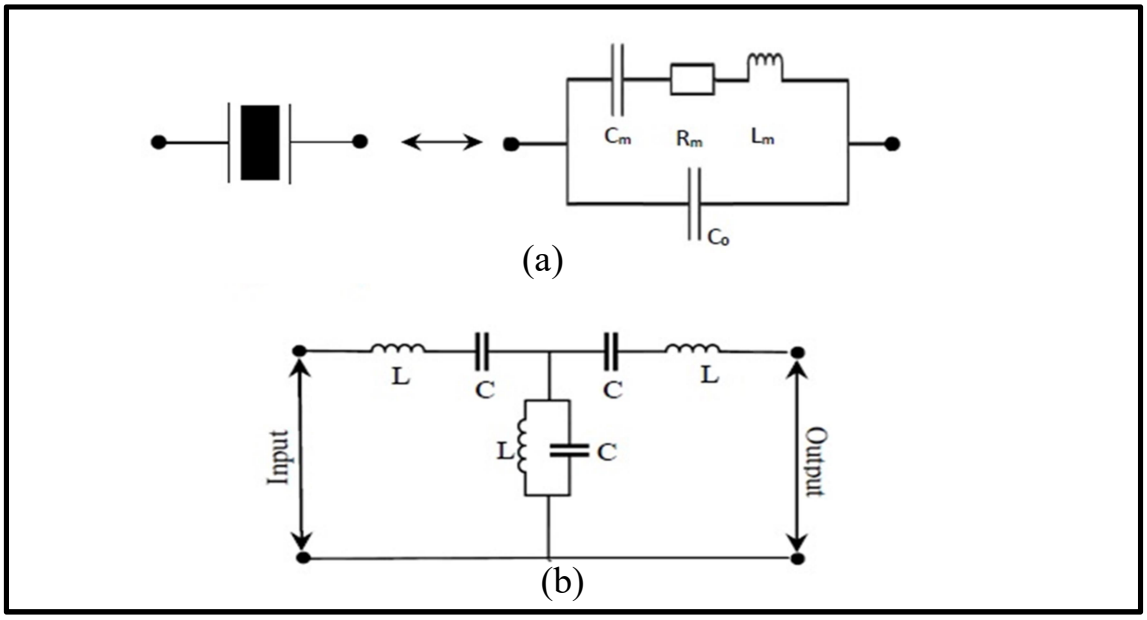

Fig 2.5: FBAR equivalent circuit diagram, (a) Single resonator FBAR, (b) Typical band pass filter (BPF)[35].

The important part of the FBAR design is to apply the design equations that required to obtain the FBAR main bandpass filter, Static Capacitance (C_o), Motional Capacitance (C_m), Motional Inductance (L_m), and Motional Resistance (R_m) are internal impedances parameters which have been provided in the equations that are required to obtain the main principle of it. The main equations are equal to as follows:[36], [37].

$$C_o = \frac{\varepsilon A}{d} \tag{2.1}$$

where: ε = the piezoelectric material permittivity

A = the thin film area (m)

d = the piezoelectric material thickness (m)

$$C_m = C_o\left[\left(\frac{f_p}{f_s}\right)^2 - 1\right] \quad (2.2)$$

where: f_s = the stop band pass filter frequency (Hz).

f_p= the pass band pass filter frequency (Hz).

$$L_m = \frac{1}{(2\pi f_s)^2 C_m} \quad (2.3)$$

$$R_m = \frac{1}{(2\pi \times f_s \times C_m \times Q)} \quad (2.4)$$

where: Q =the quality factor

From the equations(2.1, 2.2, 2.3 &3.4), it can be observed that the values of the FBAR band pass filter impedances such as C_o, C_m, L_m, and R_m will be functions of the FBAR internal physical properties, like the thin film dimensions.

2.3.4 Surface Acoustic Wave (SAW)

An IDT (Inter-Digital Transducer) electrode is attached to a piezoelectric substance in this design. On the surface of a piezoelectric substance, mechanical (sound)wave is converted back interested in electric waves. This filter has excellent selectivity at frequencies below 2 GHz, it is very small in size, and is very cheap. After this frequency, it becomes more sensitive and less discriminating. (influenced by temperature)[38]. The structure of SAW filter is shown in figure 2.6.

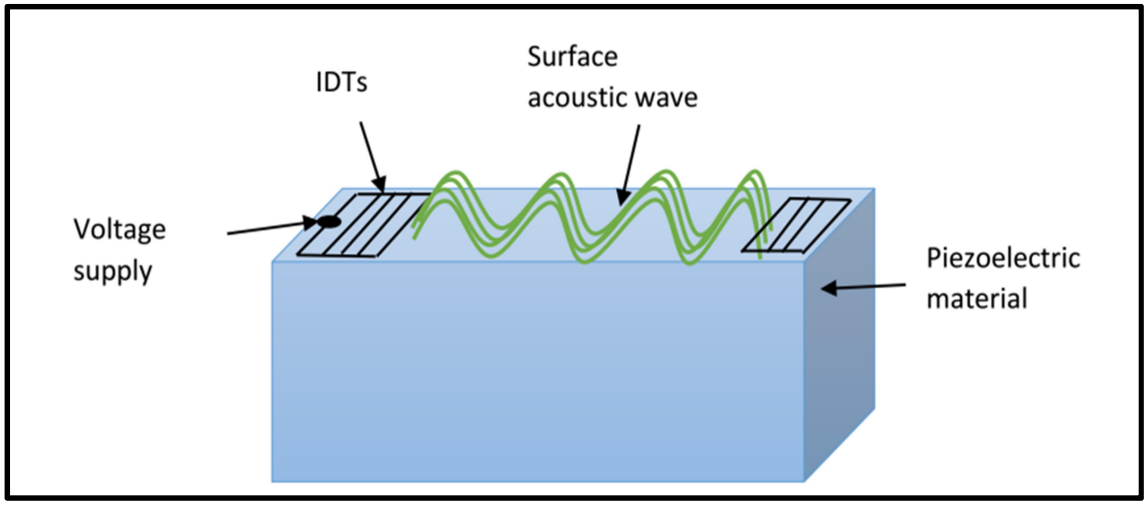

Fig 2.6: Structure of SAW filter[38].

2.3.5 Bulk Acoustic Wave (BAW)

The second variety, and the most popular, is the bipolar array microphone (BAW), which uses a piezoelectric material in its terminals to convert electrical to sonic as soon as an external voltage is functional to cathodes, in addition vice versa. This type is distinguished by its small dimensions, high selectivity, and ability to function at frequencies higher than 2 to 6 GHz. It's a crucial component of many forms of wireless communication apparatus, from smartphones and tablets to radars and satellites, and even missile guidance systems[39] .

The primary difference between them is in how the energy is stored, and all of them have favorable qualities: low size and expense, low loss rates, and low inconvenience. Moreover, they maintain a consistent temperature[40]. BAW can be set up in one of two standard ways. There has been a lot of interest in the first-generation Thin-Film Bulk Acoustic Resonator (TFBAR) due to its unique characteristics. Like its predecessors, this resonator has a cavity in the middle of a silicon substrate and is surrounded by piezoelectric material, top and bottom electrodes. This aids in keeping the waves within the piezoelectric

substance, where they can be better amplified with fewer losses. Besides having reduced input losses, it also has the benefits of being compact, well-suited to handling power, tolerant of a wider range of temperatures, and compatible with integrated circuits. Because of these characteristics, this class of resonator can operate at both middle and high frequencies.

The second type of BAW, known as the Solidly Mounted Resonator (SMR), utilizes a piezoelectric material, an upper and a lower electrode, and the bottom of this electrode is reflective layers and consists of layers with high resistance and low resistance to prevent the leakage of sound waves that are formed in the piezoelectric material, which in turn reduces the losses that are incurred as a result and increases the quality factor. figures 2.7, and 2.8 present the structure of BAW filter[41].

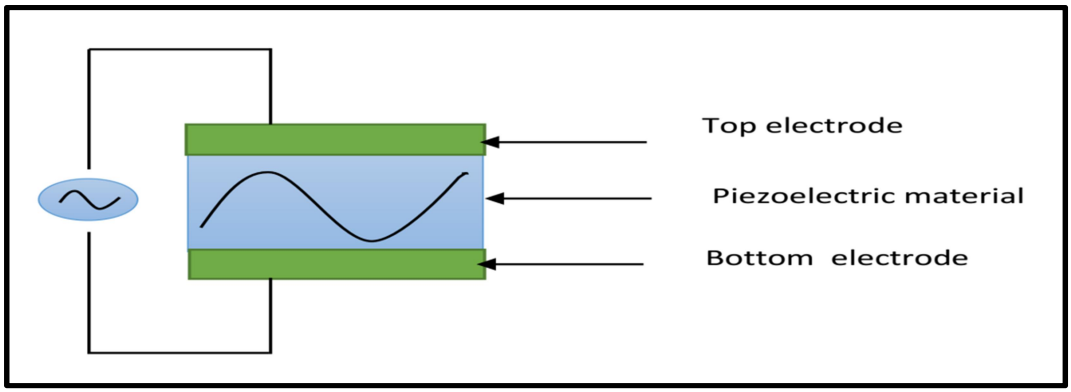

Fig 2.7: Structure of BAW filter[41].

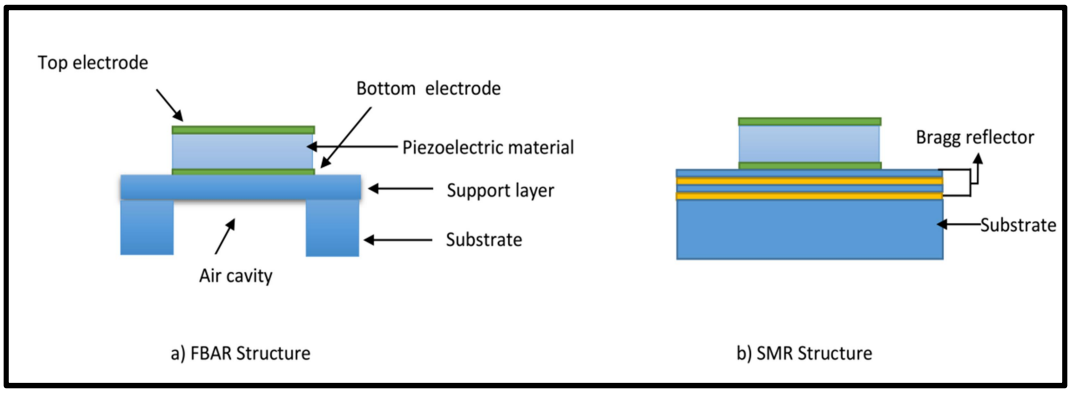

Fig 2.8: The Two Configurations of BAW filters[41].

2.4 Design and Modeling of MEMS Resonator

A critical step in the manufacture of MEMS resonators is modeling. The static and dynamic responses of the resonator can be predicted via modeling. When it comes to choosing materials, geometries, and dimensions, modeling is carried out as part of the design process. Modeling enables the examination of a working device's performance in addition to assist the designer in specifying the fabrication process. This allows us to determine the characteristics of these models by fitting the measured frequency response to them. Recent system-on-a-chip blocks consist of resonators and integrated circuits, and modeling activity is a crucial part of their construction. Different modeling techniques are used to address the design of resonators, each with its unique context and utility. Mechanical and Microelectromechanical resonator designs are the foundation of analytical models for high frequency equivalent-circuit representations of resonator physics are illustrated in figure 2.9 together with pure electrical and electromechanical representations[32].

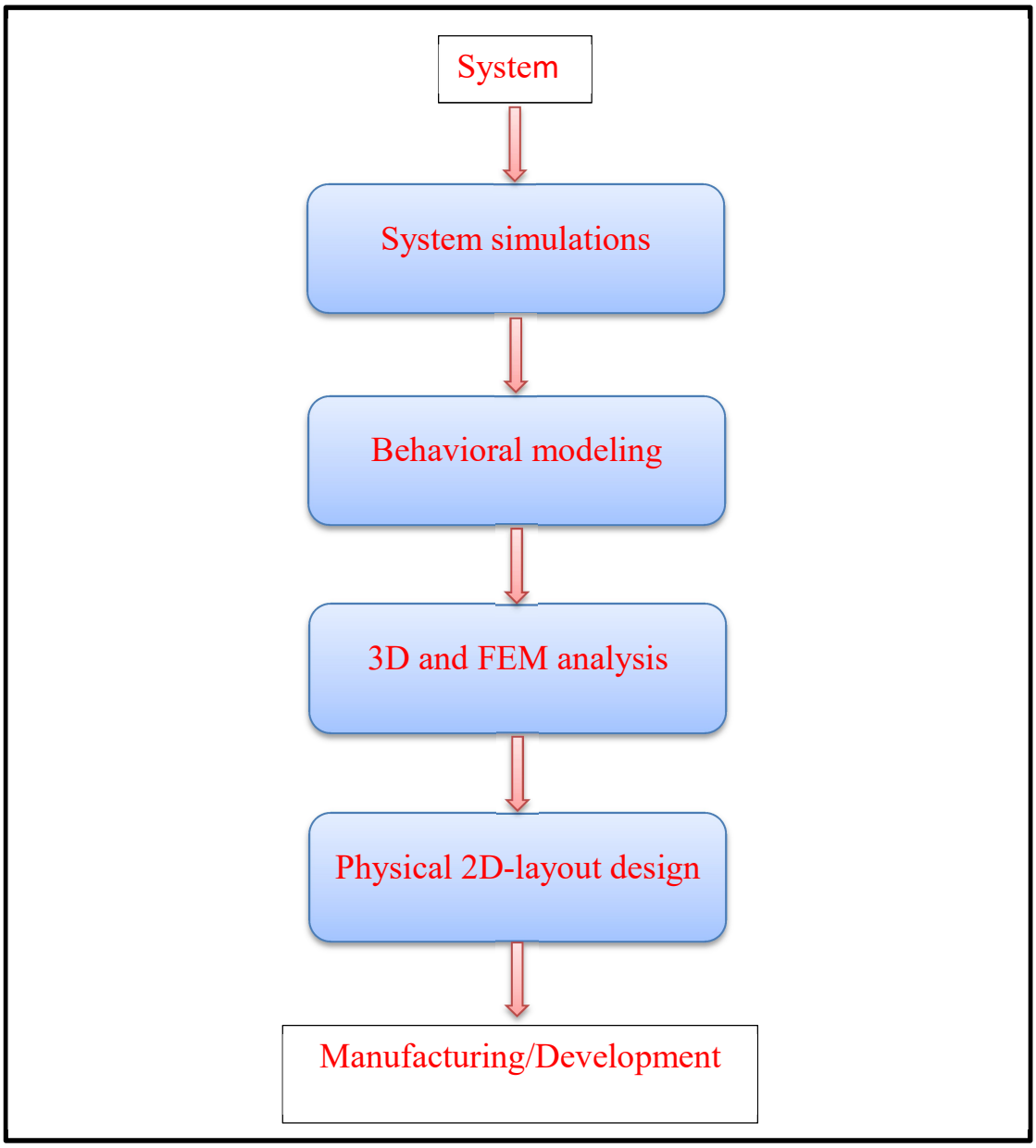

Fig 2.9: MEMS Resonator Modeling Hierarchy [32].

2.5 Applications of MEMS

The microelectromechanical resonator has many applications, most of which are shown in the table 2.2

Table 2.2: Show the applications of MEMS[42].

Electronics	Communications	Medical	Defence
Disk drive heads	Fibre-optic network components	Blood pressure sensor	Munitions guidance
Inkjet printer heads	RF Relays ، switches and filters	Muscle stimulators &drug delivery systems	Surveillance
Earthquake sensors	Voltage controlled oscillators (VCOs)	Prosthetics	Embedded sensors
Avionics pressure sensors	Splitters and Couplers	Miniature analytical instruments	Data storage
Mass data storage systems	Tuneable lasers	Pacemakers	Aircraft control

2.6 Electromechanical Sensors and Actuator

Sensors and actuators are classified into meaning that any transducer acts as either a sensor or an actuator at any given moment. Therefore, transducers can be divided into two categories: actuators, whose impose a condition on a system, and sensors, whose monitor a system[43].

Some transducers can operate as an actuator or as a sensor, but not both at the same time. This type of transducer is stated to be reversed. For example, the speaker, in addition to being an actuator can also be used as a sensor to sense the movements of the diaphragm speaker. Another example of a reversible power transformer is an accelerometer that is designed for vibration sensing, but can be used as vibration [43].

An actuator is a mechanical device that controls or create mechanical motion, which impose a situation on a system. Thus, an electromechanical actuator is a type of transducer that convert an electrical input to mechanical output to create mechanical motion as shown in figure 2.10 [43]. Motors are traditional examples of actuators that force a torque, pumps that force either a fluid velocity or a pressure, and force heads that impose a force.

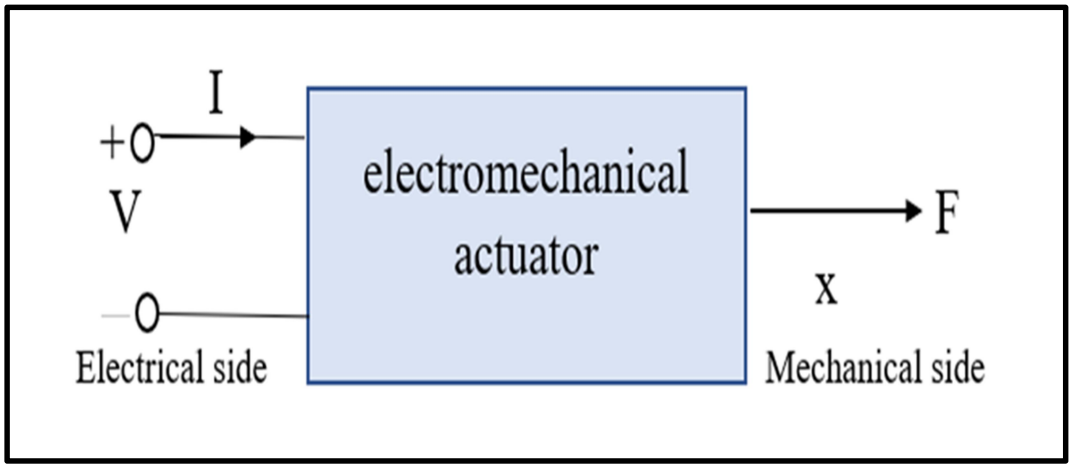

Fig 2.10: A Working Principle of Electromechanical Transducer[43].

The load effect can be minimized by high-power of the actuator, so that it causes a small disturbance with loads only. This desire to reduce the impact of the load imposed by the system on the performance of the operator usually leads to large triggers. From the definitions mean hinted at earlier it is clear that the practical, essential differences between actuators and sensors are the size required and the power level concerned. It is generally considered creating a low power device is easier than creating a high-power device. This puts the sensor relative to actuators in an advantageous position. However, in some systems, it is preferable to use one actuator that needs high energy rather than using many actuators that need low power. An example is to use a drive to run the wristwatch. If the watch has second, minute and hour hands, it can be used either gears with one motor for three engines at a time, or used three-separate motors connected to the appropriate electronics to synchronize the timing. look

at the relative cost of a larger set of gear motors, compared to three smaller engines and dominion electronics, but will always win the single gear. Although the energy level is generally the main issue that distinguishes actuators from sensor devices, the actual size of it can also play an important role.

There is a small difference in the difficulty presented in the fabrication in at conventional levels of electromechanical sensors and actuators. However, the fabrication process can become a big problem for large or very small transducers. Therefore choosing to use microelectronic technologies instead of traditional fabrication methods means moving to a system where manufacturing severe considerations restrict acceptable designs.

The difference in power and size between the typical actuators and sensors provides an entertaining background through which to discuss the trend towards the use of microelectronic fabrication to create actuators and sensors. In general, these actuators and sensors use the same conversion mechanisms as those used in micro scale. The notable exemption to this is the increasing trend of electrical thermal operation. Thermal operation is not generally used on microscale scales. Because energy needs are prohibitive and the system will operate very slowly. At the microscale, this problem are largely rejected by the use of extremely small system [43].

From the previous discussion, it is clear that there are a good reason requiring sensors have small-sized. This indicates that it is perfectly logical to miniaturize sensors, and microelectronics fabrication methods provide a reliable road to accomplish this.

2.6.1 Mechanical Sensors

Direct mechanical sensors come in a wide variety of forms, each of which has its own sensing device (typically piezoresistive, piezoelectric, or capacitive) and method of identifying characteristics. Some of these sensors have already been micro machined, while others have the potential to be. (typically strain, force and displacement)[42].

A) Piezoresistive Sensors

Because of the piezoresistive effect—change in resistivity of a substance through applied strain—gauge dimension changes cause corresponding changes in the resistance of the sensor. Silicon is a great strain sensor because the semiconductor's piezoresistive impact is much bigger than that of ordinary metals. Bulk silicon loaded by p-type or n-type impurities can be easily processed into MEMS piezoresistors[42].

B) Piezoelectric Sensors

A potential difference is created across a piezoelectric crystal when a strain (or tension) is applied to the crystal. In a similar manner, applying a potential differential to the crystal causes a displacement otherwise strain. Despite the fact that displacements are exceedingly small even at high voltages, the effect can serve as both a sensor of mechanical stress (displacement) and an actuator. In MEMS, piezoelectric materials such as quartz, lead zirconate titanate (PZT), polyvinylidene fluoride (PVDF), and zinc oxide (ZnO) are commonly used. A thin layer of a suitable substance must remain applied to devices because silicon is not piezoelectric[42].

C) Capacitive Sensors

Capacitive (or electrostatic) sensing, which combines one or more stationary conducting plates with one or more moving conducting plates, is one of the most important (and frequently used) precision sensing systems. Capacitive

detection can be traced back to the parallel-plate capacitor equation, as shown in equation(2.1). Since capacitance varies inversely with separation between plates, it can be used to detect very slight movements[42].

D) Resonant Sensors

Micro fabricated beams or spans that resonate at their resonant frequency form the basis of (MEMS) resonant sensors. They could be designed to adhere to a specific substance or fused to membranes. (as in the case of a biosensor). Implanted piezoresistors can measure changes in the resonant frequency caused by membrane movement or an accumulation of the binding material[42].

2.7 Self Test

During the life-cycle of any electronic devices, it should be passes in three stages of inspection which is of critical importance.

• Before manufacturing begins, it is imperative that any potential flaws in the design are found and fixed during the testing process.

• Second, testing is done during fabrication to confirm that no errors were made in the fabrication of a given component or device (integrated circuit, printed circuit board, etc.) that will affect the quality of operation and performance of the final system [43].

• Finally, in stage three of system operation, testing seeks to identify and fix any problems that cropped up due to normal use. In some cases, examination is performed to find the broken part so it can be replaced and the system can function normally again.

The built-in self-test methods for micro electro mechanical systems can be classified into several sections, as shown in figure 2.11.

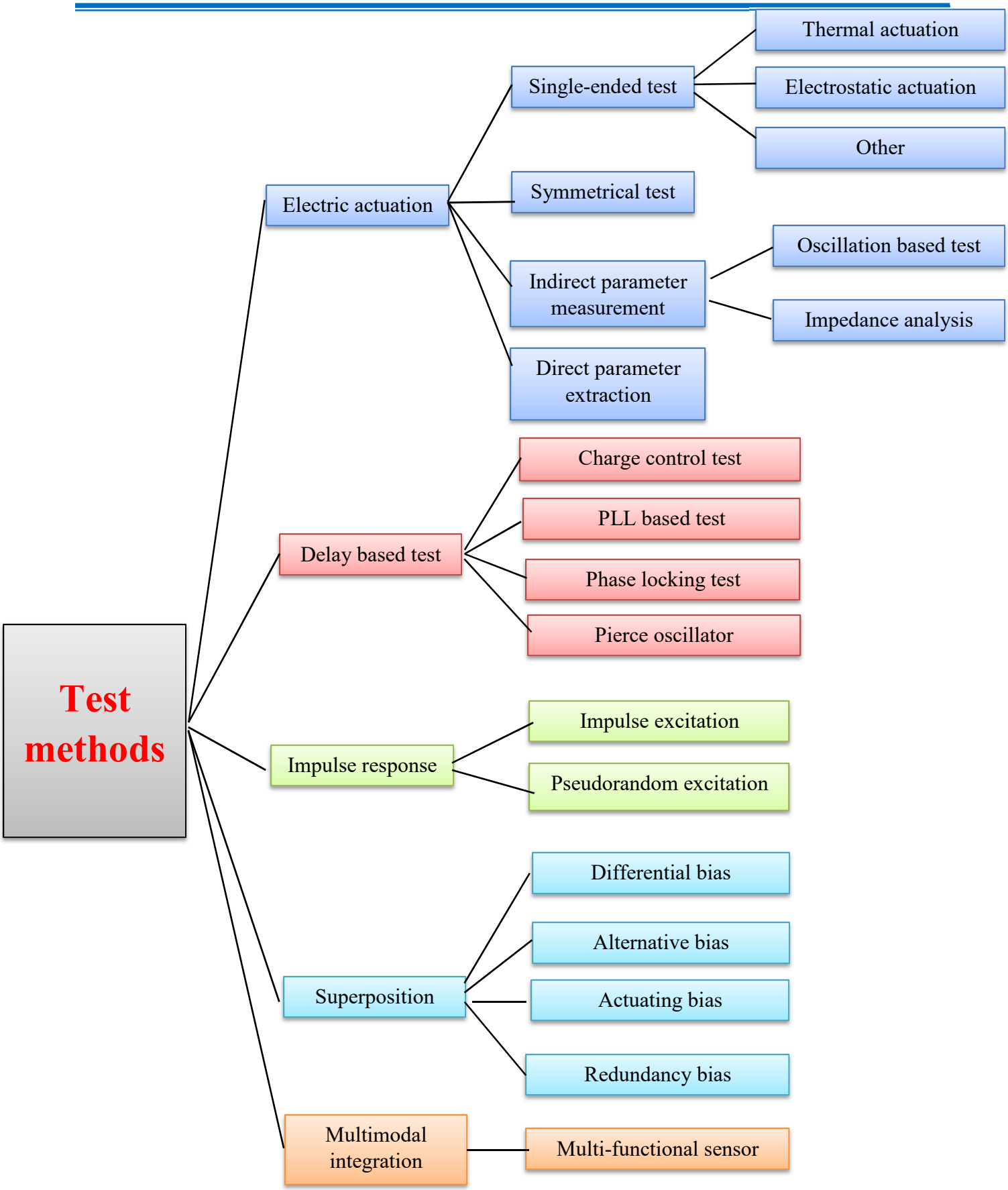

Fig 2.11: Classification of BIST techniques for MEMS devices (MEMS) [42].

The term "Built In Self Test" (BIST) refers to the practice of incorporating extra hardware features into integrated circuit designs in order to facilitate the testing of those circuits. Both voltage and charge control are commonly used methods for testing MEMS devices. The use of voltage control methods has been explored by a number of researchers. In [44],a symmetrical testing strategy is suggested in which the MEMS structure's central mass (movable capacitance plate) is split in half. It is possible to compare the two symmetrical halves by recording their reactions to the same simulation. When the gap between the two answers gets too wide, it's considered a physical flaw that needs to be documented. Unlike other methods, this one doesn't need to be calibrated against test stimulus to pick up on internal flaws. However, its usefulness is constrained by the necessity of flawless structural symmetry. Some global defects that affect both halves of a symmetrical structure at once can't be found using this technique, either. Testing MEMS structures can also be done using a sensitivity test technique[45] .To use this technique, an external test input stimulus is used to drive the Device Under Test (DUT) to the edge of its operational capability, and the resulting reaction is recorded and compared to the signature of a perfectly functioning DUT. Any MEMS device can be put through these tests to look for parametric and catastrophic failures. In order for this technique to effectively identify DUT faults, it is clear that a precise input stimuli generator and response evaluator are needed, limiting its applicability for field tests. A symmetrical partition of the fixed capacitance plate is used to combine the symmetry BIST technique with the sensitivity BIST method [45], [46].

The FBAR bandpass filter design formulae can be used to determine practical values for the bandpass filter frequencies, fs and fp, given a quality factor, Q, and the permittivity, ε, of a piezoelectric material. The material permittivity can be defined as:[14].

$$\varepsilon = \frac{Z_{Acoustic}}{V \times D} \quad (2.5)$$

where: Z Achoustic is the FBAR acoustic impedance (ohm).

V is the FBAR acoustic velocity (m/s).

D is the piezoelectric material density (Kg/m^2).

$$f_p = \frac{V}{h} \quad (2.6)$$

where: V is the FBAR acoustic velocity (m/s).

h is the FBAR thickness (m).

$$f_s = 0.85 f_p \quad (2.7)$$

where: f_p is the pass frequency (Hz).

$$Q = \frac{f_s \times d}{0.05 \times f_p \times A} \quad (2.8)$$

where: f_s is the stop frequency (Hz).

d is the thin film FBAR thickness deviation(m).

f_p is the pass frequency (Hz).

A is the FBAR area (m^2).

The previous equations make it abundantly obvious that the FBAR's physical parameters (the materials) will determine the band-pass filter's design values. When a fixed DC bias of 2.5 V and a roughly linear analysis are used, the above formulae can be used to determine the necessary FBAR design parameters. [33].

The life-cycle of any electronic devices, passes in three stages of inspection are critical importance [22].

First, during the design process, testing will diagnose and identify the design mistakes to guarantee that the manufactured devices will work properly.

Second, testing will verify seeks to diagnose any fabrication mistakes that would prohibit a given part or device (integrated circuit, printed circuit board, etc.) from delivering quality operation and performance in the final system for which it is destined [21, 22].

Third, as the system is put through its paces in the operational phase, any problems that crop up there will be identified and fixed before they can cause the system to collapse.

2.7.1 Ladder Filter

Both single-ended and balanced impulses can be processed by this filter. The most common setup, however, is a solitary end. In the ladder topology depicted in figure (2.12), two resonators are associated in series and shunt at periodic intervals. Minimum electrical impedance (Zmin) occurs at the stop frequency (f_s) of the series resonator, while maximal electrical impedance (Zmax) occurs at the pass frequency (f_p) of the shunt resonator. (Zmax). The resonator acts as a Static capacitance (C_o) at frequencies below the series resonance frequency and above the parallel resonance frequency.

It acts as a pure inductor between its series resonance frequency (f_s) besides bandpass frequency (f_p) .

The ladder filter has a sharp cutoff frequency but weak rejection of frequencies outside its pass band. Further increasing the amount of cascaded filter sections improves out-of-band rejection, but at the expense of increased insertion loss. Poor group delay is produced by the filter because of pass band ripples[32].

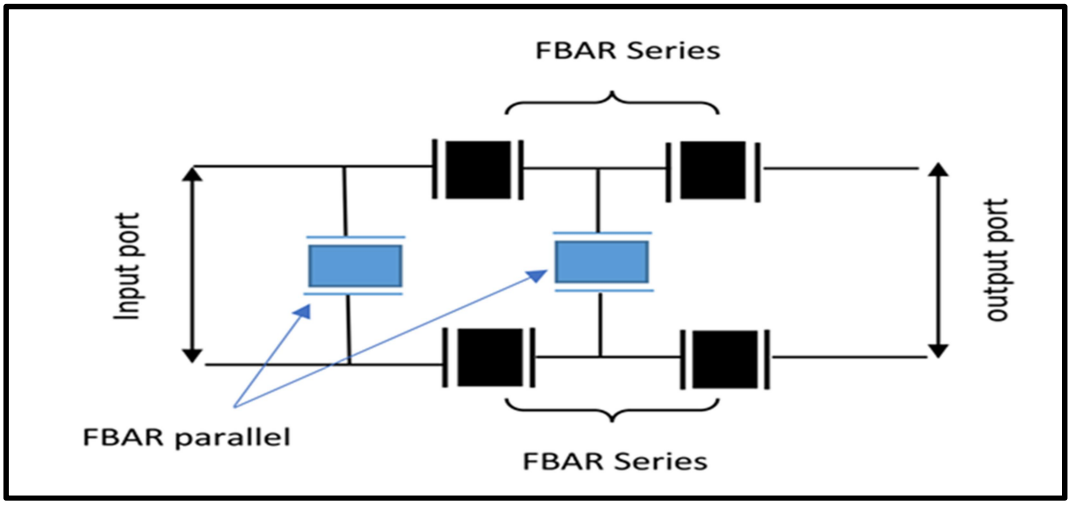

Fig 2.12: Structure of ladder topology[32].

2.7.2 Lattice Filter

When both filter inputs and outputs are in equilibrium, use this filter. Four resonators are arranged in bridge-like shapes in the lattice filter, as shown in figure 2.13. A filter's pass band is formed as soon as the frequency of the series resonator is the same as frequency of shunt resonator. One of the lattice's branches acts as an inductor, while the other acts as a capacitor. In a system with perfectly balanced branches, the transmission zero develops. Lattice filters have superior Out-of-Band (OoB) rejection but worse roll-off. When compared to a ladder filter, it results in a uniform group delay. Pass band group delta is flat because pass band wave is small[32].

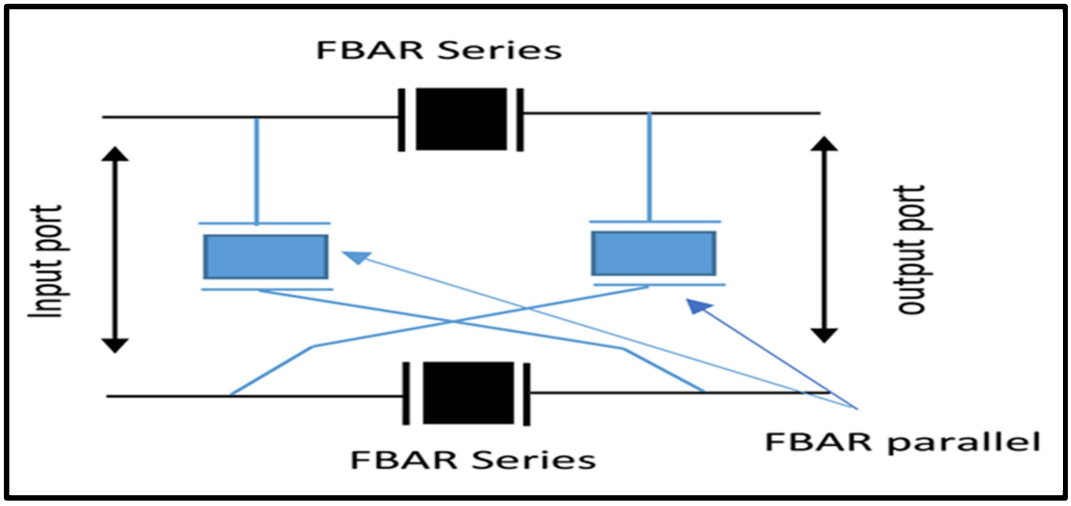

Fig 2.13: Structure of Lattice topology[32].

2.7.3 Mixed Filter

As can be seen in figure 2.14, the Mixed filter combines filters of the Ladder and Lattice types. A cross-section filter makes up one component of the filter, which is linked in series to stepping stool filter. It uses cross-section type filters to demonstrate the characteristics of both stepping stools. It features good out-of-band rejection and roll-off characteristics. The group delay is superior to the ladder filter but inferior to the lattice filter[32].

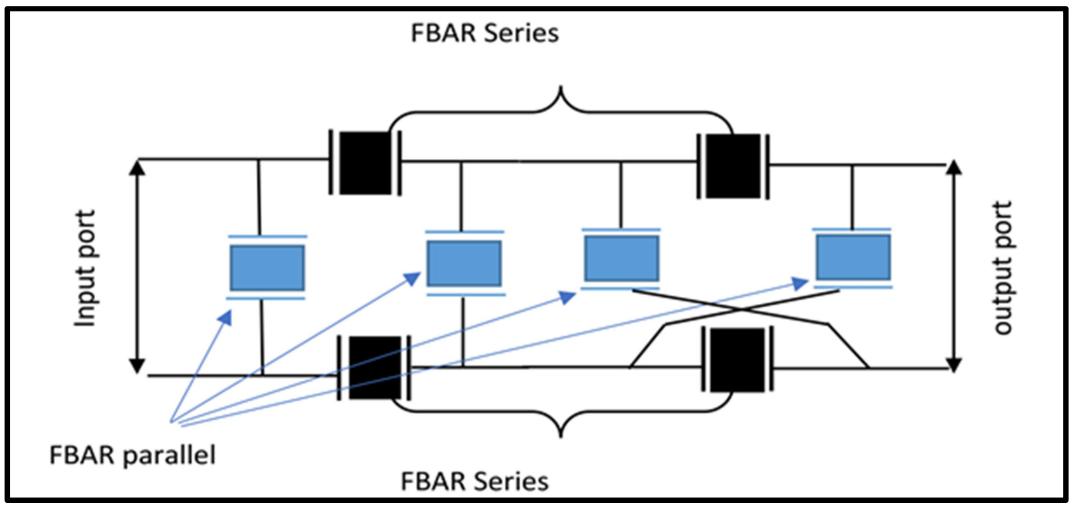

Fig 2.14: Structure of Mixed topology[32].

2.8 Constraints & Limitations

As has been mentioned in this chapter, the design equations have been introduced and can be applied to the design of either FBAR filter kind. Moreover, the design equations and the obtained FBAR design parameters make it evident that the acoustic velocity, V, of piezoelectric materials and thin film thickness, h, will largely determine resonator cutoff series and parallel frequencies[14].

In addition, unless the ratios of change in the intended FBAR frequencies are the same, the quality factor's value will shift. Hence, and in order to increase the FBAR designed frequencies only two options are available, the first option is by increasing the acoustic velocity (V) of the piezoelectric material utilized in the design, and the second option is through reducing the thin film thickness (h) of the FBAR filter. Actually the first option will highly depended upon the physical structure of the piezoelectric material utilized in the FBAR thin film design, as it is obvious, the acoustic velocity varies from one material to

another. Therefore, this design option will be highly restricted on the precise choice and careful synthesizing of the piezoelectric physical material[47], [48].

On the other hand, the second design option will be restricted by minimizing the size of the FBAR thin film structure, which also will face practical challenges because of the industrial difficulties which relating the miniaturization process when reducing the thickness of the FBAR thin film model[49], [50] .

In this study, the first design is concerning with increasing the acoustic velocity through suggesting several active samples of piezoelectric materials combinations. The second design will be adjusted to be at the minimum practically possible value of the thin film thickness (h) in order to obtain the maximum applicable FBAR design frequencies.

2.9 Chapter Summary

In this chapter, the proposed FBAR design models have been presented with detailed structural and operational illustrations. The important implementation theoretical concepts and mathematical equations necessary for clarification the suggested models have been included. Finally, the important design constraints and limitations of operation have been discussed.

Chapter Three

The Proposed Methodology

CHAPTER THREE

THE PROPOSED METHODOLOGY

3.1 Introduction

In this chapter, the proposed model of the study is discussed in details,with a proposal to implement the Micro-Electro-Mechanical System Resonator. The proposed design system model will simulate equations (2.1,2.2,2.3,2.4) using the MatLab2021b Simulink toolbox for modeling the required FBAR band-pass filter design parameters values. In this study, the system proposed for robust and efficient monitoring with controlling design for micro-electromechanical resonator system as illustrated in figure (3.1).

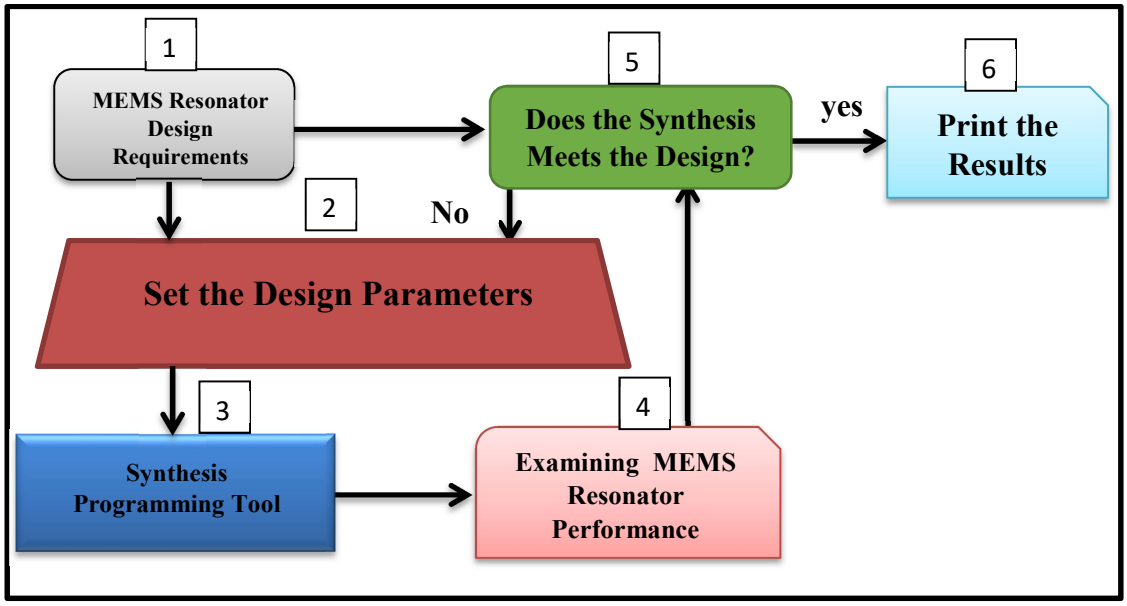

Fig 3.1: Block diagram of the planned robust micro-electromechanical resonator system.

3.2 Description of the Proposed Model

In order to understand the operation of the proposed system model, in figure 3.1, the system is explained in details as follows:

The block diagram of the micro electro mechanical resonator system of the proposed model structure contains six main block diagrams.

- The first block diagram is the resonator design requirements which will be responsible of initiating the essential requirements and demands of the design frequencies on impedances of the MEMS resonator .

- The second block diagram is called the sets of the design parameters which will be responsible of setting and adjusting the design parameters and sustaining the electronic materials.

- The third block diagram which indicated by the blue colour is called the synthesis programming tool. This is responsible of programming the software required for having control of all the proposed models actually. This model is called examining the performance obtained by the synthesis and tested in order to check if the design parameters of the frequencies on the impedances of the resonator have been adjusted.

- The fourth block diagram which is indicated by the pink colour is called the examining MEMS resonator performance for adjusting the operation in successful design domain and range .

- The 5th block diagram in this proposed model is called the checking analysis or examining the synthesis design and it will have two parts. The first is used

to access if the design parameters are well. When the results are acceptable then it will be obtained. If No, a feedback to the second block diagram that is called the set of the design parameters will be accessed in order to redesign the parameters and the overall process will be repeated until the results will be obtained in a precise and accurate values.

- The sixth block diagram is a display that shows the results.

3.3 Design Details of BIST in MEMS

The proposed model in figure (3.1) has been simulated with two different models in MATLAB program.

1- MEMS frequency dependent design model.
2- MEMS parameters dependent design model.

3.3.1 MEMS Frequency Dependent Design Model

The proposed model was designed and simulated by the MATLAB program in the form that performs the self test of the design parameters (C_o, C_m, L_m and R_m) which are internal impedances parameters and (Df_p, Df_S, f_p, f_S, and f %) through a percentage change of the resonator frequencies as shown in figure (3.2).

The idea of the self test proposed model actuator is summarized by referring to the model shown in figure (3.1), such that the MEMS resonator will set the design according to the physical parameters specifications of the piezoelectric materials provided by the synthesized programming block. The resulting MEMS designed parameters will be tested through the examining MEMS block and then the outcomes will be compared with the actual results produced along the original MEMS resonator block. If the comparison results

are not matched, the design set procedure will be repeated. Otherwise, the results will be obtained. In order to implement the proposed model, a MatLab2021b simulation program has been applied with simulink tool box utilities.

Figure (3.2) illustrates the simulation tool box of the micro electromechanical resonator structure, with obtained impedances and frequencies under the effect of percentage frequency change.

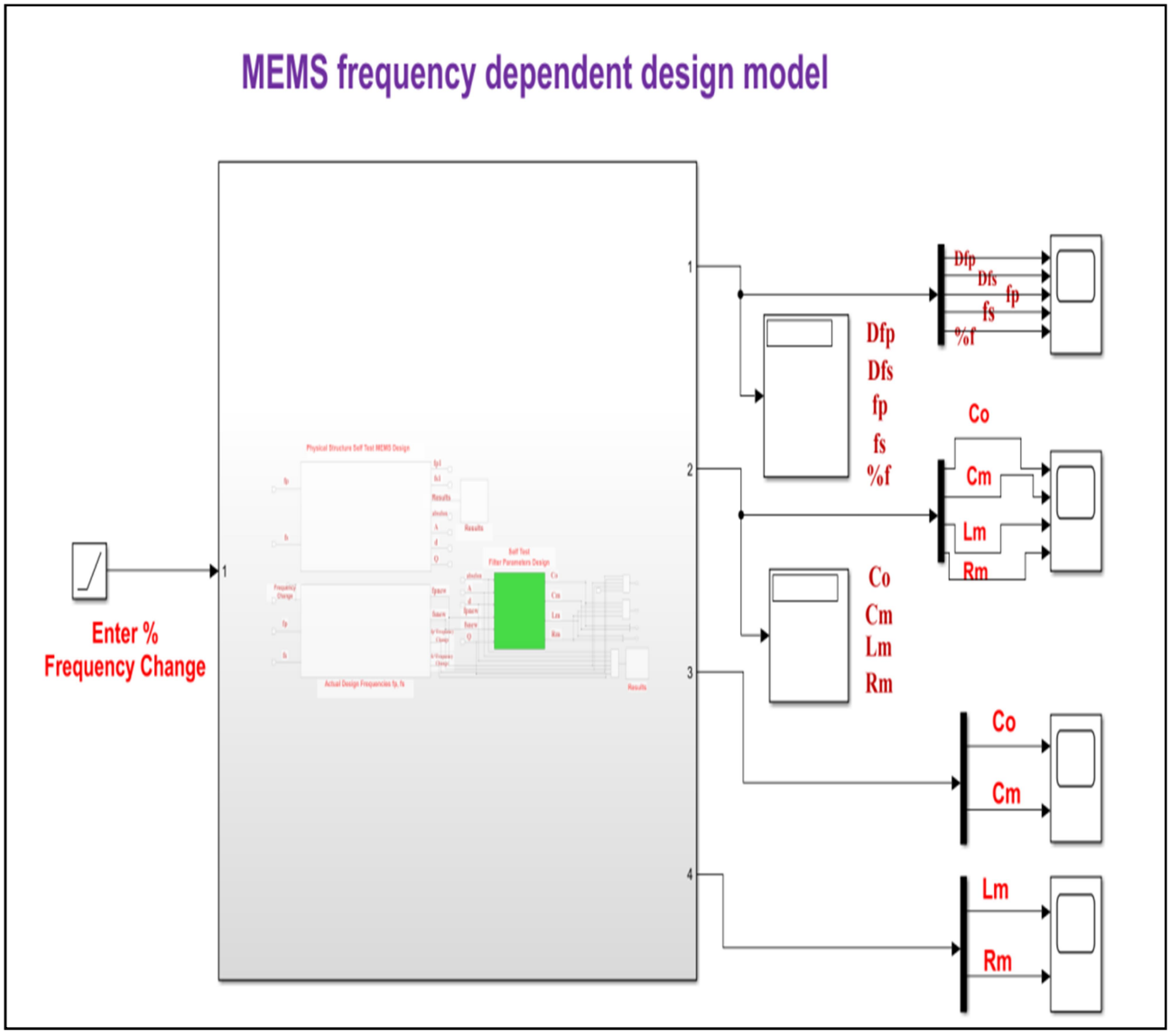

Fig 3.2: Simulation of the micro electromechanical resonator structure.

In this model, the proposed resonator frequency designed values and the corresponding resonator impedances, C_o, C_m, L_m and R_m have been designed under the influence and effect of a specified percentage change in the designed resonance frequency, f_p. This percentage change has been simulated with ramp function r(t) and the resulting designed resonator impedances as well the resonance frequency changes are recorded. This model finds the effect of percentage change in the resonance frequency on the performance of the MEMS resonator.

3.3.1.1 Solid Electro Mechanical Resonator Structure Components

The MEMS frequency self test design model, shown in figure 3.3, consists of three units:

1- Physical structure self test MEMS design.
2- Actual design frequencies f_p and f_S.
3- Self test filter parameters design.

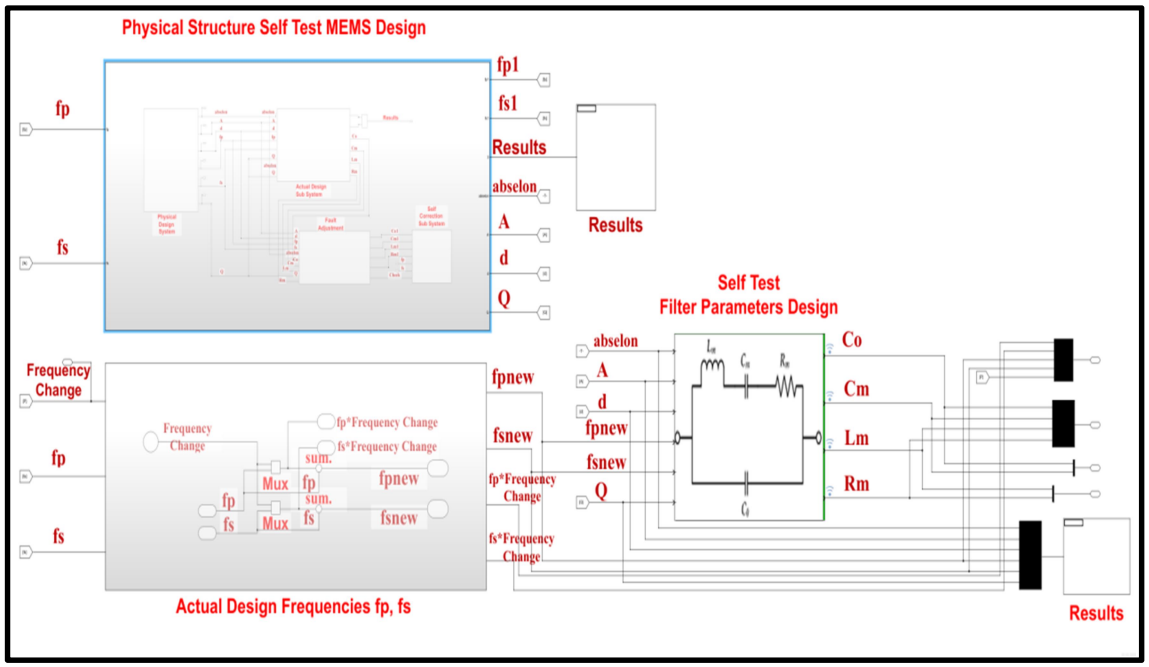

Fig 3.3: Simulink self test MEMS frequency (self test design model).

1 Physical Structure of the Self Test MEMS Design

The Physical structure self testing MEMS design consists of four sub systems as shown in figure (3.4).

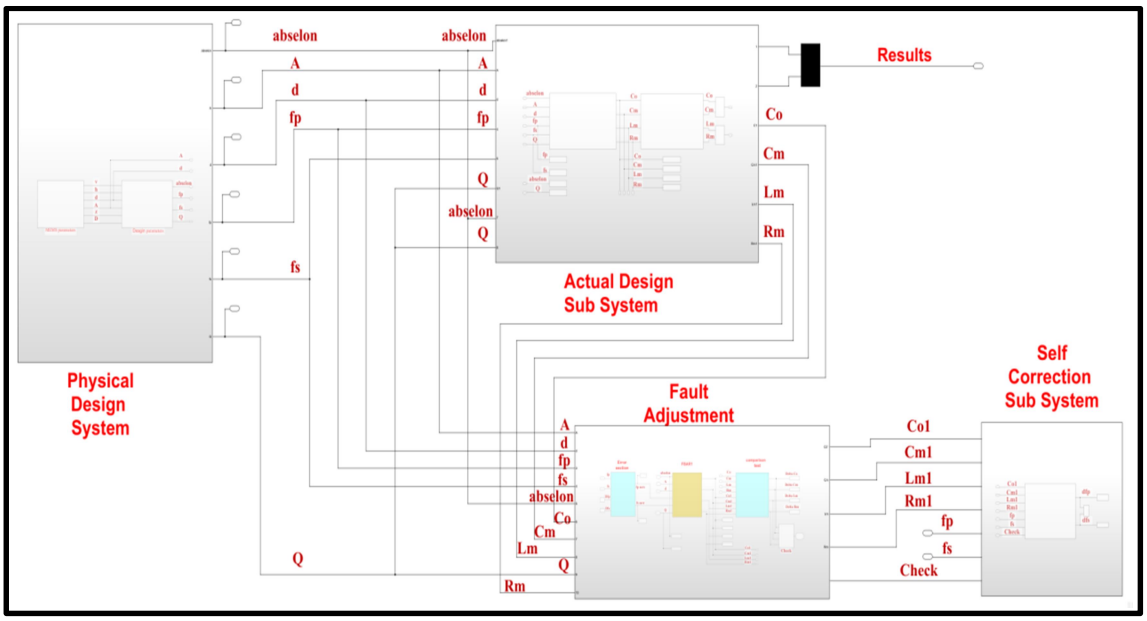

Fig 3.4: Simulink of self-test design model utilized for MEMS parameters design.

These sub systems are:

A) The physical design sub system.

B) Actual design sub system.

C) Fault adjustment.

D) Self correction sub system.

Each sub system listed in the model presented in figure (3.4), described in details in figures (3.5-3.9).

A) The Physical Design Sub System

This part is the basic part, through which the design values of the resonator are entered and then the following components are calculated through it.

1- The frequencies (fp, fs)

2- quality factor (Q)

3- material permittivity (abselon)

This subsystem consists of MEMS parameters and the design sub-system as shown in figure (3.5).

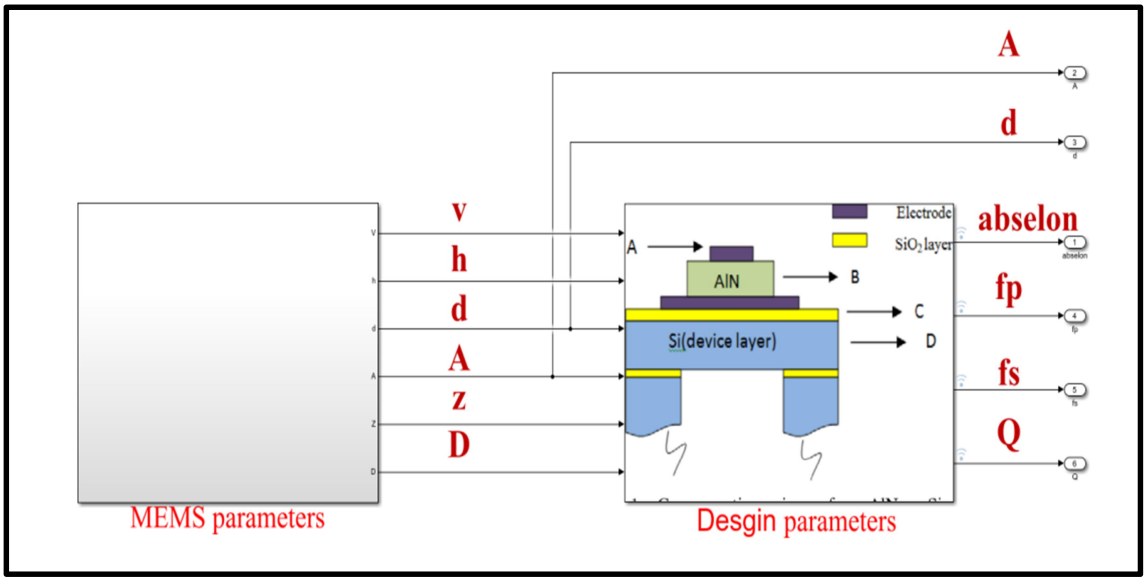

Fig 3.5: The physical design sub system of the self test design model utilized for MEMS parameters design.

Figure (3.5), represents the first subsystem in the self test design model utilized for designing the necessary frequencies in the MEMS parameters design.

The MEMS parameters system is responsible for entering the design values of the piezoelectric materials and is considered an input for the second system, which is responsible for generating the required frequencies, fp, and fs, and the quality factor from the design specifications of the piezoelectric materials and calculating the MEMS design impedances from the design equations (2.5, 2.6, 2.7, 2.8).

B) Actual Design Sub System

Through the values of FBAR area, FBAR thickness deviation, material permittivity, band pass filter frequency, and quality factor (A, d, abselon, f_p, f_S and Q) obtained in the previous sub-system, these values are considered as inputs to this system, Then it is done calculate the design impedance values of the MEMS filter (C_o, C_m, L_m and R_m) through mathematical equations (2.1, 2.2, 2.3, 2.4), as shown in figure (3.6).

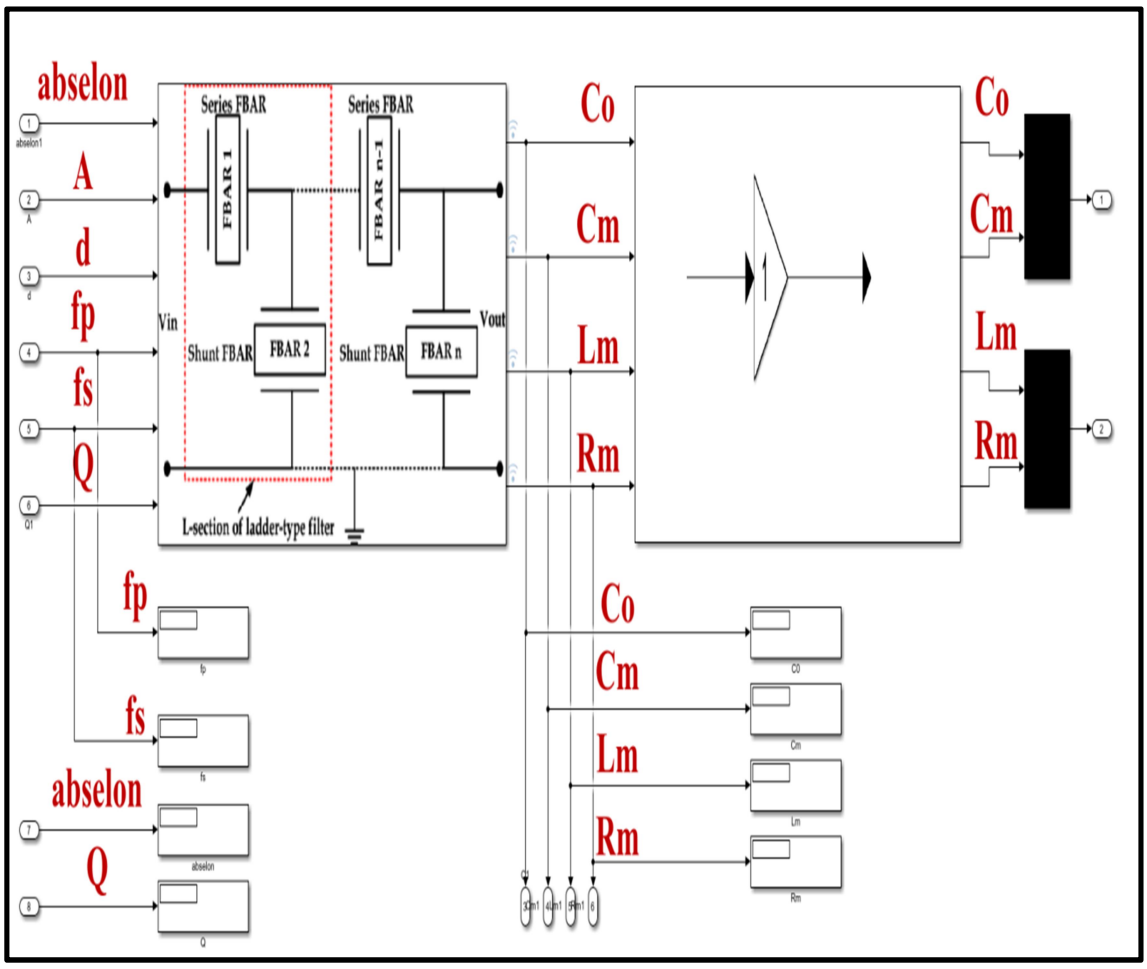

Fig 3.6: The actual design subsystem of the self test design model utilized for MEMS parameters design.

C) Fault Adjustment

Figure (3.7) shows the fault adjustment block diagram.

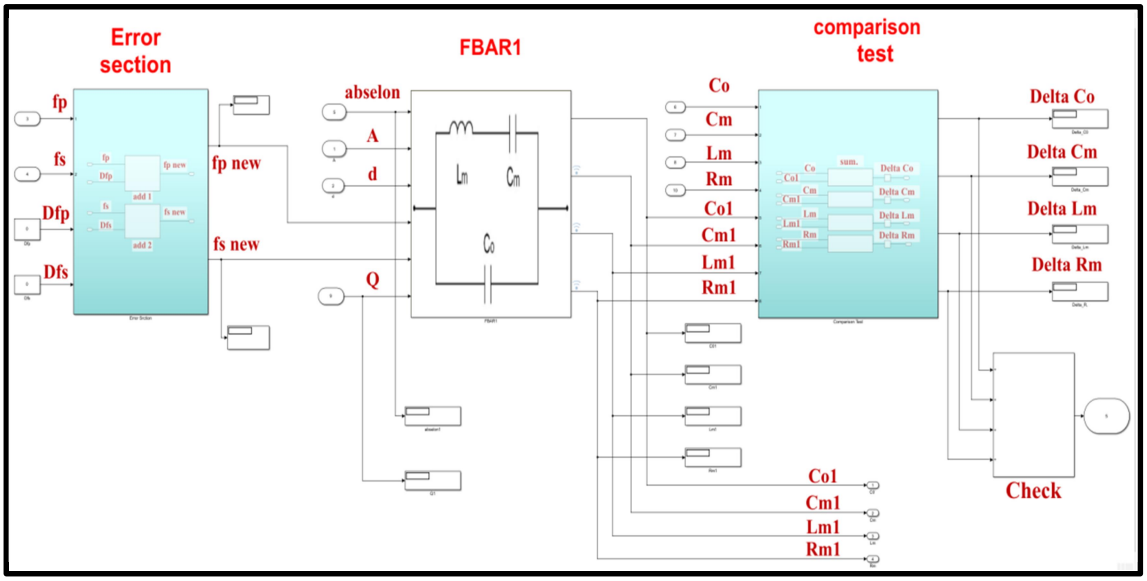

Fig 3.7: The fault adjustment subsystem of the self-test design model utilized for MEMS parameters design.

In this figure, the amount of change in frequency (error frequency) whose value is from (0) to (50%) has been added from the design frequency value to the design frequency whose value (10 GHz) is in the error section. This added frequency is an error frequency (an error occurs in the resonator), and from it, new frequencies are produced.

In the FBAR, is calculated the new impedance values using the equations (2.1, 2.2, 2.3, 2.4), which are different from the previous impedance values, called (C_o1, C_m1, L_m1 and R_m1).

In the comparison test, the difference is the values of the impedances that were taken an absolute value to avoid negative values, and through it the amount of change in the values of the resistances were calculated as shown in figure (3.8).

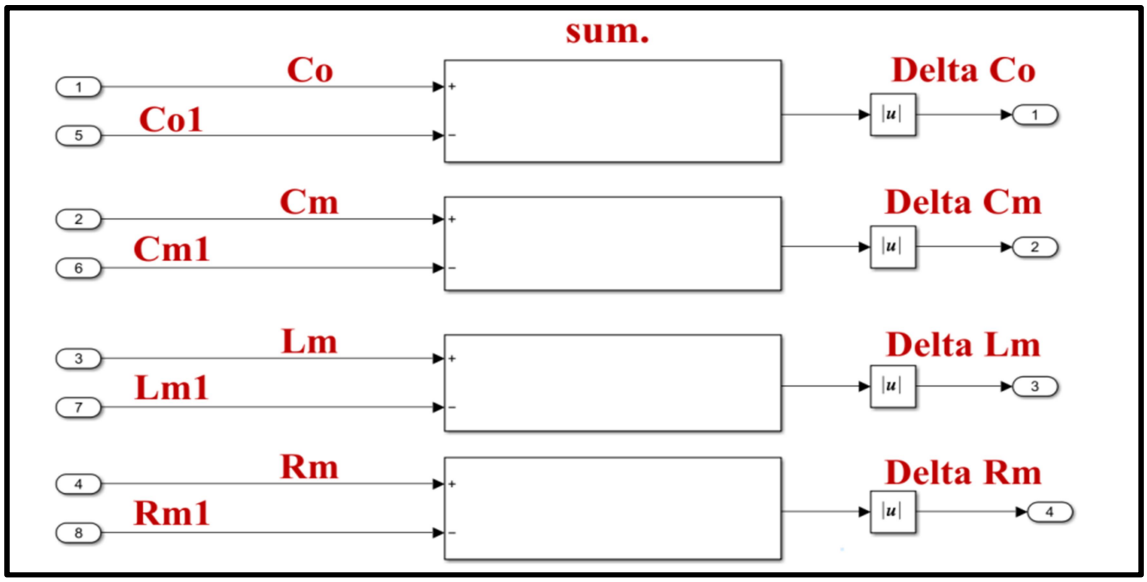

Fig 3.8: The comparison test for MEMS parameters design.

The check circuit, collects the amount of the difference between the impedances (C_o, C_m, L_m and R_m) with (C_o1, C_m1, L_m1 and R_m1) it is called (check).

D) Self Correction Sub System

Figure (3.9) shows self correction subsystem block diagram.

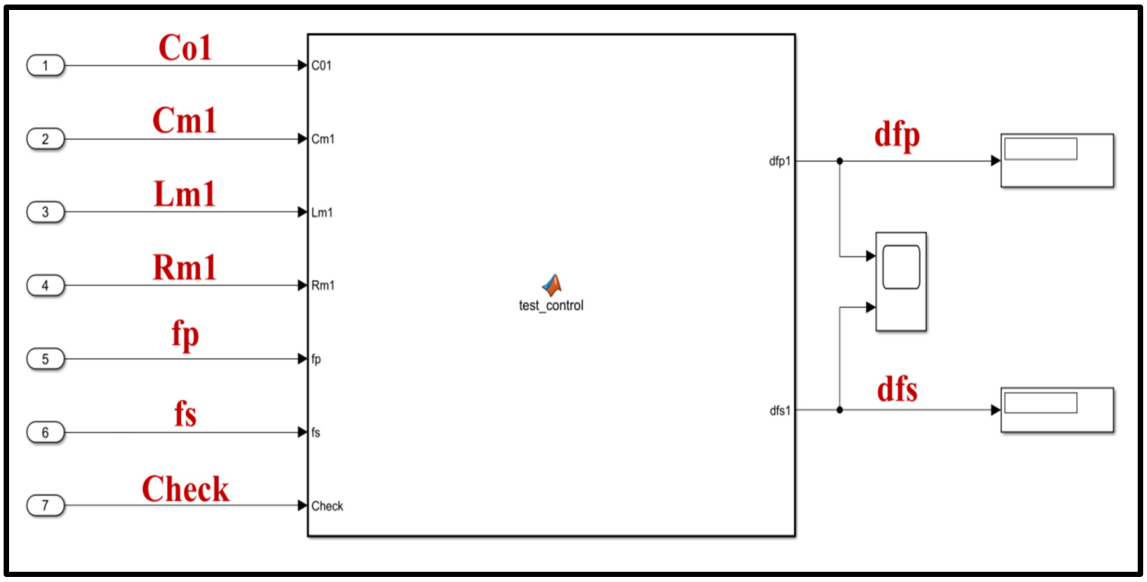

Fig 3.9: The self correction subsystem of the self-test design model utilized for MEMS parameters design.

By the values of the new impedances (C_o1, C_m1, L_m1 and R_m1) and frequencies (f_p and f_S), calculated from the fault adjustment and the check value, this system calculates the value of the current increase in frequencies (the error value) and through substitution in the equations(3.1-3.4), the amount of change in frequencies are get. By applying the equations, the amount of change is solved with two conditions.

1- If the check is equal to zero, the amount of change in delta pass band filter frequency (df_p1) and delta stop band filter frequency (df_S1) is equal to zero.

$$df_S1 = f_S \times 0 \qquad (3.1)$$

Where: f_S is the stop band filter frequency (Hz).

$$df_p1 = f_p \times 0 \qquad (3.2)$$

Where: f_p is the pass band filter frequency (Hz).

2- If the check is not equal to zero, then the change in the frequency of the delta pass band filter frequency (dfp1) and delta stop band filter frequency (dfs1) is not equal to zero as shown in the following equations:[36,37].

$$df_S1 = \left(\left(\frac{1}{2\pi \times \sqrt[2]{L_m1 \times C_m1}}\right) - 1\right) \qquad (3.3)$$

Where: L_m1 is the new internal inductance of the resonator, C_m1 is the new internal capacitance of the resonator [36,37].

$$df_p1 = \left((f_S + df_S1) \times \sqrt[2]{\left(1 + \left(\frac{C_m1}{C_o1}\right)\right)} - f_p \right) \qquad (3.4)$$

2 Actual Design Frequencies f_p, f_S

In this block, new frequencies have formed a percentage of the frequency entered through (Frequency Change) and thus through this percentage and the existing frequencies (f_p) and (f_S) we multiply the percentage with the frequencies in (Mux) An increase in the frequency is obtained which is considered the error frequency. After that collect the error frequency with the previously generated frequencies (f_p) and (f_S) in (sum.) new frequencies are obtained as shown in figure (3.10).

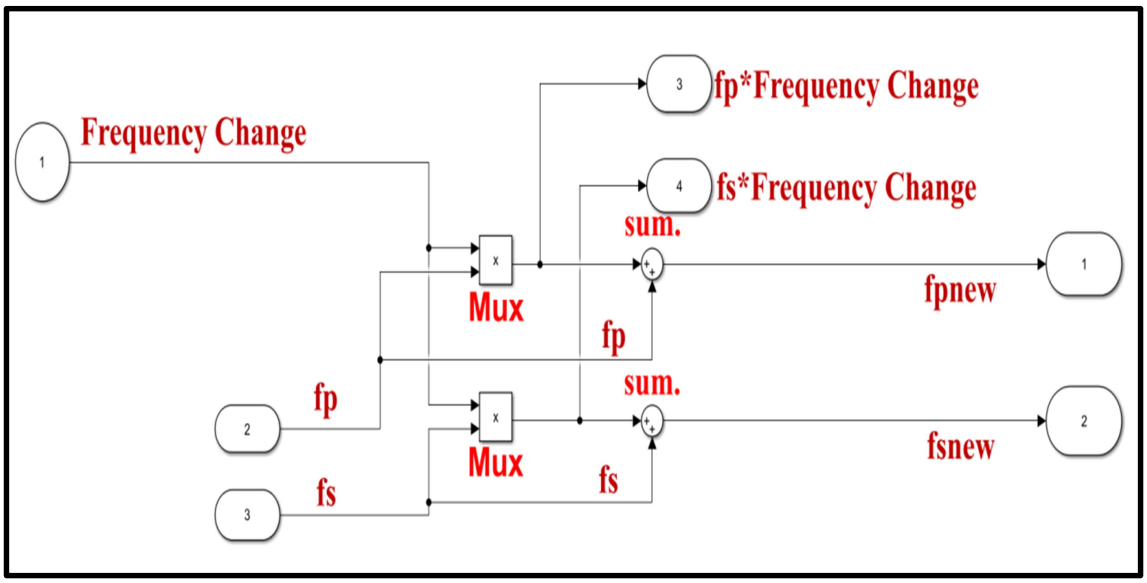

Fig 3.10: The actual design frequencies fp, fs. subsystem of the self test design model.

3 Self Test Filter Parameters Design

The sub system shown in figure (3.11) calculates the values of the new impedances through the equations (2.5,2.6,2.7,2.8,) from the values of the design components and the new frequencies.

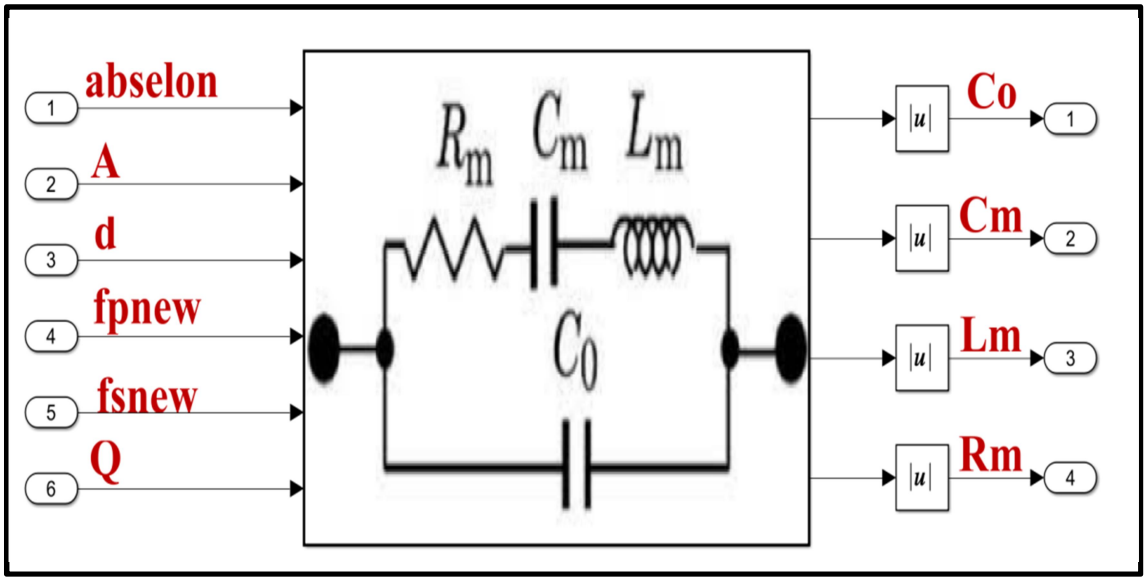

Fig 3.11: The self test filter parameters design subsystem of the selftest design model.

3.3.2 MEMS Parameters Dependent Design Model

The MEMS resonator self-test model design consists of three subsystems:

1- The actual design system

2- Sub system1

3- Self correction system

Through which the values of the resonant impedances are controlled, where the values of the resonator impedances are increase by a percentage level, as shown in the figure (3.12).

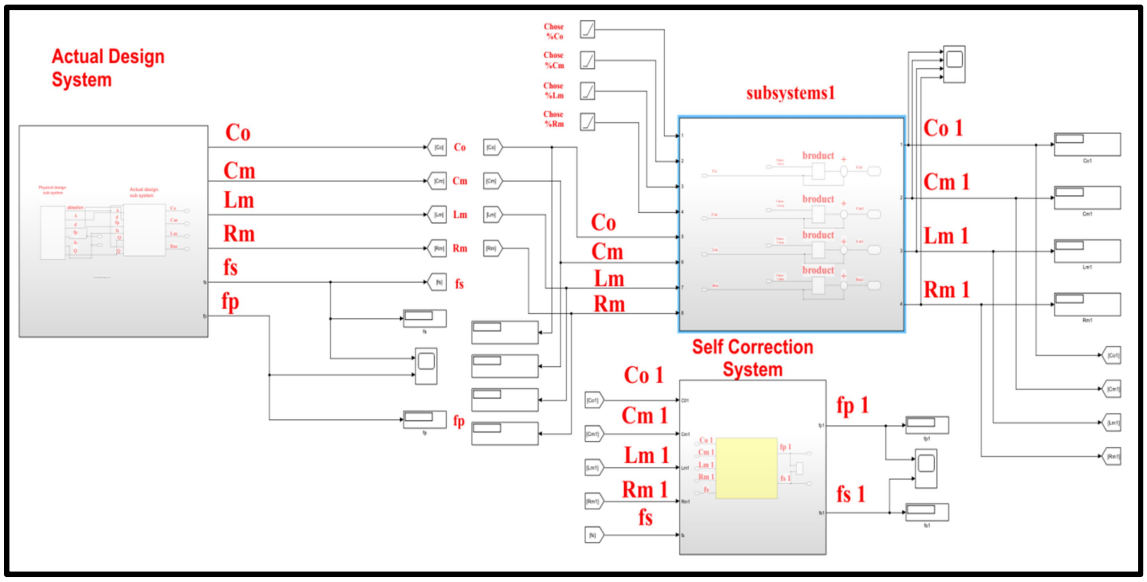

Fig 3.12: MEMS changing filter parameters self test design model.

1- Actual Design System

The MEMS design for actual design system self testing consists of two subsystems as shown in figure (3.13), and these subsystem are:

A) Physical design sub system

B) Actual design sub system

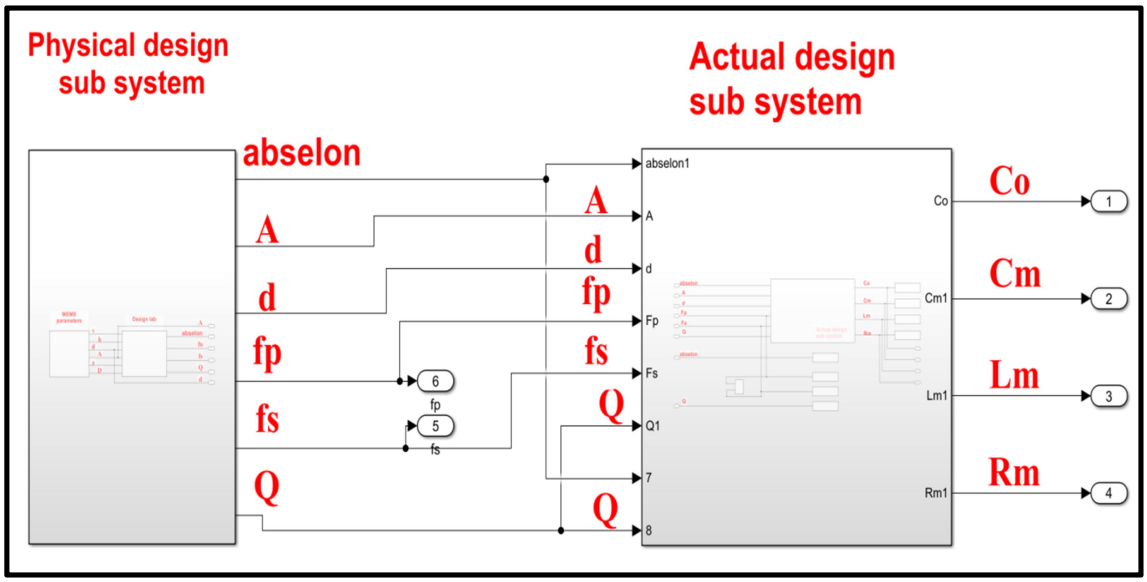

Fig 3.13: Simulink self-test design model utilized for MEMS parameters design.

Each sub system listed in the above model presented in figure (3.13), will be described in details as illustrated in figures (3.14).

A) Physical Design Sub System

This subsystem consists of two subsystems MEMS parameters & FBAR design model as shown in figure (3.14).

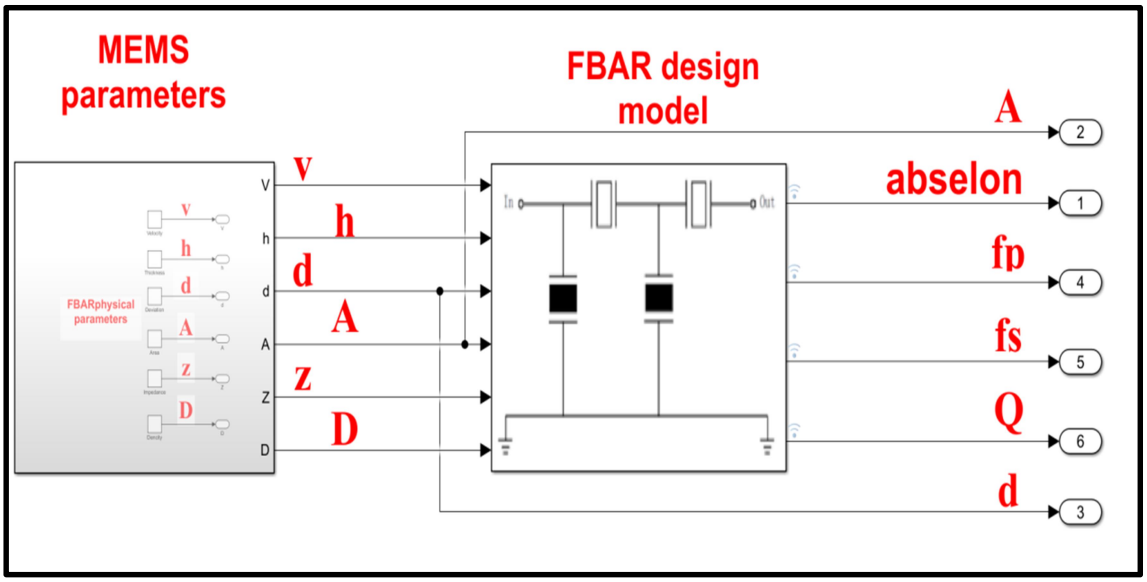

Fig 3.14: The two sub systems MEMS parameters & FBAR design model.

Figure (3.14) represents the first subsystem in the self test design model used to generate the frequencies required in the design of the MEMS parameters.

All subsystem demonstrated in figure (3.14) were performed specific tasks essential to the whole FBAR total BPFD wants. The first subsystem (MEMS Parameters) exposed in Fig. (3.14) will be responsible for initializing the (FBARPP) parameter plan values such as; (AV) (v), (TFT) (h), (TD) (d), A, (AI) (z), and (PPD) (D).

The second subsystem (FBAR Design Model) revealed in figure (3.14) will be responsible for generating (abselon), (f_p), (f_S), and (Q). By applying equations (2.5, 2.6, 2.7, 2.8) ,and as shown in figure (3.14), the output of the

first system (MEMS Parameters) is an input of the second system (FBAR design model).

B) Actual Design Sub System

This subsystem calculates the impedances (C_o, C_m, L_m and R_m) by taking the design values from the system (Physical design subsystem) as shown in figure (3.15) and applying the mentioned impedances in equations (2.1,2.2,2.3,2.4) as shown in figure (3.15).

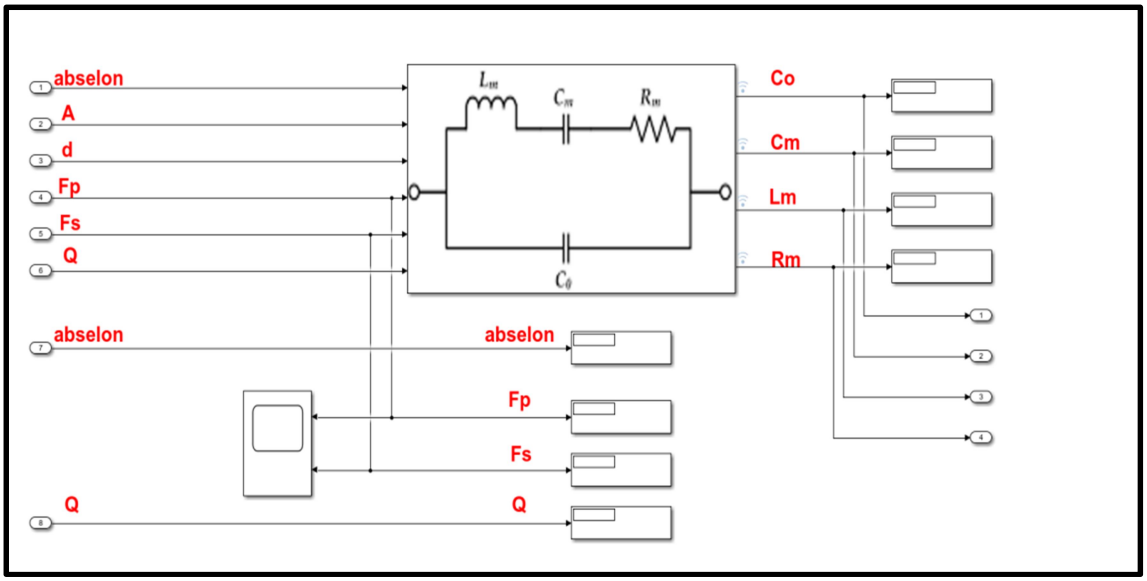

Fig 3.15: The self test filter parameters design subsystem of the self test design model.

2- Sub System1

This subsystem combines the impedances values of (C_o, C_m, L_m and R_m), extracted from equations (2.1, 2.2, 2.3, 2.4) with the percentage change (C_o%, C_m%, L_m% and R_m%), where it takes the impedance values and multiplies them by a percentage in a process called (product). Then determine its value as it is considered an error percentage values, then collects the error percentage with

the impedances values in a process called (+) and then extracts the new impedances values (C_o1, C_m1, L_m1 and R_m1), as shown in figure (3.16).

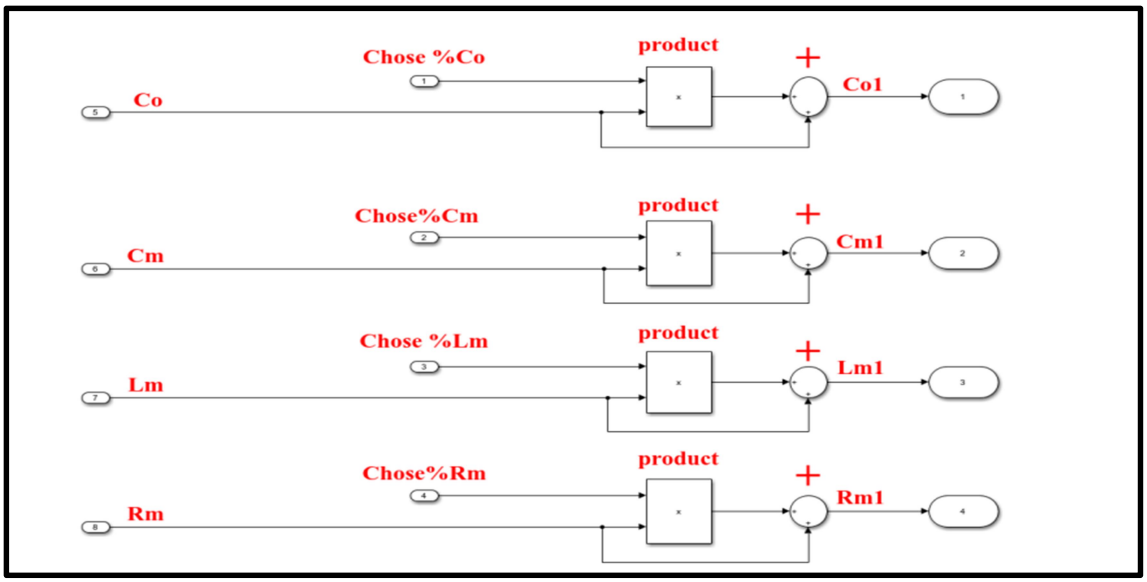

Fig 3.16: The self test filter parameters design sub system of the self test design model.

3- Self Correction System

This subsystem takes the new impedance values from sub system 1 and calculates the new frequencies (f_p1 and f_S1) by applying the following equations(3.5-3.8) as shown in figure (3.17).

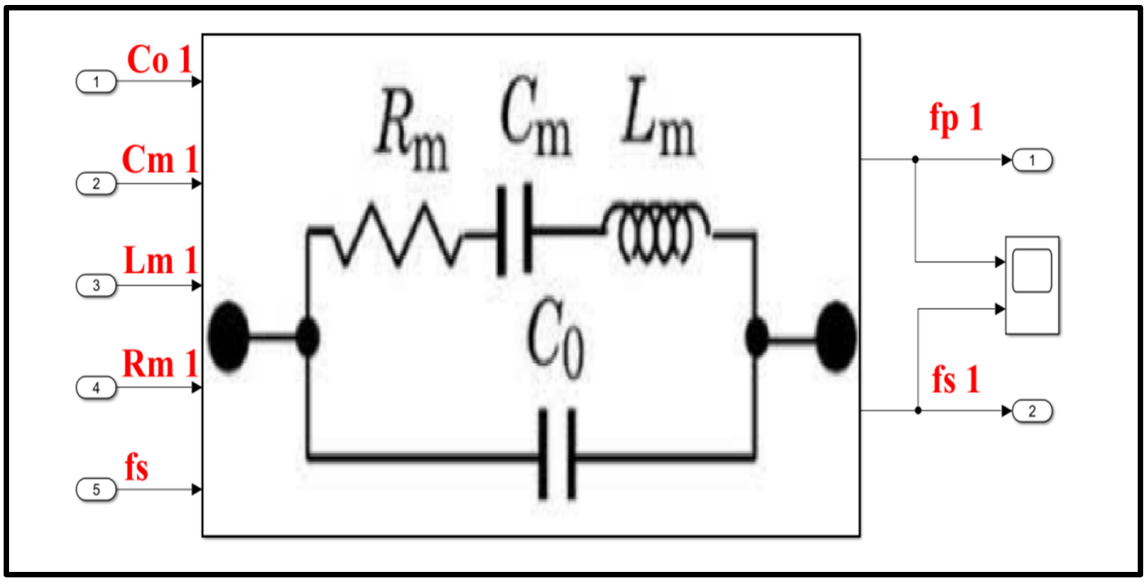

Fig 3.17: The self correction system parameters designer subsystem of the self test design model.

By applying the equations, the amount of change solved with two conditions.

1- If the percentage of the input to the impedances is equal to zero, the amount of change in pass band filter frequency (fp1) and stop band filter frequency (fs1) is equal to zero.

$$f_S 1 = f_S \times 0 \qquad (3.5)$$

Where: f_S is the stop band filter frequency (Hz).

$$f_p 1 = f_p \times 0 \qquad (3.6)$$

Where: f_p is the pass band filter frequency (Hz).

2- If the percentage of the input to the impedances is not equal to zero, the amount of change in pass band filter frequency($f_p 1$)and stop band filter frequency ($f_S 1$) is not equal to zero:[36,37].

$$f_S 1 = \left(\frac{1}{2\pi \times \sqrt[2]{L_m 1 \times C_m 1}}\right) \qquad (3.7)$$

Where: L_m1 is the internal of the new inductance of the resonator, C_m1 is the internal of the new capacitance of the resonator[36,37].

$$f_p1 = \left((f_S + f_S1) \times \sqrt[2]{\left(1 + \left(\frac{C_m1}{C_o1}\right)\right)/2} \right) \qquad (3.8)$$

Where: f_S is the stop band filter frequency (Hz), f_S1 is new stop band filter frequency (Hz), C_m1 and C_o1 are the new internal capacitances of the resonator[36,37].

3.4 Practical Circuit For Measurement Parameter

The circuit for the square wave generator utilizing Operation Amp is displayed in figure 3.18. One capacitor is associated with the reversing terminal of an operation amp with one pin associated with the ground, and a resistor for charging and releasing the capacitor is likewise associated with the transforming terminal to outpot.

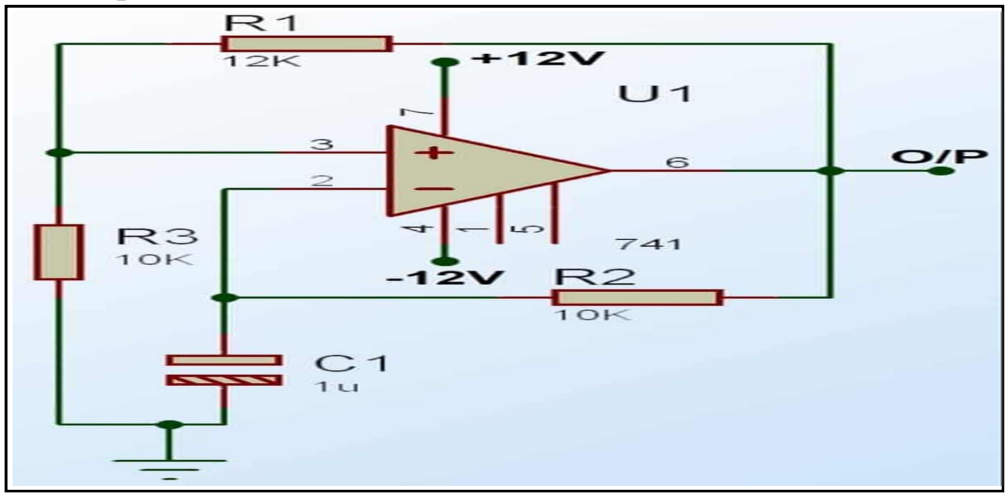

Fig 3.18: Op-Amp square wave generator circuit

Assuming the voltage at reversing terminal is V2 which it is the same amount as the voltage through the capacitor. Similarly, the voltage at the non-reversing end is V1. The difference voltage between non-reversing and reversing terminals is mentioned as differential input voltage and is given by

Vin. Fig.(3.19) show the square wave result from the circuit shown in figure.(3.18).

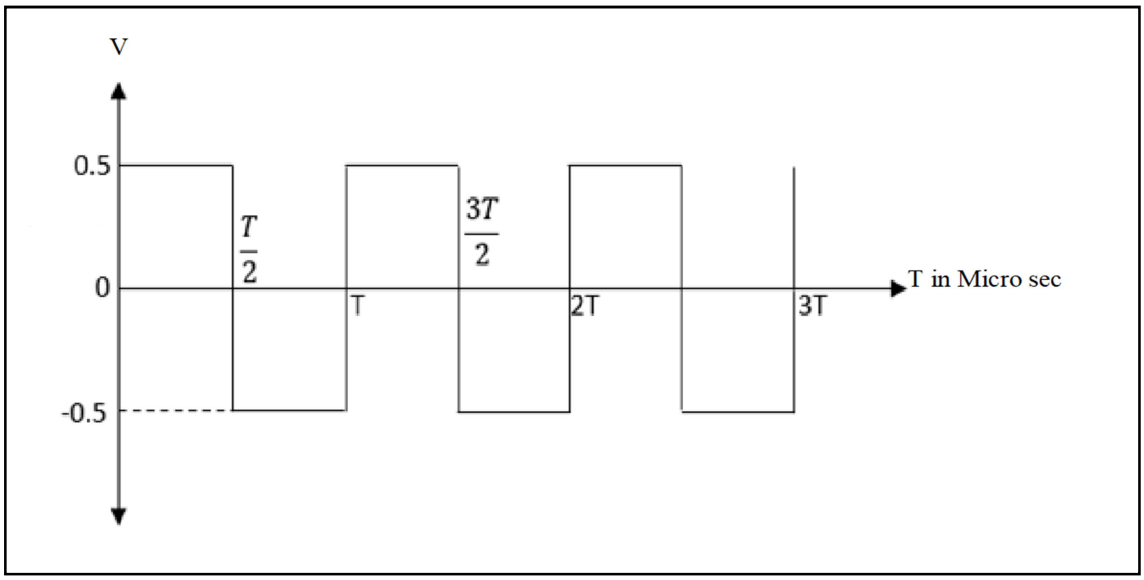

Fig 3.19: the square wave result from the circuit shown in the Figure 3.18

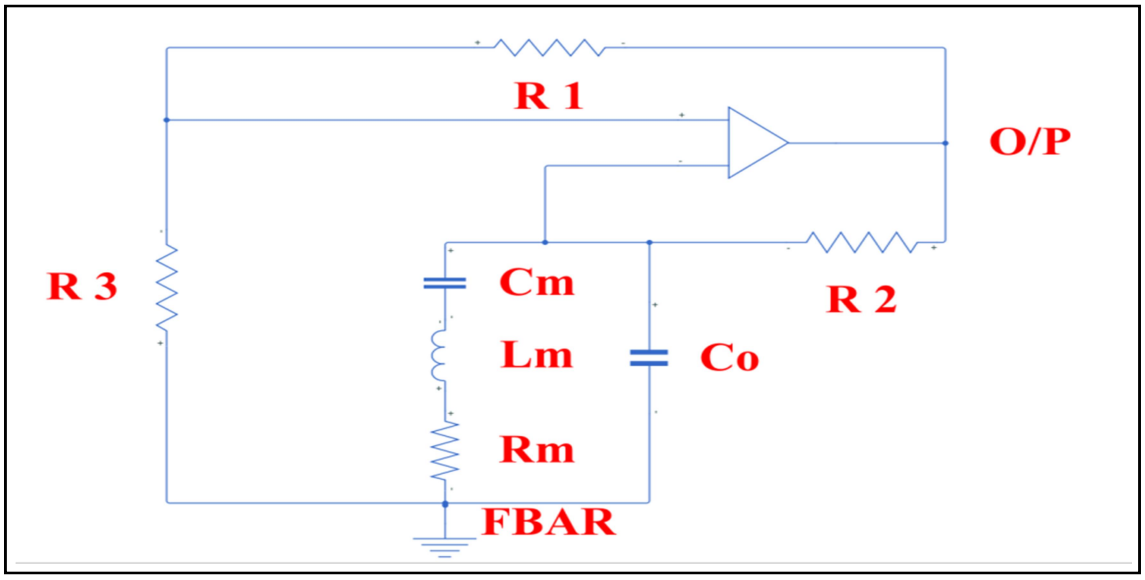

Fig 3.20: The square wave generator with the included equivalent FBAR filter

3.5 Failure Modes

Reliability engineering can be defined as the process of analyzing a product's prospective failure modes and determining how to reduce or attenuate its reaction. The failure modes depeted in table 3.1 provide an explanation for why a product or procedure might not be able to achieve the desired result. A failure mode can occur between a cause and an effect or be the cause or effect itself, depending on the circumstances.

Table 3.1: The possible failure modes in MFMS resonator

Types of failure modes		**Effect**
1- Design phase failure modes	● Functional failure modes	Eading to a deviation from the product specification
	● MEMS material failure modes	Material failure used in MEMS Devices
2- Manufacturing failure modes	**A) Front-end process defects**	
	● Local wafer defects	Affects the performance of the device and consists of pollution (dust and dust)
	● Material transport	
	● Stress effects	Influence the long-term reliability of a MEMS
	● Bonding	Minimize contaminations from particles and ambient gases
	B) Back-end process failures	
	● Wafer dicing	cause catastrophic failure which may not be detected during the

		final testing
	● Wafer handling	
	● Assembly	
3- In-use failures modes	**A) Mechanical failure modes**	
	● Fracture	Effected on the micromachined mechanical components
	● Mechanical shock resistance	Sudden acceleration defines a shock
	● Vibration	
	● Creep	occurs only in ductile materials affecting metal thin films and not silicon
	● Fatigue	fatigue occurs only for applied stresses greater than half the single-cycle fracture strength
	B) Electrical failure modes	
	● Dielectric charging	Effect on the capacitors
	● Electrical breakdown and electrostatic discharge event	
	● Electromigration	
	● Parameters design	Effect on the frequency
4- Environmental failure modes	● Radiation	Effect on the capacitors
	● Electrostatic MEMS sensors and actuators	
	● Radiation-hardening MEMS	
	● Anodic oxidation and galvanic corrosion of silicon	
	● Galvanic corrosion during release of HF	
	• Metal corrosion	

3.6 The Design Values

This part shows the design values of piezoelectric materials and the design frequencies (f_p) and (f_s) implemented with an error rate ranging from (0) to (50%) as well as the impedances (Co), (Cm), (Lm) and (Rm) implemented with the same error rate.

1- Table 3.2, illustrates the design parameters utilized in the design program with the obtained FBAR filter resulting components for a cutoff frequency of $f_p = 5GHz$, $f_s = 4.25GHz$

Table 3.2: Design parameters utilized in the model with the obtained FBAR filter resulting components at $f_p = 5GHz$, $f_s = 4.25GHz$.

FBAR Parameters	V Acoustic Velocity (m/s)	h FBAR thickness (m)	d FBAR thickness deviations (m)	A FBAR area (m^2)	Z_achoustic Acoustic Impedance (Ohm)	D FBAR Density (Kg/m^2)
	7e3	1.4e-6	2e-3	4e-4	10	1e7
f_p (Hz)	5e9					
f_s (Hz)	4.25e9					

2- Table 3.3, demonstrates the design parameters implemented in the design program with the obtained FBAR filter yielding components for a cutoff frequency of $f_p = 10GHz$, $f_s = 8.5GHz$.

Table 3.3: Design parameters utilized in the model with the obtained FBAR filter resulting components at $f_p = 10GHz$, $f_s = 8.5GHz$.

FBAR Parameters	V Acoustic Velocity (m/s)	h FBAR thickness (m)	d FBAR thickness deviations (m)	A FBAR area (m^2)	Z_achoustic Acoustic Impedance (Ohm)	D FBAR Density (Kg/m^2)
	6e3	6e-7	2e-3	4e-4	10	1e7
f_p (Hz)	10e9					
f_s (Hz)	8.5e9					

Chapter Four
Result and Discussion

CHAPTER FOUR
RESULT AND DISCUSSION

4.1 Introduction

The chapter offers the results of the MEMS frequency self test design model when the error is happened in the MEMS frequencies. This point shown with two different design frequencies which are $f_p = 5GHz$, $f_s = 4.25GHz$ and $f_p = 10GHz$, $f_s = 8.5GHz$. Then, the results of the effect of changing the filter parameters of the self test, which are (C_o, C_m, L_m and R_m) is presented.

4.2 Results of MEMS Frequency Dependent Design Model

This section presents the results of the first circuit shown in figure (3.2) in the previous chapter. The test here will be according to variable frequencies and as follows:

4.2.1 When $f_p = 5GHz$ and $f_s = 4.25GHz$

The proposed model presented in figure (3.2) have been successfully designed, simulated, and implemented with the designed specifications illustrated in Table (3.1). Figures (4.1 &4.2) show the simulation of that model without a change in the percentage of frequency (i.e. steady state case).

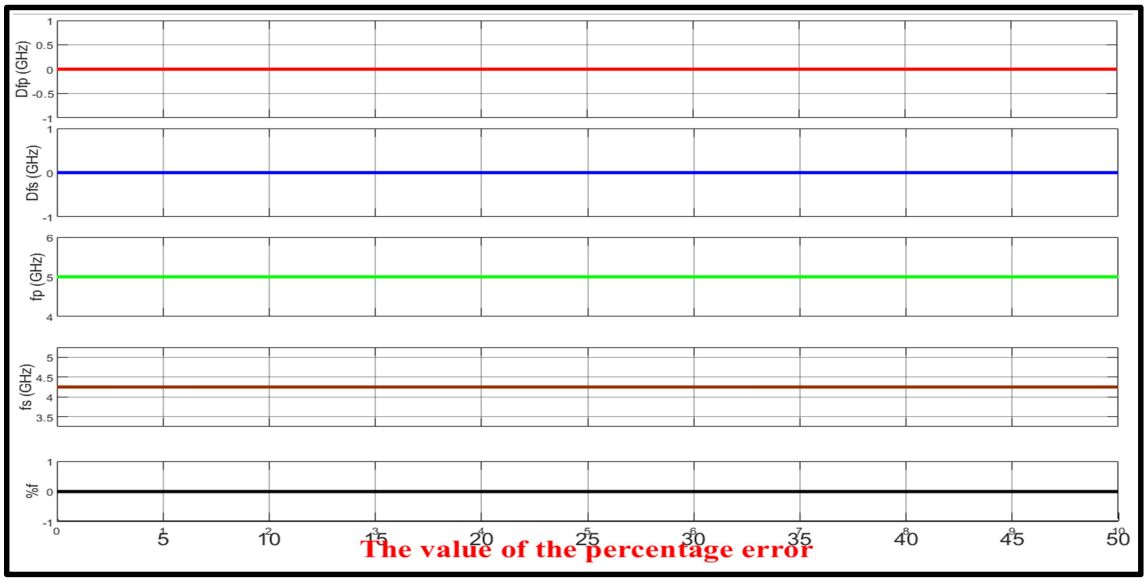

Fig. 4.1: Results of frequencies for the MEMS frequency self test design model in the steady state case with $f_p = 5GHz$, $f_s = 4.25GHz$.

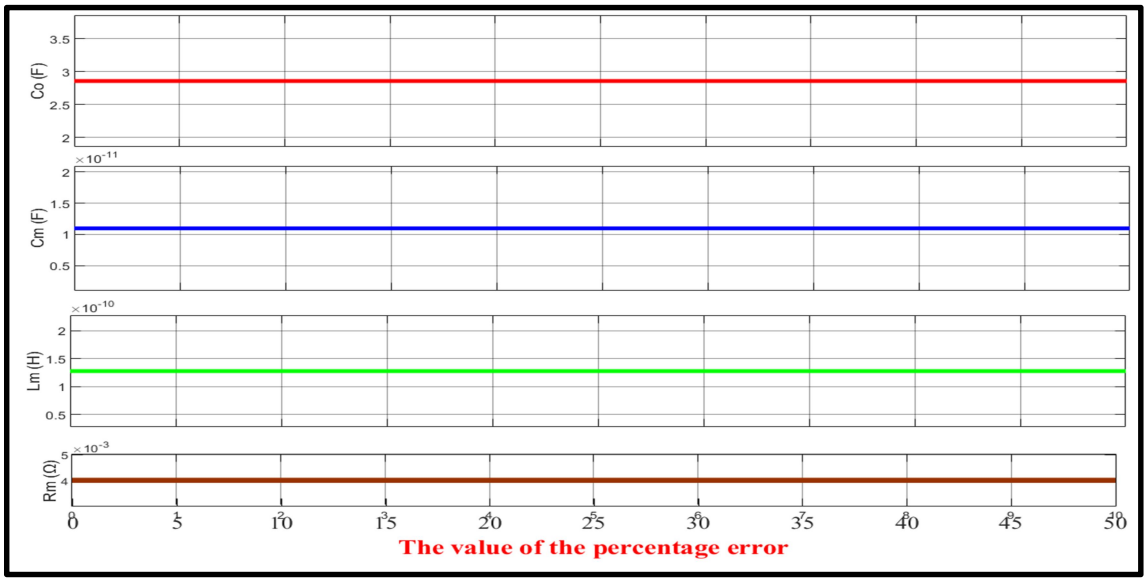

Fig. 4.2: Results of parameters for the MEMS frequency self test design model in the steady state case with $f_p = 5GHz$, $f_s = 4.25GHz$.

The figures (4.1&4.2) show that actuator works in normal case without errors in frequencies and parameters. Table (4.1) shows the values of (Df_p, Df_S, f_p, f_S, f %, C_o, C_m, L_m and R_m).

Table 4.1: Frequencies and parameter values for the MEMS frequency self test design model in the steady state case with $f_p = 5GHz$, $f_s = 4.25GHz$.

variables	Symbol	Values
Delta pass frequency	$\mathbf{Df_p}$	**0**
Delta stop frequency	$\mathbf{Df_S}$	**0**
Pass frequency	$\mathbf{f_p}$	**5 GHz**
Stop frequency	$\mathbf{f_s}$	**4.25 GHz**
Frequency percentage	**f %**	**0**
Parallel plate capacitor	$\mathbf{C_o}$	**28.57 PF**
Series plate capacitor	$\mathbf{C_m}$	**10.97 PF**
Series inductance	$\mathbf{L_m}$	**127.8 PH**
Series resistance	$\mathbf{R_m}$	$\mathbf{4.015 * 10^{-3}\ \Omega}$

The percentage variation in the designed frequency has been adjusted from 0-50%, and simulated successfully, with the resulting self test MEMS actuator frequencies alternations values as shown in figures (4.3 &4.4).

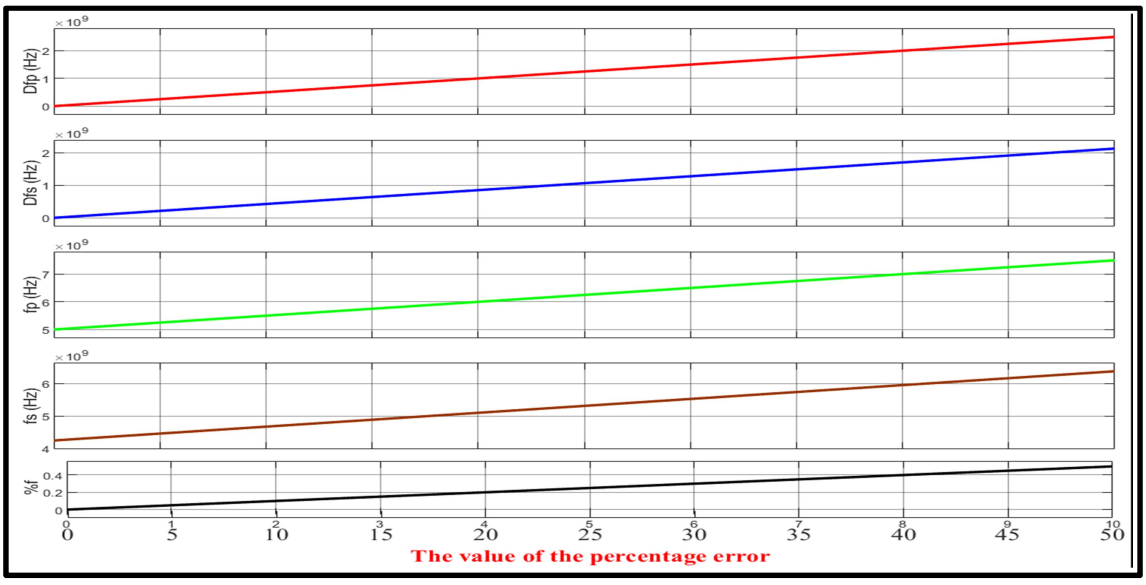

Fig. 4.3: Results of frequencies for the MEMS frequency self test design model with $f_p = 5GHz$, $f_s = 4.25GHz$ when variation the designed frequency from 0-50%.

Figure (4.3) shows that the resulting self test MEMS actuator frequency alternations values in (Df_p and Df_s) will be as percentage ratio from the actually designed frequencies (f_p and f_s), and are linearly increased with the increase in the designed frequency. While figure (4.4) shows that the capacitances of the MEMS actuator will not be affected by these variations. The reason is a follows, the design structure of these capacitances is independent of the operating MEMS frequency. Also, figure (4.4) illustrates the motion inductance and resistance of the MEMS actuator are highly inverse-proportional to the percentage variations in the operating designed frequency. The reason for this is that the structural characteristics of the MEMS L_m and R_m impedances depend on the frequency of MEMS. Table (4.2) shows the values of Df_p, Df_S, f_p, f_S, f%, C_o, C_m, L_m and R_m according to figures (4.3 &4.4).

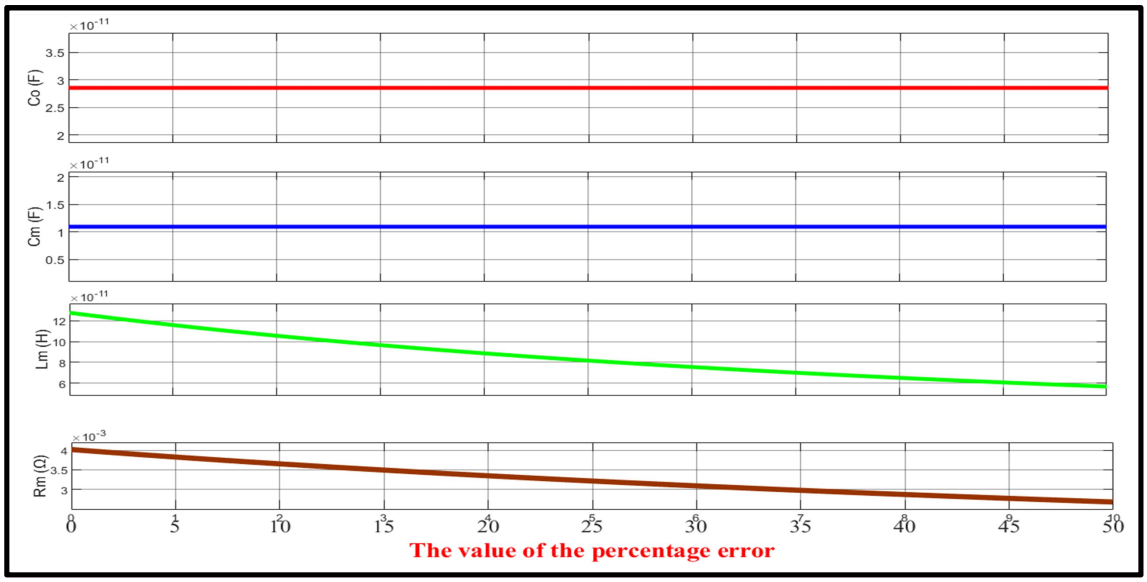

Fig. 4.4: Results of parameters for the MEMS frequency self test design model with $f_p = 5GHz$, $f_s = 4.25GHz$ when variation in the designed frequency from 0-50%.

Table 4.2: The values of frequencies and parameters for the MEMS frequency self test design model with $f_p = 5GHz$, $f_s = 4.25GHz$ when variation the designed frequency from 0-50%**.**

Symbol	Values according variation in the designed frequency from 0-50%.		
	0%	**25%**	**50%**
Df_p	**0**	**1.25 GHz**	**2.5 GHz**
Df_S	**0**	**1.063 GHz**	**2.125 GHz**
f_p	**5 GHz**	**6.25 GHz**	**7.5 GHz**
f_s	**4.25 GHz**	**5.313 GHz**	**6.375 GHz**
%f	**0 %**	**25 %**	**50 %**
C_o	**28.57 PF**	**28.57 PF**	**28.57 PF**
C_m	**10.97 PF**	**10.97 PF**	**10.97 PF**
L_m	**127.8 PH**	**81.75 PH**	**56.8 PH**
R_m	$4.015 * 10^{-3}\ \Omega$	$3.21 * 10^{-3}\ \Omega$	$2.675 * 10^{-3}\ \Omega$

4.2.2 When $f_p = 10\ GHz$ and $f_s = 8.5\ GHz$

The planned model offered in figure (3.2) have been effectively designed, simulated, and employed with the designed specifications illustrated in table (3.2).

The system was firstly simulated without a change in the percentage of frequency (i.e. at steady state) as shown in figures (4.5 &4.6).

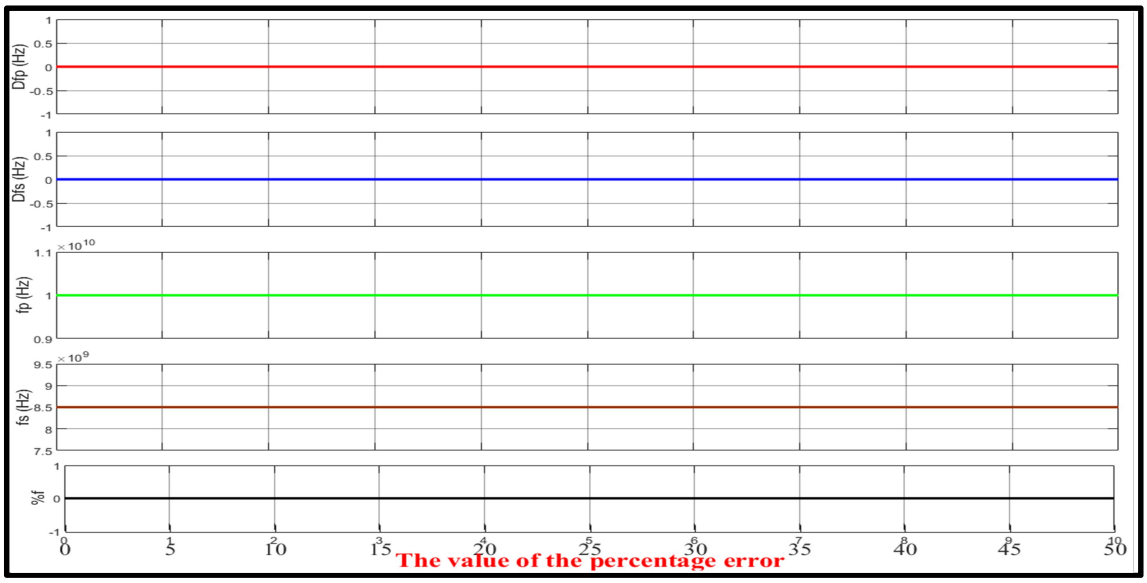

Fig. 4.5: Results of frequencies for the MEMS frequency self test design model in the steady state case with $f_p = 10GHz$, $f_s = 8.5GHz$.

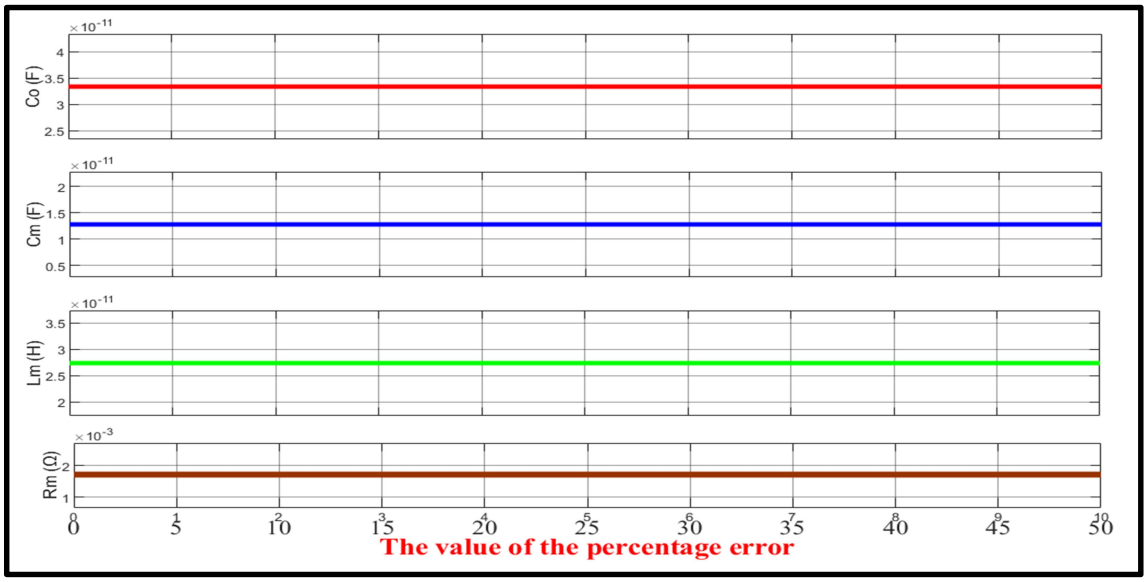

Fig. 4.6: Results of parameters for the MEMS frequency self test design model in the steady state case with $f_p = 10GHz$, $f_s = 8.5GHz$.

Figures (4.5 & 4.6) show that the actuator operates without errors in frequencies and parameters. Table (4.3) shows the values of Df_p, Df_S, f_p, f_S, f %, C_o, C_m, L_m and R_m in normal case (i.e. steady state case) .

Table 4.3: Frequencies and parameters values for the MEMS frequency self test design model in the steady state case with $f_p = 10\text{GHz}$, $f_s = 8.5\text{GHz}$.

Symbol	Values
$\mathbf{Df_p}$	**0**
$\mathbf{Df_S}$	**0**
$\mathbf{f_p}$	**10 GHz**
$\mathbf{f_s}$	**8. 5 GHz**
%f	**0**
$\mathbf{C_o}$	**33 PF**
$\mathbf{C_m}$	**12.8 PF**
$\mathbf{L_m}$	**27.38 PH**
$\mathbf{R_m}$	$\mathbf{1.721 * 10^{-3}\ \Omega}$

By comparing table 4.3 with table 4.1 ,it can be seen that the values of L_m and R_m decrease when the designed frequencies increase. In the same comparison, table 4.3 shows that the values of C_o and C_m increase when the designed frequencies increase.

Additionally, the percentage variation in the designed frequency has been adjusted from 0-50%. Figures (4.7&4.8) show results of frequencies and parameters of the MEMS frequency self test design model in this case.

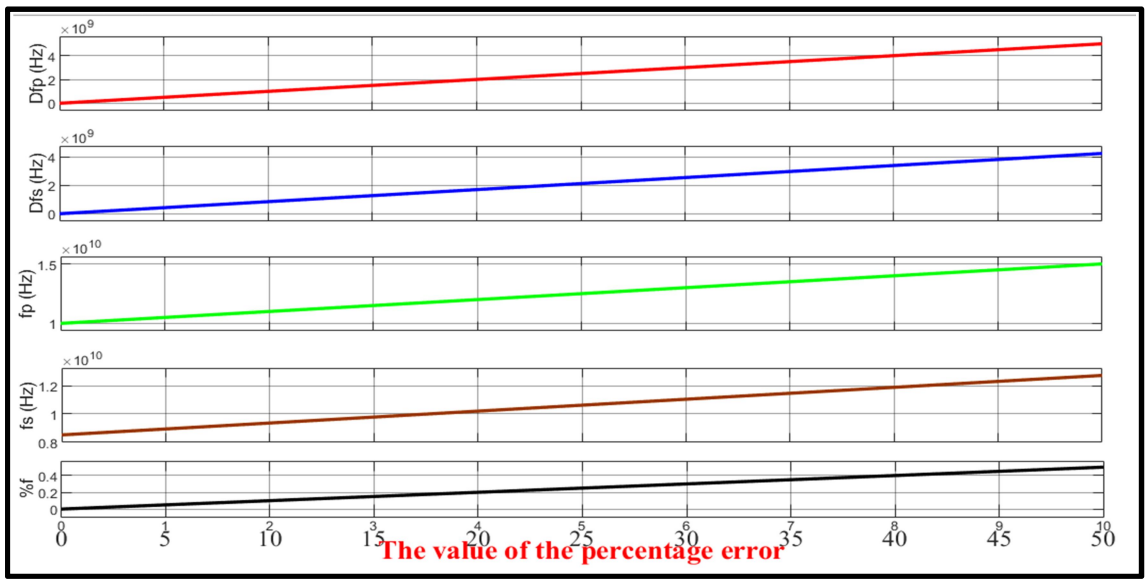

Fig. 4.7: Results of frequencies for the MEMS frequency self test design model with $f_p = 10GHz$, $f_s = 8.5GHz$ when variation the designed frequency from 0-50%.

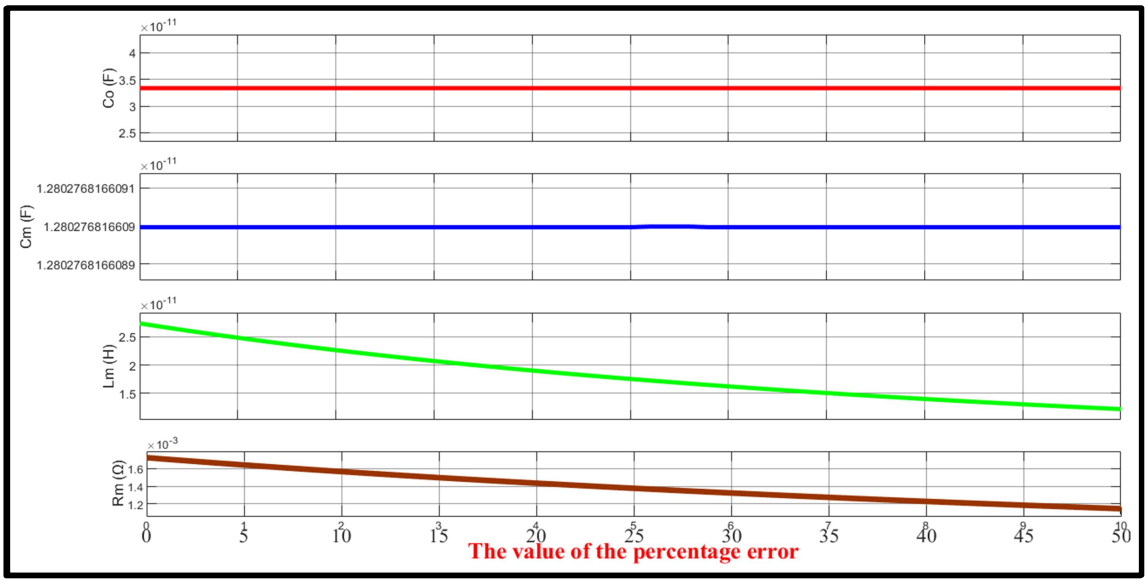

Fig. 4.8: Results of parameters for the MEMS frequency self test design model with $f_p = 10GHz$, $f_s = 8.5GHz$ when variation the designed frequency from 0-50%.

Figure (4.7) also shows that the values of Df_p and Df_S are linearly increased with the increased percentage ratio error of the designed frequency actuator. In addition, it can be seen that the range of Df_p and range of Df_S in the case of MEMS frequency self test design model with $f_p = 10GHz$, $f_s = 8.5GHz$

are larger than their ranges in the case of MEMS frequency self test design model with $f_p = 5GHz$, $f_s = 4.25GHz$. Therefore, it can be said that ranges of Df_p and Df_S in the case of MEMS frequency self-test design model with variation in the designed frequency from 0-50% are linearly increased with the increase of f_p and f_S together.

Farther more, figure (4.8) shows that the values of capacitances of the MEMS actuator will not be affected by this variation in the designed frequency. Additionally, the same figure also show that values of L_m and R_m impedances depend on the frequency of MEMS. In other word, values of L_m and R_m are highly inverse-proportional to the percentage variations in the operating designed frequency. Table (4.4) shows the values of Df_p, Df_S, f_p, f_S, %f, C_o, C_m, L_m and R_m according to figures (4.6 &4.7).

Table 4.4: The values of frequencies and parameters for the MEMS frequency self test design model with $f_p = 10GHz$, $f_s = 8.5GHz$ when the variation in the designed frequency is changed from 0-50%**.**

Symbol	**Values according to the variation in the designed frequency from 0-50%.**		
	0%	**25%**	**50%**
Df_p	**0**	**2.5 GHz**	**5 GHz**
Df_S	**0**	**2.125 GHz**	**4.25 GHz**
f_p	**10 GHz**	**12.5 GHz**	**15 GHz**
f_s	**8.5 GHz**	**10.36 GHz**	**12.75 GHz**
%f	**0**	**25 %**	**50 %**
C_o	**33.33 PF**	**33.33 PF**	**33.33 PF**
C_m	**12.8 PF**	**12.8 PF**	**12.8 PF**
L_m	**27.38 PH**	**17.53 PH**	**12.15 PH**
R_m	**$1.721 * 10^{-3}$ Ω**	**$1.376 * 10^{-3}$ Ω**	**$1.145 * 10^{-3}$ Ω**

4.3 Results of MEMS Parameters Dependent Design Model

This section illustrates the results of the circuit shown in figure (3.12). The test here will be based on variable frequencies and will be explained as follows:

4.3.1 when $f_p = 5GHz$ and $f_s = 4.25GHz$

Firstly, the system was simulated without a change in the percentage of internal MEMS designed impedances, (C_o, C_m, L_m, & R_m) as shown in figures (4.9 &4.10).

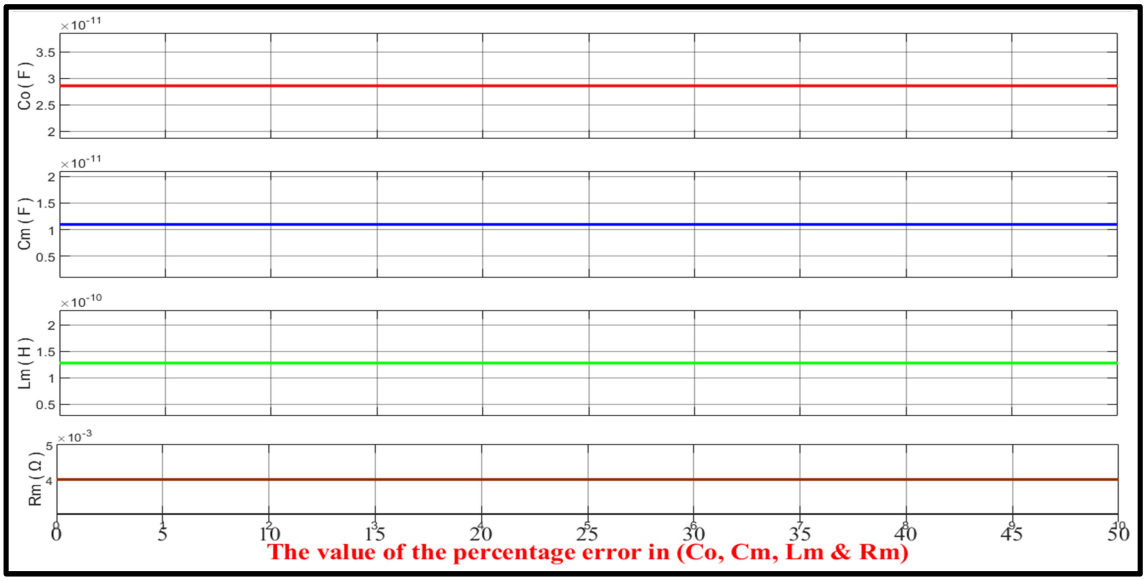

Fig. 4.9: Parameters of the self test MEMS actuator without any change in the percentage of internal MEMS designed impedances with $f_p = 5GHz$, $f_s = 4.25GHz$.

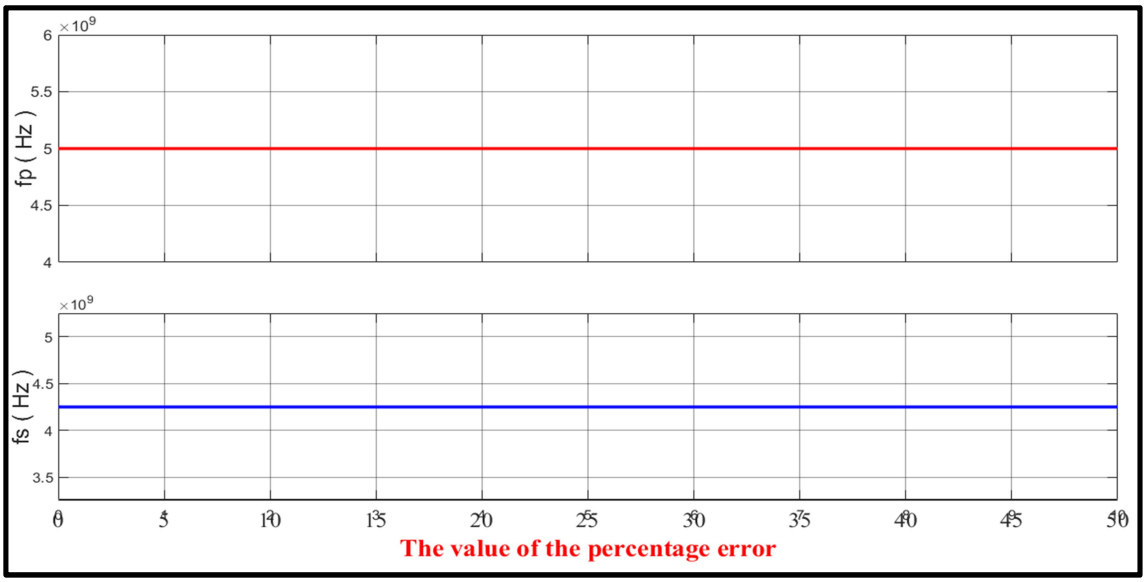

Fig. 4.10: Frequencies of the self test MEMS actuator without any change in the percentage of internal MEMS designed impedances with $f_p = 5\text{GHz}$,

$$f_s = 4.25\text{GHz}.$$

The above figures show that the actuator runs in a normal case. In other words, the above figures show that the actuator runs without a change in the percentage of internal MEMS designed impedances. Therefore, output frequencies stay constant at all times.

Secondly, the percentage variation ratio in the internal MEMS designed capacitance (C_o) has been adjusted from 0-50% with stay the values of other parameters constant. Figure 4.11 displays the percentage change action in the designed MEMS internal capacitance (C_o), which will be applied to test the MEMS designed frequencies which are shown in figure (4.12).

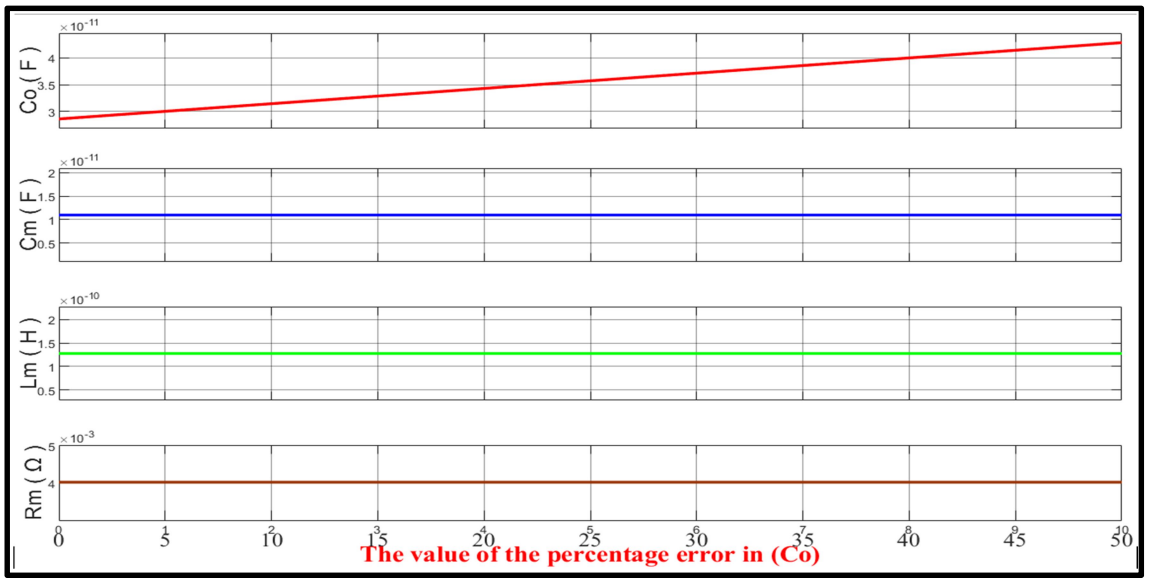

Fig. 4.11: Percentage change in the designed MEMS capacitance (C_o) of the self test MEMS actuator with stay the values of other parameters constant in the case of $f_p = 5GHz$, $f_s = 4.25GHz$.

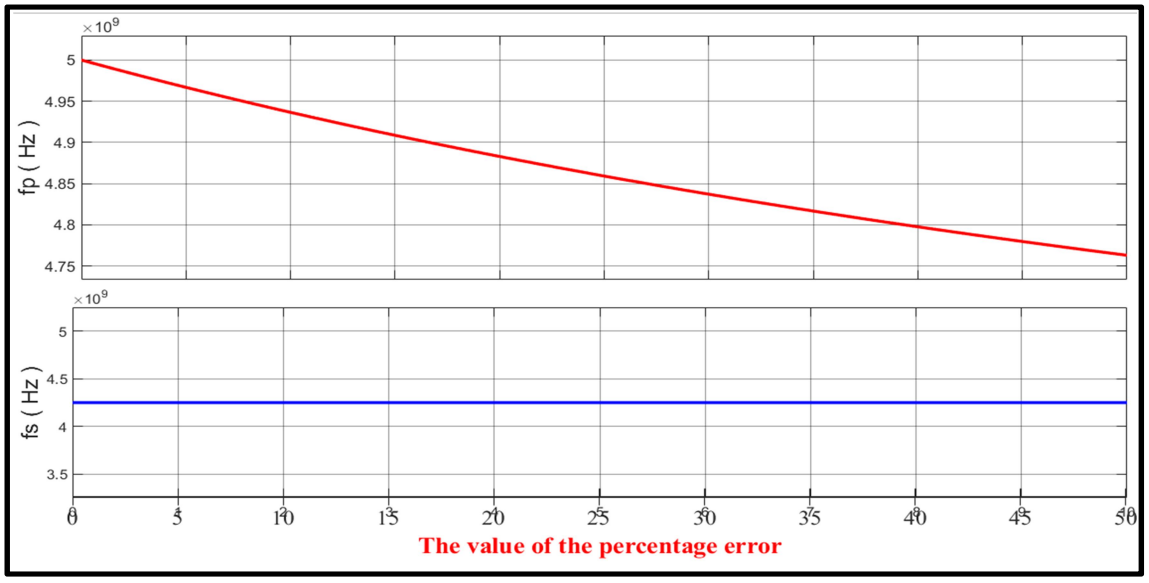

Fig. 4.12: MEMS designed frequencies according to percentage change in (C_o) in the case of $f_p = 5GHz$, $f_s = 4.25GHz$.

From figure (4.12), it can be seen that the change in the designed frequency (f_p) will exponentially decay with a percentage change in the internal MEMS designed capacitance (C_o). Whereas, the same figure shows that there is no change in the designed frequency (f_S) for the same percentage change in the internal MEMS designed capacitance (C_o). Also, table (4.5) displays the values of fp and fs according to percentage change in C_o.

Table 4.5: The values of C_o, f_p and f_s according to percentage change in C_o for the self test MEMS actuator with $f_p = 5\text{GHz}$, $f_s = 4.25\text{GHz}$.

percentage change in C_o	**Values of C_o, f_p, and f_S**		
	C_o	**f_p**	**f_S**
0%	**28.57 PF**	**5 GHz**	**4.25 GHz**
10%	**31.41 PF**	**4.935 GHz**	**4.25 GHz**
20%	**34.28 PF**	**4.88 GHz**	**4.25 GHz**
30%	**37.15 PF**	**4.837 GHz**	**4.25 GHz**
40%	**40 PF**	**4.798 GHz**	**4.25 GHz**
50%	**42.9 PF**	**4.760 GHz**	**4.25 GHz**

Now, the effect of changing the internal MEMS designed capacitance (C_m) on the MEMS designed frequencies will be tested. Figure (4.13) displays the percentage change in the designed MEMS internal capacitance (C_m), which will be applied to test the MEMS designed frequencies, which are shown in figure (4.14).

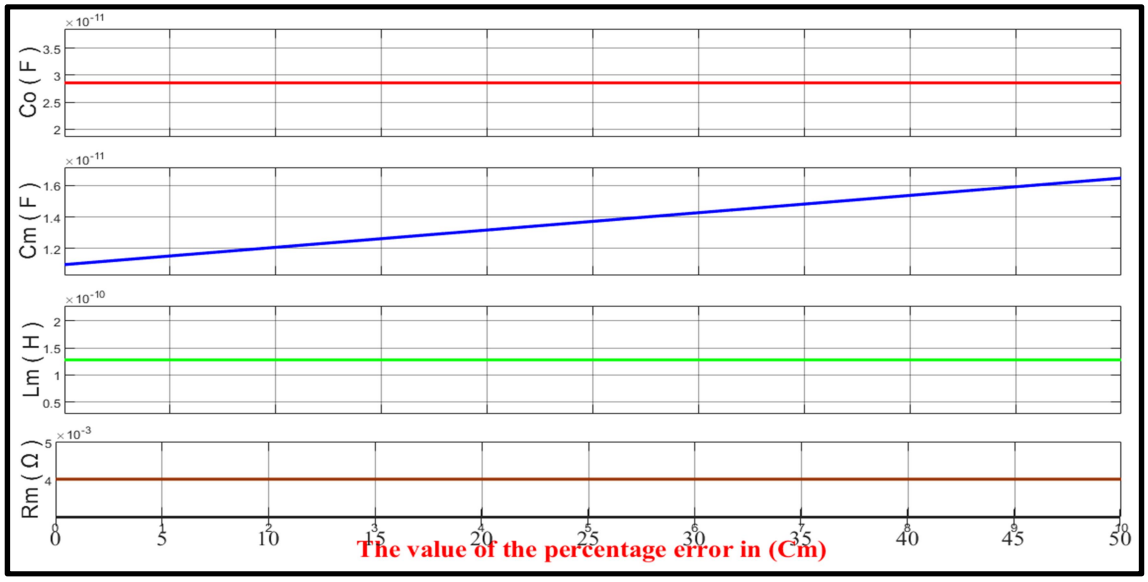

Fig. 4.13: Percentage change in the designed MEMS capacitance (C_m) of the self test MEMS actuator with keeping the values of other parameters constant in the case of $f_p = 5GHz$, $f_s = 4.25GHz$..

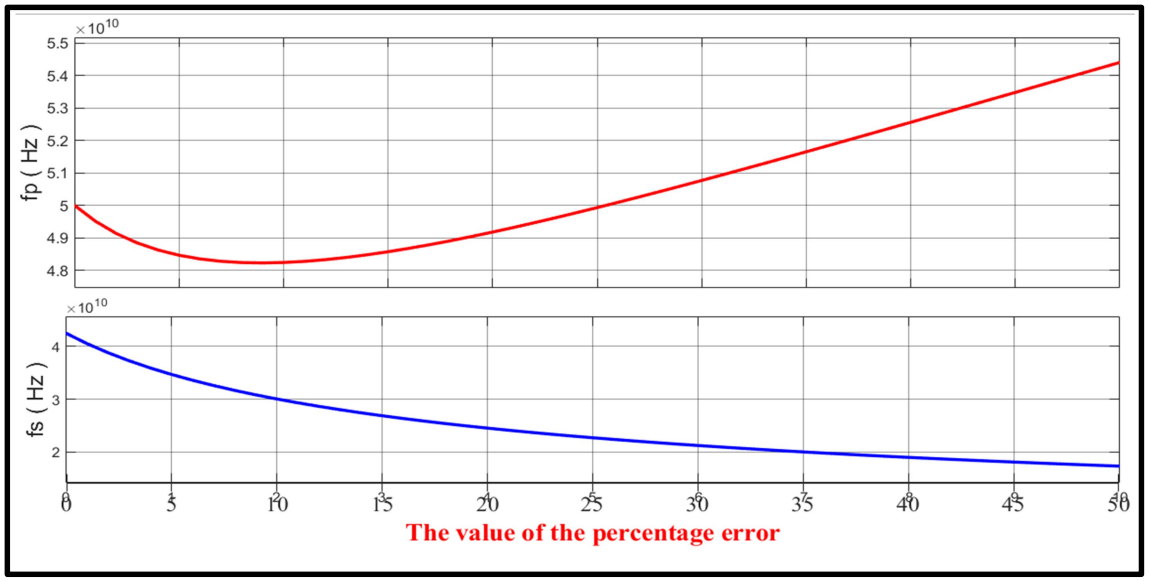

Fig. 4.14: MEMS designed frequencies according to percentage change in C_m in the case of $f_p = 5GHz$, $f_s = 4.25GHz$.

From figure (4.14), it can be seen that the change in the designed frequency (f_p) decreased when the Percentage change of C_m changes from 0%

to 20%, and it is increased in residual changing. Also, the same figure shows that the change in the designed frequency (f_s) exponentially decays with a percentage change in the internal MEMS designed capacitance (C_m). Table (4.6) displays the values of fp and fs according to percentage change in C_m.

Table 4.6: The values of C_m, f_p and f_s according to percentage change in C_m for the self test MEMS actuator with $f_p = 5\text{GHz}$, $f_s = 4.25\text{GHz}$.

percentage change in C_m	**Values of C_m, f_p, and f_s**		
	C_m	**f_p**	**f_s**
0%	**10.97 PF**	**5 GHz**	**4.25 GHz**
10%	**12.05 PF**	**4.824 GHz**	**4.052GHz**
20%	**13.17 PF**	**4.917 GHz**	**3.88GHz**
30%	**14.25 PF**	**5.007 GHz**	**3.727 GHz**
40%	**15.36 PF**	**5.255 GHz**	**3.59 GHz**
50%	**16.47 PF**	**5.44 GHz**	**3.471 GHz**

In addition, the effect of changing the internal MEMS designed impedance (L_m) on the MEMS designed frequencies will be taken. Figure (4.15) demonstrates the percentage change in the designed MEMS internal impedance (L_m). On the other side, figure (4.16) offers the MEMS design frequencies according to changing the internal MEMS designed impedance (L_m).

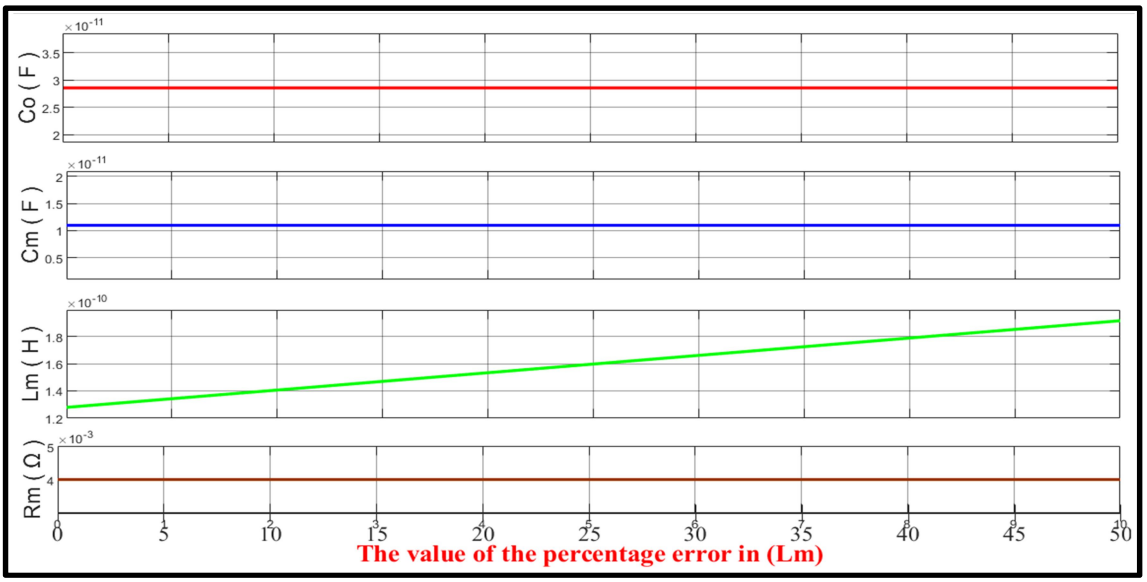

Fig. 4.15: Percentage change in the designed MEMS impedance (L_m) of the self test MEMS actuator with keeping the values of other parameters constant in the case of $f_p = 5GHz$, $f_s = 4.25GHz$.

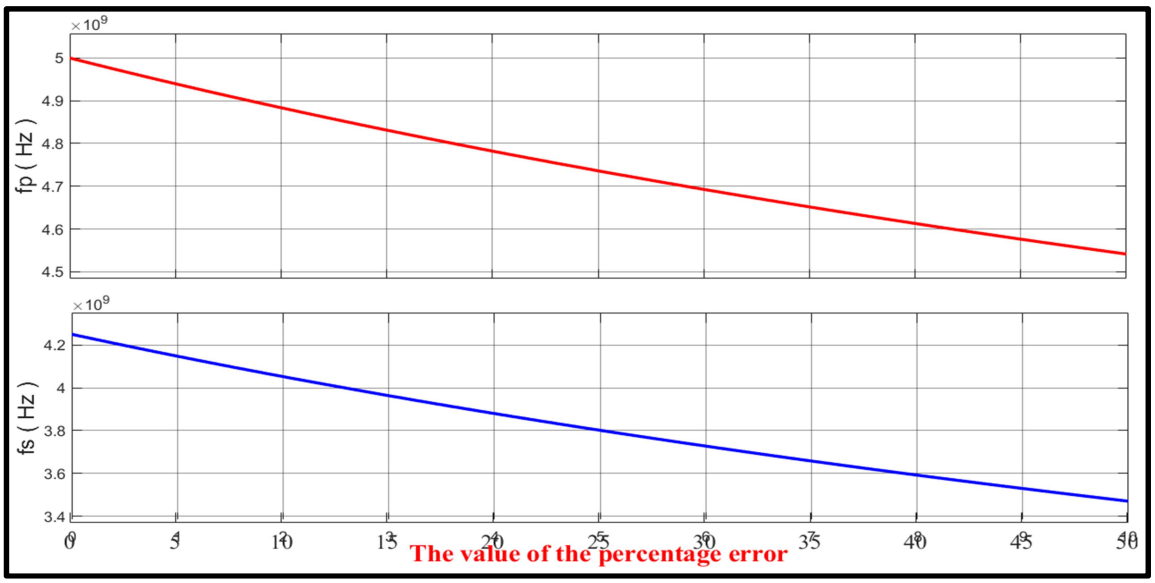

Fig. 4.16: MEMS designed frequencies according to percentage change in L_m in the case of $f_p = 5GHz$, $f_s = 4.25GHz$.

The above figure shows that the values of the designed frequencies (f_p and f_s) exponentially decrease when the percentage ratio change of L_m changes. Table (4.7) displays the values of f_p and fs according to percentage change in L_m.

Table 4.7: The values of L_m& f_p and f_s according to percentage change in L_m for the self test MEMS actuator with $f_p = 5GHz$, $f_s = 4.25GHz$.

percentage change in L_m	Values of L_m, f_p, and f_s		
	L_m	f_p	f_s
0%	**127.8 PH**	**5 GHz**	**4.25 GHz**
10%	**140.6 PH**	**4.888 GHz**	**4.055 GHz**
20%	**153.2 PH**	**4.782 GHz**	**3.880 GHz**
30%	**166.1 PH**	**4.695 GHz**	**3.730 GHz**
40%	**178.9 PH**	**4.618 GHz**	**3.594 GHz**
50%	**191.7 PH**	**4.541 GHz**	**3.470 GHz**

Furthermore, will investigate how the changing in internal MEMS designed resistance (R_m) affects the MEMS designed frequency. The percentage change in the intended MEMS internal resistance is shown in figure (4.17). Instead, figure (4.18) provides the MEMS design frequencies in response to varying the internal MEMS designed resistance (R_m).

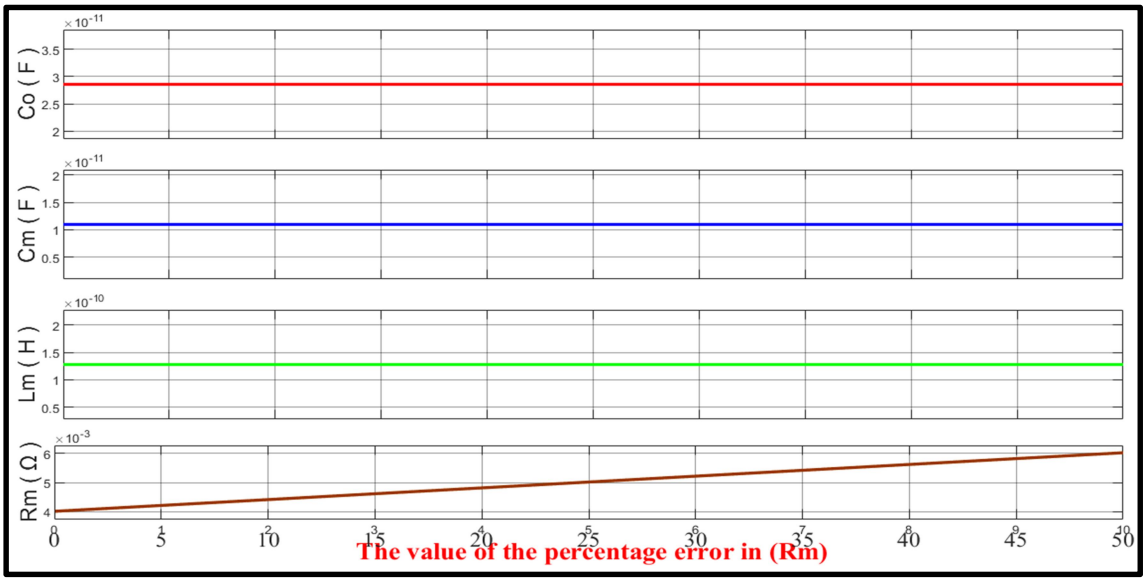

Fig. 4.17: Percentage change in the designed MEMS resistance (R_m) of the self test MEMS actuator with holding the values of other parameters constant in the case of $f_p = 5GHz$, $f_s = 4.25GHz$.

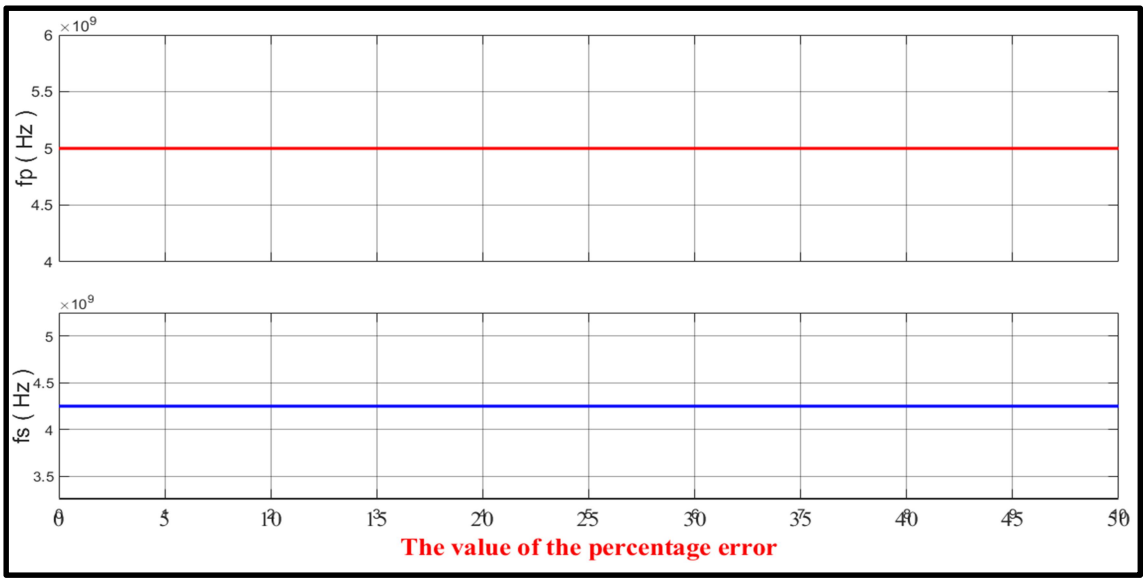

Fig. 4.18: MEMS designed frequencies according to percentage change in R_m in the case of $f_p = 5GHz$, $f_s = 4.25GHz$.

From figure (4.18), it can be seen that the variation in both designed frequencies (f_p and f_s) is constant (no change) whatever the percentage change in the internal MEMS designed resistance (R_m). In other words, the value of the resistance is not considered in calculations of the values of the design frequencies for the self test MEMS actuator.

Finally, the percentage variation ratio in the internal MEMS designed impedances (C_o, C_m, L_m, & R_m) has been adjusted from 0-50%. Figure (4.19) shows the percentage change in the designed MEMS internal impedances (C_o, C_m, L_m, & R_m). On the other hand, figure (4.20) suggests the MEMS design frequencies (f_p and f_s) according to changing the internal MEMS designed impedances (C_o, C_m, L_m, & R_m).

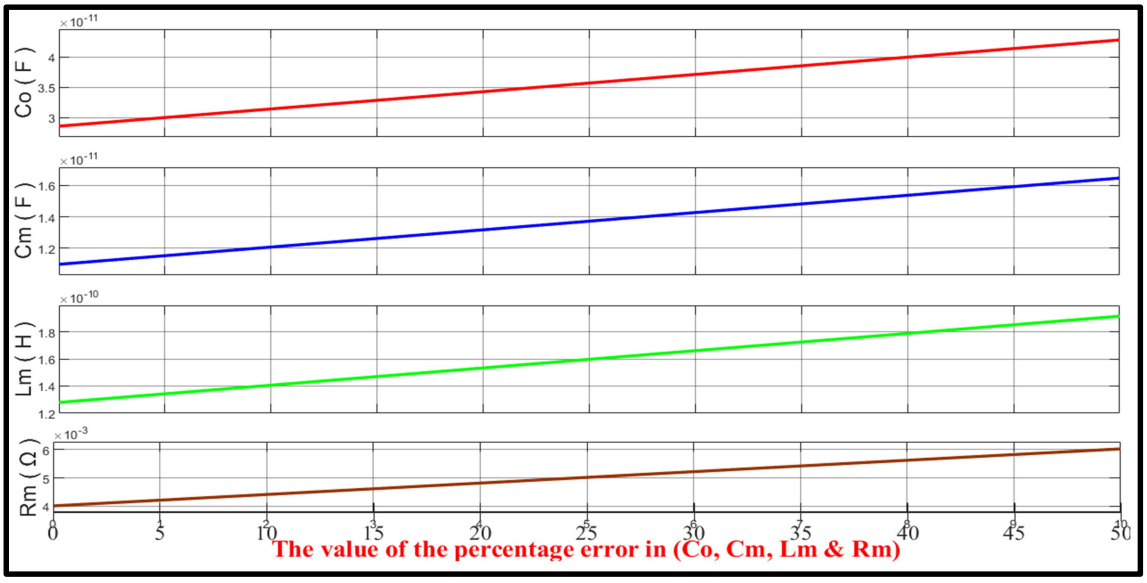

Fig. 4.19: Percentage change in the designed MEMS impedances (C_o, C_m, L_m, & R_m) of the self test MEMS actuator in the case of $f_p = 5GHz$, $f_s = 4.25GHz$.

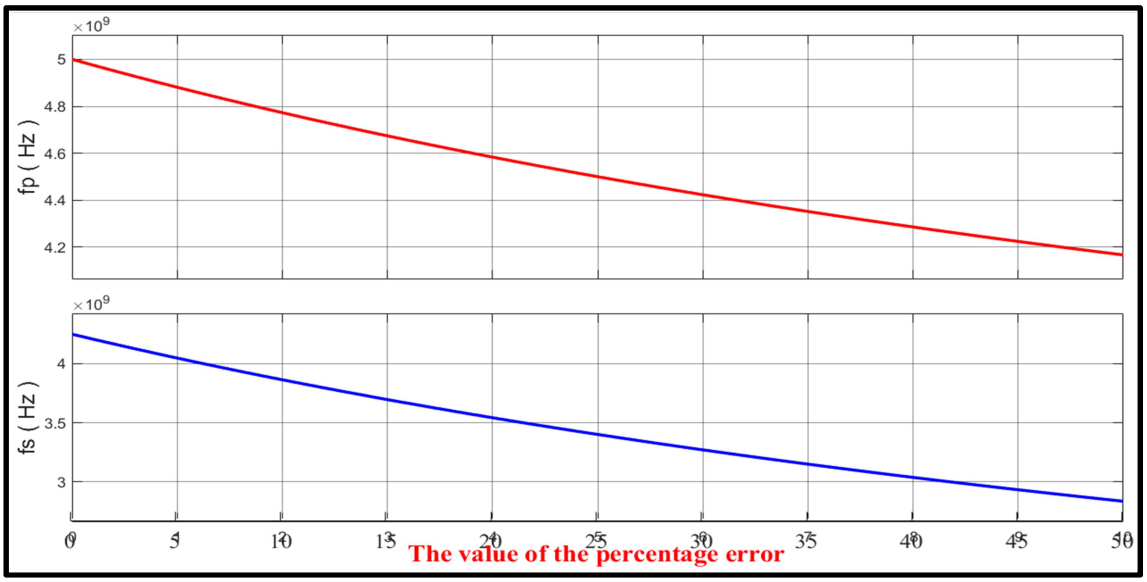

Fig. 4.20: MEMS designed frequencies according to percentage change in C_o, C_m, L_m, & R_m in the case of $f_p = 5GHz$, $f_s = 4.25GHz$.

The above figure illustrated that the values of the designed frequencies (f_p and f_s) exponentially decrease when the Percentage ratio change of C_o, C_m, L_m, & R_m changes. Table (4.8) displays the values of f_p and f_s according to percentage change in C_o, C_m, L_m, & R_m .

Table 4.8: The values of C_o, C_m, L_m, & R_m, f_p and f_s according to percentage change in C_o, C_m, L_m, & R_m for the self test MEMS actuator with $f_p = 5\text{GHz}$, $f_s = 4.25\text{GHz}$.

percentage change	Values of C_o, C_m, L_m, & R_m, f_p and f_s					
	C_o	C_m	L_m	R_m	f_p	f_s
0%	**28.57 PF**	**10.97 PF**	**127.8 PH**	**4.015 mΩ**	**5 GHz**	**4.25 GHz**
10%	**31.41 PF**	**12.05 PF**	**140.6 PH**	**4.416 mΩ**	**4.775 GHz**	**3.864GHz**
20%	**34.28 PF**	**13.17 PF**	**153.2 PH**	**4.818 mΩ**	**4.583 GHz**	**3.542 GHz**
30%	**37.15 PF**	**14.25 PF**	**166.1 PH**	**5.218 mΩ**	**4.423 GHz**	**3.269 GHz**
40%	**40 PF**	**15.36 PF**	**178.9 PH**	**5.620 mΩ**	**4.285 GHz**	**3.035 GHz**
50%	**42.9 PF**	**16.47 PF**	**191.7 PH**	**6.024 mΩ**	**4.167 GHz**	**2.834 GHz**

From table (4.8), it can be concluded that the percentage change in the designed MEMS impedances (C_o, C_m, L_m, & R_m) has a dominant effect on the MEMS designed frequencies.

4.3.2 When $f_p = 10\text{GHz}$ and $f_s = 8.5\text{GHz}$

This subsection is similar to the previous subsection but the difference is in the frequencies that will be relied upon are $f_p = 10\text{GHz}$, $f_s = 8.5\text{GHz}$. Firstly, will be considered two cases to find out how the MEMS-designed frequencies are affected. The first case shows the MEMS frequencies design when no change in the percentage of internal MEMS designed impedances, (C_o, C_m, L_m, & R_m). Figure (4.21) shows the values of the MEMS parameters, and figure (4.22) offers the MEMS frequencies design. The second case shows the MEMS frequencies design when the percentage variation ratio in the internal MEMS designed resistance (R_m) has been adjusted from 0-50% with keeping the values of other parameters constant. The percentage change in the intended MEMS internal resistance is shown in figure (4.23). Instead, figure (4.24) provides the MEMS design frequencies in response to varying the internal MEMS designed resistance (R_m).

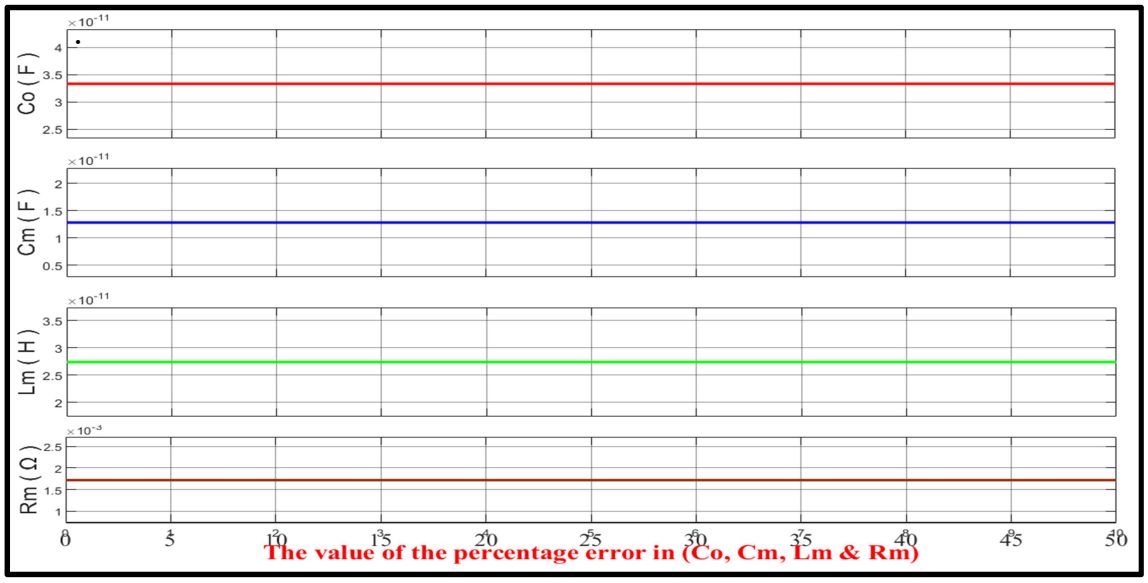

Fig. 4.21: Parameters of the self test MEMS actuator without any change in the percentage of internal MEMS designed impedances with $f_p = 10\text{GHz}$, $f_s = 8.5\text{GHz}$.

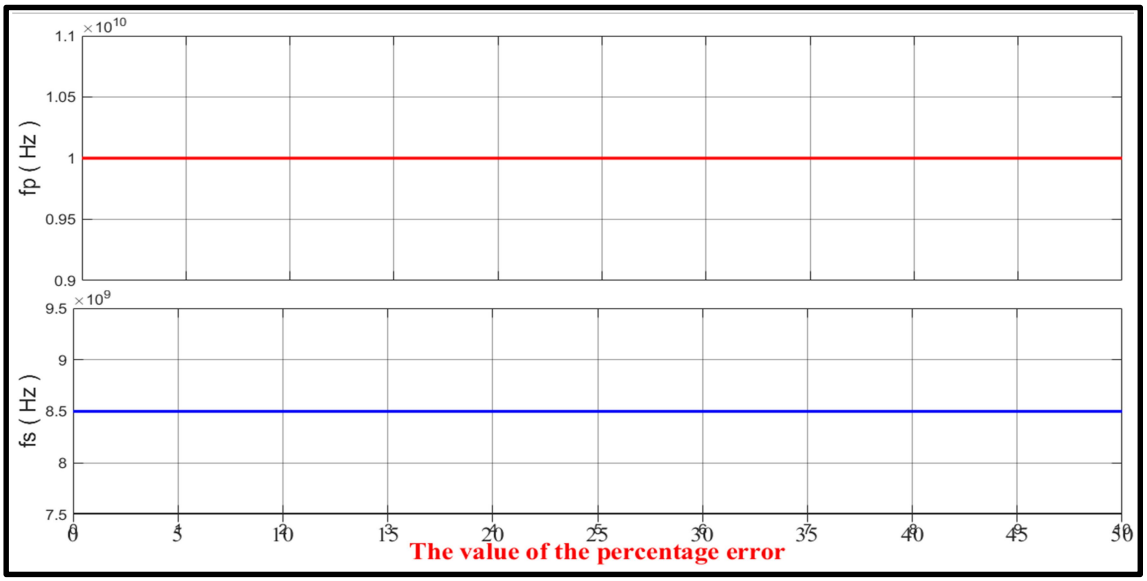

Fig. 4.22: Frequencies of the self test MEMS actuator without any change in the percentage of internal MEMS designed impedances with $f_p = 10\text{GHz}$, $f_s = 8.5\text{GHz}$.

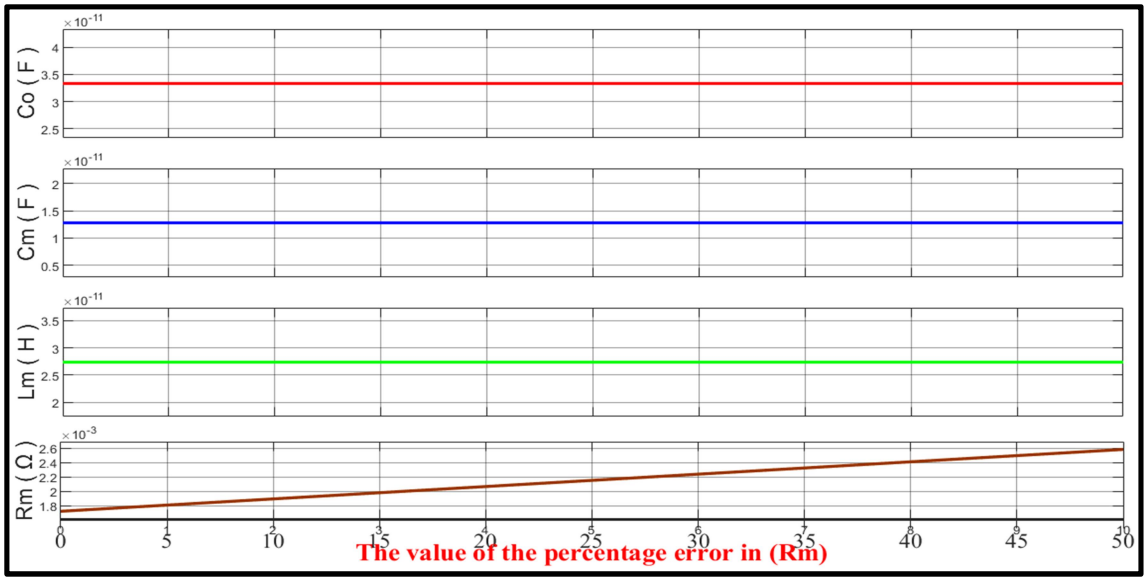

Fig. 4.23: Percentage change in the designed MEMS resistance (R_m) of the self test MEMS actuator with holding the values of other parameters constant in the case of $f_p = 10\text{GHz}$, $f_s = 8.5\text{GHz}$.

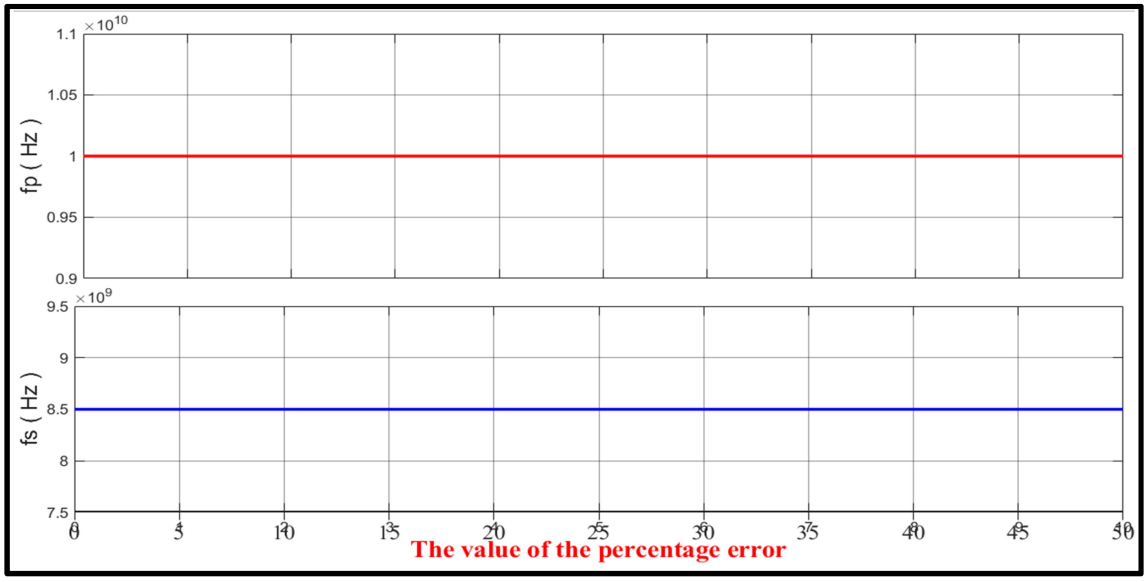

Fig. 4.24: MEMS designed frequencies according to percentage change in R_m in the case of $f_p = 10\text{GHz}$, $f_s = 8.5\text{GHz}$.

From the figures (4.24), it can be concluded that the MEMS designed frequencies (f_p & f_s) are not changed for any value of R_m when the percentage variation ratio in the internal MEMS-designed resistance (R_m) has been adjusted from 0-50%.

Now, the percentage variation ratio in the internal MEMS designed capacitance (C_o) has been adjusted from 0-50% with holding the values of other parameters constant. Figure (4.25) displays the percentage change in the designed MEMS internal capacitance (C_o), which will be applied to test the MEMS designed frequencies, as shown in figure (4.26).

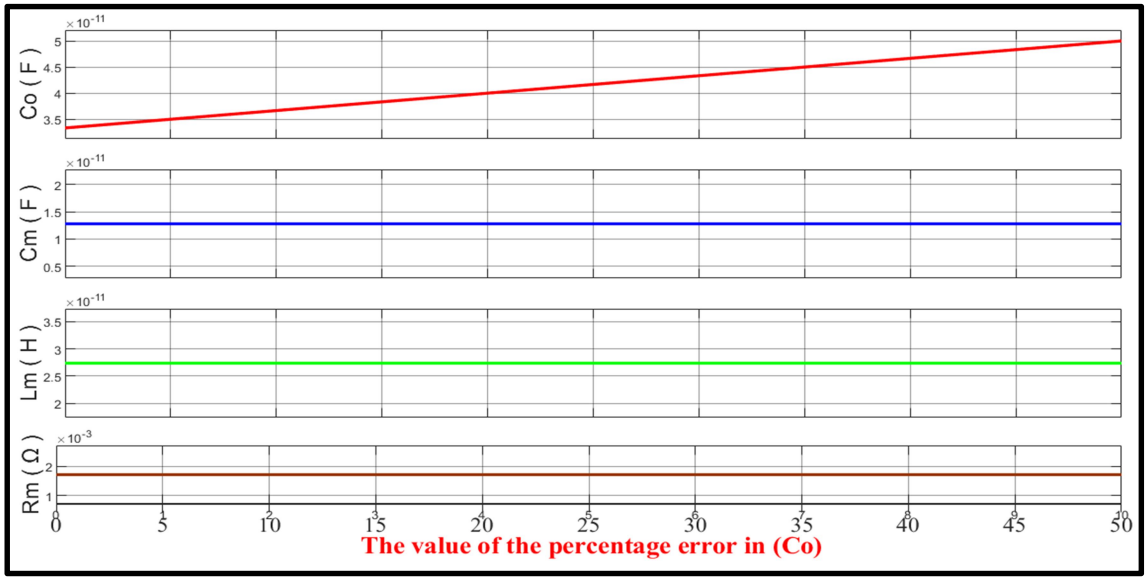

Fig. 4.25: Percentage change in the designed MEMS capacitance (C_o) of the self test MEMS actuator with keeping the values of other parameters constant in the case of $f_p = 10\text{GHz}$, $f_s = 8.5\text{GHz}$.

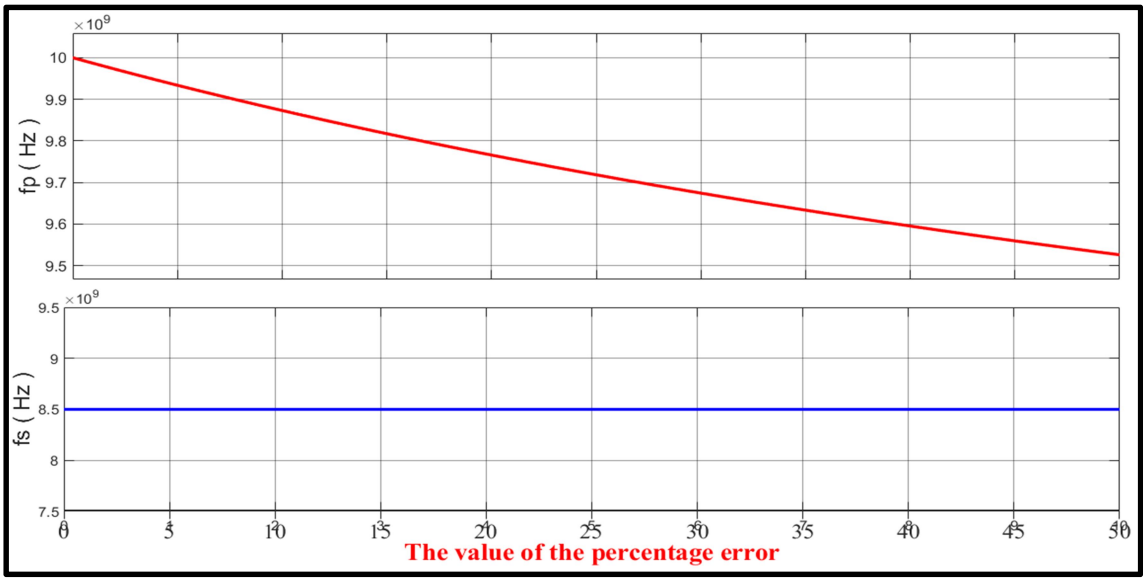

Fig. 4.26: MEMS designed frequencies according to percentage change in C_o in the case of $f_p = 10GHz$, $f_s = 8.5GHz$.

The figures (4.25, 4.26) show that the f_p is the only effect frequency, from the MEMS designed frequency, by the change in the value of Co, which is mentioned in the previous case when the stander frequencies are $f_p = 5GHz$, $f_s = 4.25GHz$. Therefore, it can be concluded that the behavior of fs and fp for any value of stander MEMS frequencies is not changed when the value of co changes. Also, table (4.9) displays the values of fp and fs according to percentage change in (C_o) in the case of $f_p = 10GHz$, $f_s = 8.5GHz$.

Table 4.9: The values of C_o, f_p and f_s according to percentage change in C_o for the self test MEMS actuator with $f_p = 10GHz$, $f_s = 8.5GHz$.

percentage change in C_o	**Values of C_o, f_p, and f_S**		
	C_o	**f_p**	**f_S**
0%	**33.33 PF**	**10 GHz**	**8.5 GHz**
10%	**36.67 PF**	**9.837 GHz**	**8.5 GHz**
20%	**40 PF**	**9.766 GHz**	**8.5 GHz**
30%	**43.33 PF**	**9.674 GHz**	**8.5 GHz**
40%	**46.66 PF**	**9.595 GHz**	**8.5 GHz**
50%	**50 PF**	**9.525 GHz**	**8.5 GHz**

In addition, the effect of changing the internal MEMS designed capacitance (C_m) on the MEMS designed frequencies will be tested. Figure (4.27) displays the percentage change in the designed MEMS internal capacitance (C_m), which will be applied to test the MEMS designed frequencies, as shown in figure (4.28).

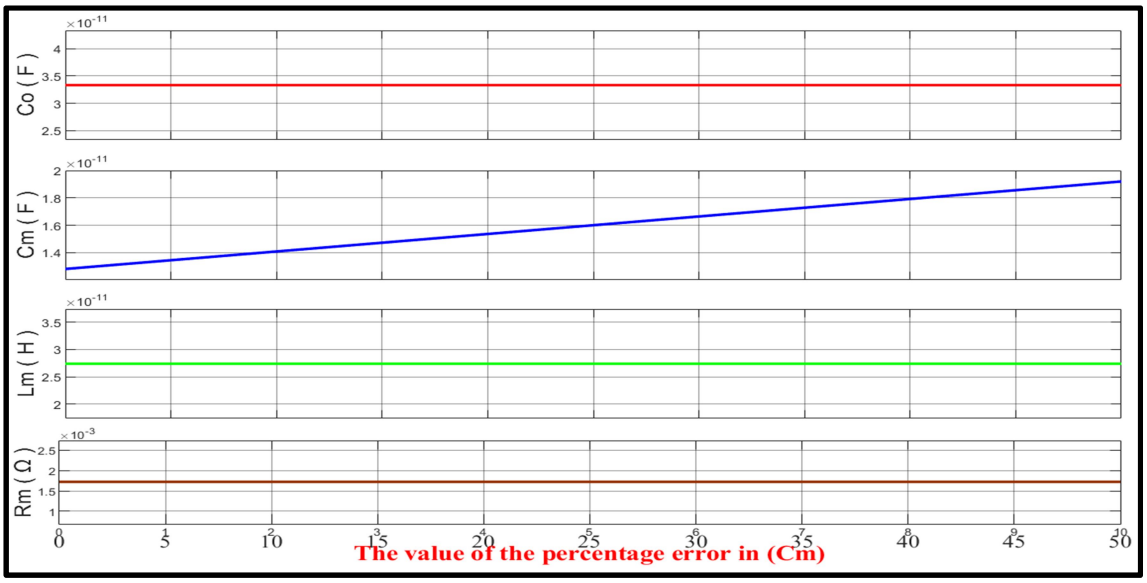

Fig. 4.27: Percentage change in the designed MEMS capacitance (C_m) of the self test MEMS actuator with keeping the values of other parameters constant in the case of $f_p = 10\text{GHz}$, $f_s = 8.5\text{GHz}$.

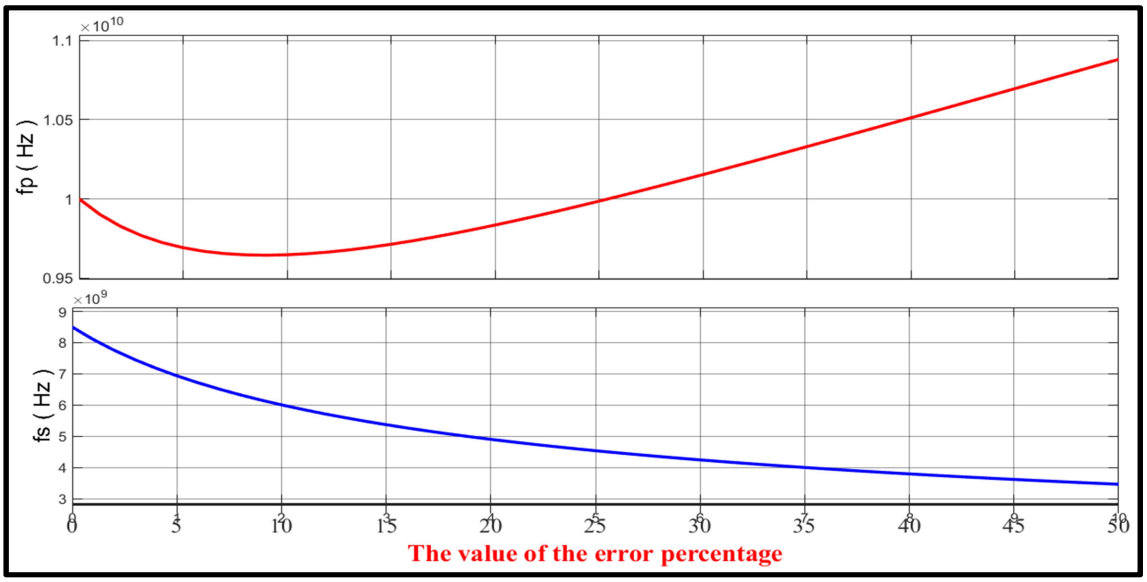

Fig. 4.28: MEMS designed frequencies according to percentage change in C_m in the case of $f_p = 10GHz$, $f_s = 8.5GHz$.

From figure (4.28), it can be seen that the behavior of fs and fp in the case of $f_p = 10GHz$ and $f_s = 8.5GHz$ is similar to the behavior of fs and fp in the case of $f_p = 5GHz$ and $f_s = 4.25GHz$ when the percentage variation ratio in the internal MEMS designed capacitance (C_m) has been adjusted from 0-50% with stay the values of other parameters constant. The difference here is only the range of changing C_m becomes large than that in the case of $f_p = 5GHz$ and $f_s = 4.25GHz$. Table (4.10) displays the values of f_p and f_s according to percentage change in C_m in the case of $f_p = 10GHz$, $f_s = 8.5GHz$.

Table 4.10: The values of C_m, f_p and f_s according to percentage change in C_m for the self test MEMS actuator with $f_p = 10GHz$, $f_s = 8.5GHz$.

percentage change in C_m	**Values of C_m, f_p, and f_S**		
	C_m	**f_p**	**f_S**
0%	**12.8 PF**	**10 GHz**	**8.5 GHz**
10%	**14.08 PF**	**9.647 GHz**	**8.104 GHz**
20%	**15.36 PF**	**9.835 GHz**	**7.759 GHz**
30%	**16.65 PF**	**10.15 GHz**	**7.455 GHz**
40%	**17.93 PF**	**10.51 GHz**	**7.185 GHz**
50%	**19.20 PF**	**10.88 GHz**	**6.940 GHz**

Furthermore, the effect of changing the internal MEMS designed impedance (L_m) on the MEMS designed frequencies will be considered. Figure (4.29) demonstrates the percentage change in the designed MEMS internal impedance (L_m). On the other side, figure (4.30) presents the MEMS design frequencies according to changing the internal MEMS designed impedance L_m.

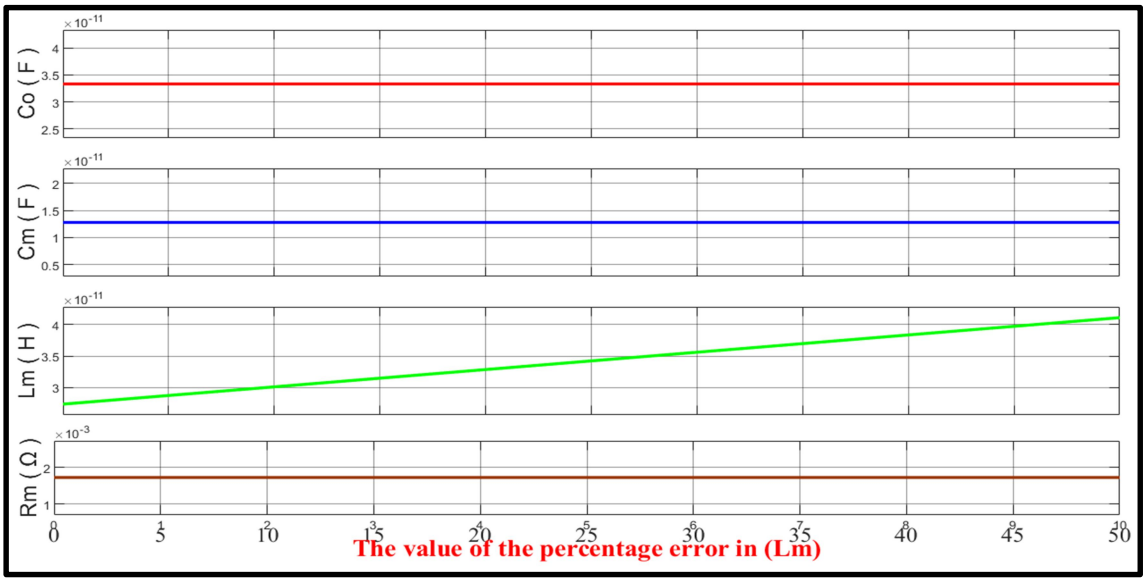

Fig. 4.29: Percentage change in the designed MEMS impedance (L_m) of the self test MEMS actuator with holding the values of other parameters constant in the case of $f_p = 10GHz$, $f_s = 8.5GHz$.

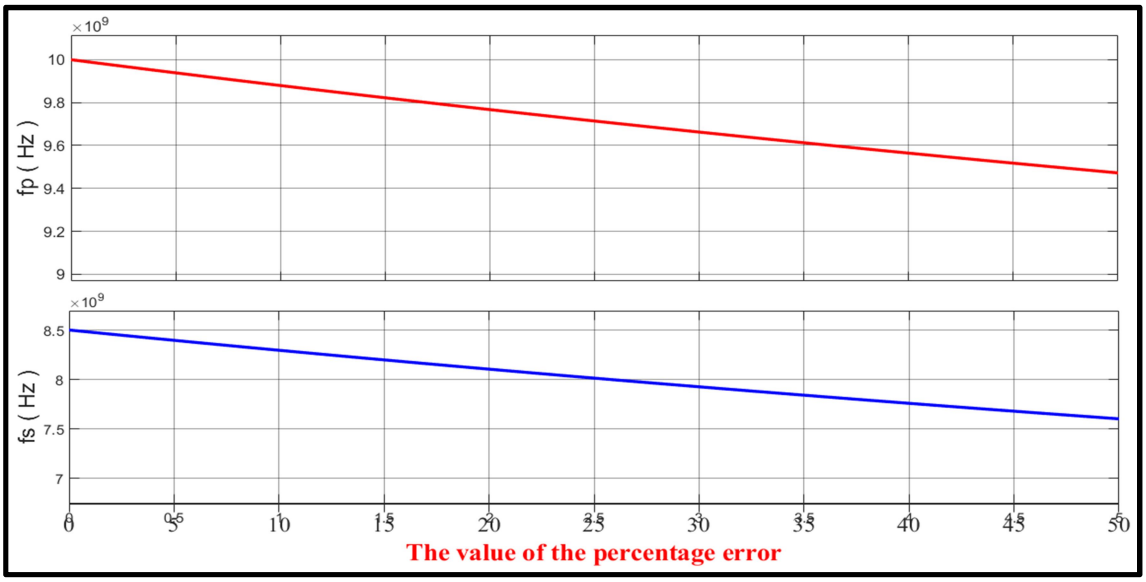

Fig. 4.30: MEMS designed frequencies according to percentage change in L_m in the case of $f_p = 10GHz$, $f_s = 8.5GHz$.

Figure (4.30) shows that the values of the designed frequencies (f_p and f_s) exponentially decrease when the percentage ratio change of L_m changes. This point is mentioned in the previous case when the stander frequencies are $f_p = 5GHz$, $f_s = 4.25GHz$. The difference here is only the range of changing L_m becomes small than that in the case of $f_p = 5GHz$ and $f_s = 4.25GHz$. Table (4.11) displays the values of f_p and fs according to percentage change in L_m in the case of $f_p = 10GHz$, $f_s = 8.5GHz$.

Table 4.11: The values of L_m& f_p and f_s according to percentage change in L_m for the self test MEMS actuator with $f_p = 10GHz$, $f_s = 8.5GHz$.

percentage change in L_m	Values of L_m, f_p, and f_s		
	L_m	f_p	f_s
0%	**27.38 PH**	**10 GHz**	**8.5 GHz**
10%	**30.12 PH**	**9.767 GHz**	**8.104 GHz**
20%	**32.89 PH**	**9.564 GHz**	**7.760 GHz**
30%	**34.60 PH**	**9.385 GHz**	**7.455 GHz**
40%	**38.34 PH**	**9.226 GHz**	**7.184 GHz**
50%	**41.07 PH**	**9.120 GHz**	**6.960 GHz**

Finally, the percentage variation ratio in the internal MEMS designed impedances (C_o, C_m, L_m, & R_m) has been adjusted from 0-50%. Figure (4.31) shows the percentage change in the designed MEMS internal impedances (C_o, C_m, L_m, & R_m). On the other hand, figure (4.32) suggest the MEMS design frequencies (f_p and f_s) according to changing the internal MEMS designed impedances (C_o, C_m, L_m, & R_m).

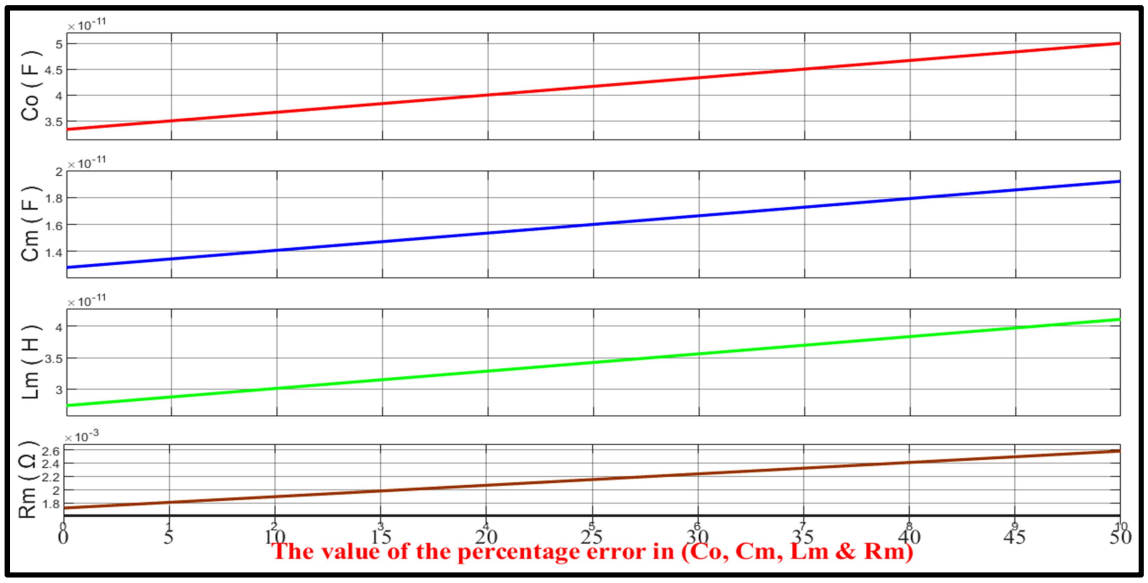

Fig. 4.31: Percentage change in the designed MEMS impedances (C_o, C_m, L_m, & R_m) of the self test MEMS actuator in the case of $f_p = 10GHz$, $f_s = 8.5GHz$

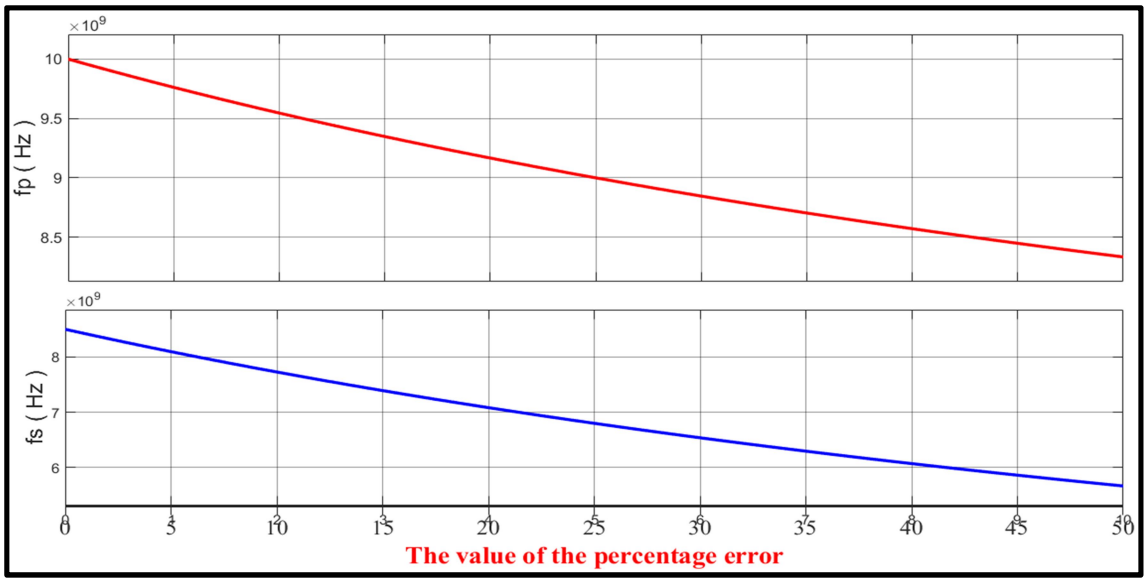

Fig. 4.32: MEMS designed frequencies according to percentage change in C_o, C_m, L_m, & R_m in the case of $f_p = 5GHz$, $f_s = 4.25GHz$.

Figure (4.32) offered that the values of the designed frequencies (f_p and f_s) exponentially decrease when the percentage ratio change of C_o, C_m, L_m, & R_m changes. Table (4.12) displays the values of f_p and f_s according to percentage change in C_o, C_m, L_m, & R_m .

Table 4.12: The values of C_o, C_m, L_m, & R_m, f_p and f_s according to percentage change in C_o, C_m, L_m, & R_m for the self test MEMS actuator with $f_p = 10GHz$, $f_s = 8.5GHz$.

percentage change	Values of C_o, C_m, L_m, & R_m, f_p and f_s					
	C_o	**C_m**	**L_m**	**R_m**	**f_p**	**f_s**
0%	**33.33 PF**	**12.8 PF**	**27.38 PH**	**1.721 mΩ**	**10 GHz**	**8.5 GHz**
10%	**36.67 PF**	**14.08 PF**	**30.12 PH**	**1.892 mΩ**	**9.544 GHz**	**7.725 GHz**
20%	**40 PF**	**15.36 PF**	**32.89 PH**	**2.065 mΩ**	**9.166GHz**	**7.083 GHz**
30%	**43.33 PF**	**16.65 PF**	**34.60 PH**	**2.237 mΩ**	**8.845 GHz**	**6.535 GHz**
40%	**46.66 PF**	**17.93 PF**	**38.34 PH**	**2.409 mΩ**	**8.571 GHz**	**6.071 GHz**
50%	**50 PF**	**19.20 PF**	**41.07 PH**	**2.585 mΩ**	**8.335 GHz**	**5.665 GHz**

Chapter Five Conclusion and future research directions

CHAPTER FIVE
CONCLUSIONS AND FUTURE RESEARCH DIRECTIONS

5.1 Introduction

In this exploration, the conclusions about the results that appeared in chapter four are presented. This chapter is divided into three sections, the first section suggests the conclusion about the results of the MEMS frequency self-test design model. The second section illustrates the conclusion about the results of the MEMS changing filter parameter self-test design model. The third section explains the future research directions for the proposed work.

5.2 The MEMS Frequency Dependent Design Model

From the results of the circuit shown in figure (3.2), where the results of it are shown in chapter four and when the percentage variation in the designed frequency has been adjusted from 0-50 %, the following points can be concluded:

1- The Df_p, and Df_S are linearly proportional with the increase in the percentage variation which can be related to the aging failure mode.
2- The values of the capacitances of the MEMS actuator will not be affected by these percentage variations.
3- The motional inductance and resistance of the MEMS actuator are highly inverse-proportional to the percentage variations in the operating designed frequency.

4- The ranges of Df_p and Df_S values in the case of MEMS frequency self-test design model with the variation in the designed frequency from 0-50% are linearly increased with the increase of the threshold designed frequencies (5 GHz and 10 GHz).
5- The values of L_m and R_m decrease when the threshold designed frequencies increase.
6- The values of C_o and C_m increase when the threshold designed frequencies increase.

5.3 The Effect of Changing the Filter Parameters of the Self-Test Model

The results of the circuit shown in figure (3.12) included a number of cases. Therefore, the conclusions of these results can be simplified into the following:

The effect of changing C_o, it can be concluded that the change in the value of C_o starting 0 to 50% shows a decrease in the value of f_p, while the value of f_S remains constant**.** Also, it can be concluded that the change in the value of C_m starting 0 to 10% shows a decrease in value of f_p, while the change in the value of C_m starting 10% to 50% causes an increase in value of f_p. Also, it can be concluded from this case that the change in value of C_m causes a decrease in value of f_S. Also, it can be concluded that the change in the value of L_m from 0 to 50% causes a decrease in the values of f_p and f_S. The change in the value of R_m from 0 to 50% has not affected the values of f_S and f_p. Finally, it can be concluded that the change in the values of all parameters from 0 to 50% causes a decrease in the values of f_p and f_S.

5.4 Future Research Directions

By reviewing the simulation details of this study and analyzing the results obtained, we can recommend several suggestions to future researchers in this field to complete a systematic research and investigation in a scientific manner and within a well-studied work plan. The following suggestions might be recommended:

1) It is possible to continue the work using the proposed systems in this study and developing a self-test at resonant frequencies higher than 10 GHz.
2) Studying the effects of partial changes in the designed resonant frequencies with new high values on the impedance values designed by these systems.
3) Design a compensation system that can performs a correction in the value of frequencies when the error happens.

References

References

[1] N. S. Kale, “Introduction to MEMS; their applications as sensors for chemical & bio sensing,” in *2015 19th International Symposium on VLSI Design and Test*, Jun. 2015, no. January, pp. 1–2, doi: 10.1109/ISVDAT.2015.7208158.

[2] R. L. Filler and J. R. Vig, “Resonators for the microcomputer compensated crystal oscillator,” in *Proceedings of the 43rd Annual Symposium on Frequency Control*, 1989, pp. 8–15, doi: 10.1109/FREQ.1989.68852.

[3] H. A. C. Tilmans, M. Elwenspoek, and J. H. J. Fluitman, “Micro resonant force gauges,” *Sensors Actuators A Phys.*, vol. 30, no. 1–2, pp. 35–53, Jan. 1992, doi: 10.1016/0924-4247(92)80194-8.

[4] A.-C. Wong, J. R. Clark, and C. T.-C. Nguyen, “Anneal-activated, tunable, 68 MHz micromechanical filters,” *Dig. Tech. Pap.*, vol. 10, pp. 7–10, 1999.

[5] M. I. Pupin, “Wave Transmission over Non-Uniform Cables and Long-Distance Air-Lines,” *Trans. Am. Inst. Electr. Eng.*, vol. XVII, pp. 445–512, 1900, doi: 10.1109/T-AIEE.1900.4764144.

[6] G. A. Campbell, “XXX. On loaded lines in telephonic transmission,” *London, Edinburgh, Dublin Philos. Mag. J. Sci.*, vol. 5, no. 27, pp. 313–330, Mar. 1903, doi: 10.1080/14786440309462928.

[7] K. W. Wagner, “Spulen- und Kondensatorleitungen,” *Arch. für Elektrotechnik*, vol. 8, no. 2–3, pp. 61–92, Feb. 1919, doi: 10.1007/BF01597052.

[8] A. Ling *et al.*, “Broadband microwave absorbing materials based on MWCNTs’ electromagnetic wave filtering effect,” *Compos. Part B Eng.*, vol. 171, pp. 214–221, Aug. 2019, doi:

10.1016/j.compositesb.2019.04.034.

[9] O. J. Zobel, "Theory and Design of Uniform and Composite Electric Wave-filters," *Bell Syst. Tech. J.*, vol. 2, no. 1, pp. 1–46, Jan. 1923, doi: 10.1002/j.1538-7305.1923.tb00001.x.

[10] A. S. Algamili *et al.*, "A review of actuation and sensing mechanisms in MEMS-based sensor devices," *Nanoscale Res. Lett.*, vol. 16, pp. 1–21, 2021.

[11] S. W. Park and E. Sanchez-Sinencio, "RF Oscillator Based on a Passive RC Bandpass Filter," *IEEE J. Solid-State Circuits*, vol. 44, no. 11, pp. 3092–3101, Nov. 2009, doi: 10.1109/JSSC.2009.2031061.

[12] R. P. Sallen and E. L. Key, "A practical method of designing RC active filters," *IRE Trans. Circuit Theory*, vol. 2, no. 1, pp. 74–85, Mar. 1955, doi: 10.1109/TCT.1955.6500159.

[13] B. John, C. M. Philip, and A. J. George, "Design and Implementation of Built in Self Test (BIST) forVLSI Circuits using Verilog," vol. 3, no. 05, pp. 3–6, 2015, doi: 10.17577/IJERTCONV3IS05037.

[14] N. Zhang, L. Mei, C. Wang, Z. Deng, J. Yang, and Q. Guo, "A Switchable Bandpass Filter Employing RF MEMS Switches and Open-Ring Resonators," *IEEE Trans. Electron Devices*, vol. 64, no. 8, pp. 3377–3383, Aug. 2017, doi: 10.1109/TED.2017.2712643.

[15] S. K. Roy, V. T. K. Sauer, J. N. Westwood-Bachman, A. Venkatasubramanian, and W. K. Hiebert, "Improving mechanical sensor performance through larger damping," *Science (80-.).*, vol. 360, no. 6394, p. eaar5220, Jun. 2018, doi: 10.1126/science.aar5220.

[16] D. Fedasyuk, R. Holyaka, and T. Marusenkova, "A Tester of the MEMS Accelerometers Operation Modes," in *2019 3rd International Conference*

on Advanced Information and Communications Technologies (AICT), Jul. 2019, pp. 227–230, doi: 10.1109/AIACT.2019.8847840.

[17] C. Zhao *et al.*, "A Resonant MEMS Accelerometer With 56ng Bias Stability and 98ng/Hz 1/2 Noise Floor," *J. Microelectromechanical Syst.*, vol. 28, no. 3, pp. 324–326, Jun. 2019, doi: 10.1109/JMEMS.2019.2908931.

[18] Y. Liu, Y. Cai, Y. Zhang, A. Tovstopyat, S. Liu, and C. Sun, "Materials, Design, and Characteristics of Bulk Acoustic Wave Resonator: A Review," *Micromachines*, vol. 11, no. 7, p. 630, Jun. 2020, doi: 10.3390/mi11070630.

[19] S. Yandrapalli, S. E. Kucuk, B. Atakan, V. Plessky, and L. G. Villanueva, "Fabrication and Analysis of Thin Film Lithum Niobate Resonators for 5GHz Frequency and Large K t 2 Applications," in *2021 IEEE 34th International Conference on Micro Electro Mechanical Systems (MEMS)*, Jan. 2021, pp. 967–969, doi: 10.1109/MEMS51782.2021.9375401.

[20] H. J. Santos, *Introduction to microelectromechanical (MEM) microwave systems*. 1999.

[21] R. Abdolvand, B. Bahreyni, J. Lee, and F. Nabki, "Micromachined Resonators: A Review," *Micromachines*, vol. 7, no. 9, p. 160, Sep. 2016, doi: 10.3390/mi7090160.

[22] L.-W. Hung, *High-Q low-impedance MEMS resonators*. University of California, Berkeley, 2011.

[23] Yu-Wei Lin, Seungbae Lee, Sheng-Shian Li, Yuan Xie, Zeying Ren, and C.-C. Nguyen, "Series-resonant VHF micromechanical resonator reference oscillators," *IEEE J. Solid-State Circuits*, vol. 39, no. 12, pp. 2477–2491, Dec. 2004, doi: 10.1109/JSSC.2004.837086.

[24] C. Nguyen, “MEMS technology for timing and frequency control,” *IEEE Trans. Ultrason. Ferroelectr. Freq. Control*, vol. 54, no. 2, pp. 251–270, 2007, doi: 10.1109/TUFFC.2007.240.

[25] J. Perkins, “LED & HB-LED Packaging: Technology & Marketing Trends,” *Addit. Conf. (Device Packag. HiTEC, HiTEN, CICMT)*, vol. 2010, no. DPC, pp. 001137–001176, Jan. 2010, doi: 10.4071/2010DPC-Keynote3_LEDs.

[26] N. S. Khan, “Modeling and characterization of RF MEMS resonators.” The University of Texas at Arlington, 2009.

[27] K. Asadi, J. Yu, and H. Cho, “Nonlinear couplings and energy transfers in micro- and nano-mechanical resonators: intermodal coupling, internal resonance and synchronization,” *Philos. Trans. R. Soc. A Math. Phys. Eng. Sci.*, vol. 376, no. 2127, p. 20170141, Aug. 2018, doi: 10.1098/rsta.2017.0141.

[28] H. C. Nathanson, W. E. Newell, R. A. Wickstrom, and J. R. Davis, “The resonant gate transistor,” *IEEE Trans. Electron Devices*, vol. 14, no. 3, pp. 117–133, Mar. 1967, doi: 10.1109/T-ED.1967.15912.

[29] J. Taylor and Q. Huang, *CRC handbook of electrical filters*. CRC Press, 1997.

[30] S. A. Chandorkar, M. Agarwal, R. Melamud, R. N. Candler, K. E. Goodson, and T. W. Kenny, “Limits of quality factor in bulk-mode micromechanical resonators,” in *2008 IEEE 21st International Conference on Micro Electro Mechanical Systems*, Jan. 2008, pp. 74–77, doi: 10.1109/MEMSYS.2008.4443596.

[31] H. Campanella, *Acoustic wave and electromechanical resonators: concept to key applications*. Artech House, 2010.

[32] B. Charlot, S. Mir, F. Parrain, and B. Courtois, "Generation of electrically induced stimuli for MEMS self-test," *J. Electron. Test.*, vol. 17, pp. 459–470, 2001.

[33] H. V Allen, S. C. Terry, and D. W. De Bruin, "Accelerometer systems with self-testable features," *Sensors and Actuators*, vol. 20, no. 1–2, pp. 153–161, Nov. 1989, doi: 10.1016/0250-6874(89)87113-6.

[34] L. Zimmermann *et al.*, "Airbag application: a microsystem including a silicon capacitive accelerometer, CMOS switched capacitor electronics and true self-test capability," *Sensors Actuators A Phys.*, vol. 46, no. 1–3, pp. 190–195, Jan. 1995, doi: 10.1016/0924-4247(94)00888-O.

[35] S. Wang and N. Yao, "A RSU-aided distributed trust framework for pseudonym-enabled privacy preservation in VANETs," *Wirel. Networks*, vol. 25, pp. 1099–1115, 2019.

[36] N. Guo, L. Ma, and T. Gao, "Independent Mix Zone for Location Privacy in Vehicular Networks," *IEEE Access*, vol. 6, pp. 16842–16850, 2018, doi: 10.1109/ACCESS.2018.2800907.

[37] M. Z. Koohi, W. Peng, and A. Mortazawi, "An Intrinsically Switchable Balanced Ferroelectric FBAR Filter at 2 GHz," in *2020 IEEE/MTT-S International Microwave Symposium (IMS)*, Aug. 2020, pp. 131–134, doi: 10.1109/IMS30576.2020.9223799.

[38] T. Onuta, Y. Wang, S. E. Lofland, and I. Takeuchi, "Multiferroic Operation of Dynamic Memory Based on Heterostructured Cantilevers," *Adv. Mater.*, vol. 27, no. 2, pp. 202–206, Jan. 2015, doi: 10.1002/adma.201402974.

[39] Y. Jang, J.-D. Ha, S.-J. Lee, J. Lim, S.-M. Han, and D. Ahn, "Compact Size and Wideband Triplexer Using SAW Resonators and LC

Components," in *2018 IEEE/MTT-S International Microwave Symposium - IMS*, Jun. 2018, pp. 856–859, doi: 10.1109/MWSYM.2018.8439454.

[40] B. Kim *et al.*, "Temperature Dependence of Quality Factor in MEMS Resonators," *J. Microelectromechanical Syst.*, vol. 17, no. 3, pp. 755–766, Jun. 2008, doi: 10.1109/JMEMS.2008.924253.

[41] M. Villarroya *et al.*, "CMOS-SOI platform for monolithic integration of crystalline silicon MEMS," *Electron. Lett.*, vol. 42, no. 14, pp. 800–801, 2006.

[42] N. Deb and R. D. Blanton, "Built-in self test of CMOS-MEMS accelerometers," in *Proceedings. International Test Conference*, 2002, pp. 1075–1084.

[43] B. Charlot, S. Mir, F. Parrain, and B. Courtois, "Electrically induced stimuli for MEMS self-test," in *Proceedings 19th IEEE VLSI Test Symposium. VTS 2001*, 2001, pp. 210–215.

[44] M. Aikele *et al.*, "Resonant accelerometer with self-test," *Sensors Actuators A Phys.*, vol. 92, no. 1–3, pp. 161–167, 2001.

[45] X. Xiong, Y.-L. Wu, and W.-B. Jone, "A dual-mode built-in self-test technique for capacitive MEMS devices," *IEEE Trans. Instrum. Meas.*, vol. 54, no. 5, pp. 1739–1750, 2005.

[46] R. Puers, D. De Bruyker, and A. Cozma, "A novel combined redundant pressure sensor with self-test function," *Sensors Actuators A Phys.*, vol. 60, no. 1–3, pp. 68–71, 1997.

[47] N. Zhang, Z. Deng, and F. Sen, "CPW Tunable Band-Stop Filter Using Hybrid Resonator and Employing RF MEMS Capacitors," *IEEE Trans. Electron Devices*, vol. 60, no. 8, pp. 2648–2655, Aug. 2013, doi: 10.1109/TED.2013.2270359.

[48] S. M. Mirebrahimi, M. Dousti, and S. Afrang, "MEMS tunable filters based on DGS and waveguide structures: A literature review," *Analog Integr. Circuits Signal Process.*, vol. 108, no. 1, pp. 141–164, 2021.

[49] W. Y. Sam and Z. Zakaria, "A review on reconfigurable integrated filter and antenna," *Prog. Electromagn. Res. B*, vol. 63, pp. 263–273, 2015.

[50] V. N. R. Vanukuru and V. K. Velidi, "Millimeter-wave CMOS 30/80 GHz sharp-rejection dual-band bandstop filters using TFMS open-stepped-impedance resonators," *IEEE Trans. Circuits Syst. II Express Briefs*, vol. 68, no. 1, pp. 201–205, 2020.

الخلاصة

على مدى السنوات الأخيرة، أظهرت النظم الكهروميكانيكية الدقيقة (MEMS) الإمكانات الحرجة لتطبيقات تحديد ومعالجة الإشارات عالية التكرار، يرجع ذلك إلى ميزاتها المذهلة مثل المدى الضئيل وعامل الجودة ، واستهلاك الطاقة المنخفض، وتكلفة الإنتاج المنخفضة. يمكن استخدام دوائر الاتصالات عبر الترددات اللاسلكية لتلبية الطلب المتزايد على مكونات RF التي يمكن أن تطلبها أجهزة الاتصالات اللاسلكية متعددة النطاقات ومتعددة الأوضاع في المستقبل. قد توفر رنانات MEMS خياراً قابلاً للتحقيق بدلاً عن تقنية الكوارتز الحالية المحملة بالعيوب الكبيرة مثل الحجم الكبير نسبيًا والتكلفة العالية وانعدام التوافق مع رقائق IC.

في هذه الأطروحة، تم تصميم ومحاكاة تكنولوجيا حديثة لتصميم اختبار ذاتي، والذي يمثل عمل مرشح نطاق تمرير الرنين الذي يولد الترددات المطلوبة عن طريق إدخال البيانات المتعلقة بالخصائص الفيزيائية للمواد الكهرضغطية. باستخدام تقنية الفحص الذاتي والتصحيح، يمكن استخدام النظام المقترح وقيم التصميم المستخرجة للمقاومات والمكثفات والمحاثات المكافئة لحذف أي انحراف في أداء المرشح. تمت محاكاة النظام المقترح واختباره على ترددات تمرير عالية fp = 10 GHz و عامل الجودة Q=85% في اكتشاف التغيرات في الترددات والمعلمات. كانت السعة الحركية Cm هي المعلمة الرئيسية التي أثرت على تردد الإخراج حيث تم اعتبارها كدالة لتحديد حالة فشل المواد في نظام MEMS. انخفض تردد التوقف من 8.5 جيجاهرتز إلى 3.47 جيجاهرتز بينما زاد تردد التمرير من 10 جيجاهرتز إلى 10.88 جيجاهرتز. من ناحية أخرى ، كان للمعلمات الأخرى السعة الثابتة (Co) والحث الحركي (Lm) والمقاومة الحركية (Rm) تأثير أقل على تردد خرج المذبذب.

وزارة التعليم العالي والبحث العلمي
جامعة بابـل / كلية الهندسة
قسم الهندسة الكهربائية

اختبار ذاتي مدمج لرنان مايكرو الكترو ميكانيكي

رســـالـــــة
مقدمة الى كلية الهندسة في جامعة بابل
كجزء من متطلبات نيل درجة الماجستير في علوم الهندسة الكهربائية/الهندسة الكهربائية/إلكترونيك

من قبل
علي جاسم مُحَمَّد عبيد

اشـراف
الأستاذ الدكتور قيس كريم عمران

1444هـ 2023م